Thermal energy from surface waters

The thermal effects and underlying processes during thermal energy extraction from surface waters; a case study in the canals of Amsterdam

D.F.L. van 't Westende (Thierry)

Technische Universiteit Delft

TU Delft

waternet
waterschap amstel gooi en vecht
gemeente amsterdam

Thermal energy from surface waters

The thermal effects and underlying processes during thermal energy extraction from surface waters; a case study in the canals of Amsterdam

by

D.F.L. van 't Westende (Thierry)

to obtain the degree of Master of Science
at the Delft University of Technology,
to be defended publicly on We June 18, 2021 at 10:00 AM.

Student number:	4171691	
Project duration:	November, 2019 – June, 2021	
Thesis committee:	Dr. ir. F. H. M. van der Ven,	TU Delft
	Prof. dr. ir. J. P. van der Hoek,	TU Delft/Waternet
	Dr. ir. J. M. Bloemendal,	TU Delft
	Ir. S. Mol,	Waternet

An electronic version of this thesis is available at `http://repository.tudelft.nl/`.
Cover image: 'Zicht op Ketelhuisbrug' by @iljabertrand

TU Delft
Delft University of Technology

waternet
waterschap amstel gooi en vecht
gemeente amsterdam

Voorwoord

Voor u ligt mijn master thesis die het einde vormt van mijn studietijd aan de TU Delft. Het onderwerp van deze thesis gaat over het winnen van warmte uit oppervlaktewateren en in dit geval specifiek in de wereldberoemde grachten van Amsterdam. Deze duurzame warmte kan vervolgens ingezet worden om bijvoorbeeld huizen te verwarmen of warm water te maken. Het idee om juist dit onderwerp op te pakken is gegroeid vanuit mijn overtuiging dat klimaatverandering één van de grootste toekomstige bedreigingen voor de mensheid zal gaan vormen. Het is daarom van levensbelang om naar dit soort duurzame energiebronnen te zoeken en zo de uitstoot van broeikasgassen in de atmosfeer drastisch te verlagen. Mijn hoop is dat deze thesis daar een heel klein steentje aan mag bijdragen.

Dit onderzoek is in samenwerking met Waternet uitgevoerd, het waterbedrijf van Amsterdam. Ik ben Waternet dankbaar dat ik dit onderwerp heb mogen onderzoeken en voor de faciliteiten die Waternet mij ter beschikking heeft gesteld tijdens mijn onderzoek. Het is mijns inziens bijzonder en een groot goed dat er binnen Waternet een onderzoeksafdeling is met een ruime blik op de maatschappelijke vraagstukken rond water en dat er ook voldoende ruimte is om deze vraagstukken te onderzoeken.

Binnen Waternet wil ik allereerst mijn thesis begeleider aldaar bedanken, Stefan. De regelmatige gesprekken die we hebben gehad tijdens het schrijven van deze thesis, ook over onderwerpen niet per se aan deze thesis gerelateerd, hebben mij telkens gemotiveerd en gaven me weer energie. Ik wil daarnaast ook Jan Willem bedanken voor het opzetten van de meetcampagne, de leuke dagen varen in de grachten en de zoektocht naar samenwerking met Deltares. Verder heb ik leuke gesprekken gehad met Jan waarin we onze tegelijkertijd opgedane kennis over de modellering van oppervlaktewateren goed konden delen.

Vanuit Deltares wil ik Roland bedanken voor het wegwijs maken in de modelsoftware. Voor specifieke vragen over het model kon ik altijd bij jou terecht en voorzag je me van deskundig advies.

Vanuit de TU Delft wil ik allereerst Martin bedanken voor de begeleiding bij deze thesis. Het is fijn om met jou een traject als deze in te mogen gaan. De kalmte en het geduld die je bracht in onze overleggen zijn in mijn ogen belangrijk om tot iets goeds te kunnen komen. Verder wil ik Frans van de Ven bedanken voor zijn positieve energie en enthousiasme rondom het onderwerp aquathermie, evenals Jan Peter van der Hoek, van wie ik ook het genoegen heb deze thesis bij Waternet te hebben kunnen uitvoeren.

Tot slot wil ik Ilja bedanken voor het ontwerpen van de omslag van dit rapport en natuurlijk haar steun en liefde in het afronden van deze thesis. Het is een kwestie van de lange adem gebleken. Uiteraard wil ik ook mijn vrienden bedanken, zowel mijn vrienden uit mijn geliefde stad Middelburg als mijn studievrienden, de Mubraba's, voor de mooie tijd de afgelopen jaren. Tot slot, wil ik uiteraard mijn familie ook bedanken, mijn moeder, vader, broer en zussen voor hun onvoorwaardelijke steun en geloof in mij gedurende mijn hele studietijd en al die tijd daarvoor.

Ik wens u veel leesplezier,

D.F.L. van 't Westende (Thierry)
Delft, 28th of June 2021

Abstract

In order to achieve the goals in the Paris Climate Agreement of 2015 and stabilize the global warming of the atmosphere, an energy transition towards sustainable energy sources without emission of greenhouse gasses is vital. Historically, water has a large role in sustainable energy solutions by means of energy extraction and storage through its potential energy in areas with sufficient difference in altitude. In absence of height difference, another way of retrieving energy from water is by thermal extraction. In this study, the possibility of thermal energy extraction from a city canal is studied in a modelling case study.

Cities have the largest footprint in global energy use. In the Netherlands, the largest part of this urban energy demand is used for control of indoor climate of the built environment, with an overall higher heating demand rather than a cooling demand. This study focuses on the capital city of the Netherlands, Amsterdam, which originally is a harbour city situated in the middle of a river delta and therefore also contains a high amount of surface water area. This provides an interesting opportunity in which sustainable thermal energy could be extracted from the many famous canals in the inner city using so-called Surface Water Heat (SWH) systems.

SWH systems can extract thermal energy from surface waters directly, but often these systems are combined with Aquifer Thermal Energy Systems (ATES) for storage of energy in underground aquifers to overcome the time lag between energy recovery and usage. Solar radiation energy heats surface waters during summer. This heat can be extracted by a SWH heat exchanger and subsequently be stored underground in an ATES. During the colder months this thermal energy is pumped up out of the subsurface and can be used for various heating purposes.

Currently, research towards aquathermal energy solutions is still in a pioneering phase. As a consequence, there are only a few systems operable. In the city canals of Amsterdam, SWH systems have not been implemented at all. A reason for this can be found in a lack of knowledge about natural water temperature variations in these waters and the unknown thermal effects related to SWH. This study is an answer to this knowledge gap and an attempt is made to provide insight in the thermal effects of SWH on a city canal in Amsterdam. The Amsterdam city canals are a unique water system in open connection with larger waterways and they are part of a hydrodynamically complex interaction between sea and the river Rhine. Until date, such a study, not being restricted to the boundaries of the respective water body, is scarce or even non-existent.

The case study location is situated at the Jacob van Lennepkanaal in Amsterdam, where a collective of civilians has recently started the exploratory phase for installation of the first SWH city canal system for heating of their own district. To respond to this societal development, this specific case study location was chosen. To be able to model the SWH system for this neighbourhood, the first part of this thesis focuses on system layout and related system characteristics. It was found that open-loop SWH systems are often applied at district level. Secondly, a reference surface water temperature model without SWH systems was built and validated upon meteorological forcing with local water temperature measurements. The third part of the followed method was to apply the modelled SWH system to this validated three-dimensional thermodynamic model. For this purpose, the Delft3D model was chosen, which computes the RANS equations under the hydrostatic assumption. Several scenarios were calculated with varying temperature difference through the SWH heat exchanger and distance between system intake and outfall.

The modelling results for the van Lennepkanaal case show that SWH systems used for heating purposes, thereby cooling the surface water, produce a negatively buoyant flow, causing the discharged cold water plume to sink to the bottom. Existing thermal stratification in the city canals is enhanced and hydrodynamic mixing processes are not strong enough to disturb this stratification built-up. Further away along the plume, in the far-field, a combination of buoyant spreading and the process of passive diffusion mix the water column and the temperature decrease, induced by the SWH system, becomes uniformly spread over the entire water column. Currently, steady state one-dimensional models are often used for assessment of SWH

thermal effects. It was demonstrated that these models are useful and accurate, provided that the right heat exchange coefficient is used and near-field mixing at the outfall is represented correctly. These models can be used to study for example the time-averaged extent of the cold water plume, but fail to provide insight in time-varying and spatial characteristics of the canal. Local changes in bed level height, attraction of ambient water by the intake and intersections with lateral canals also influence the thermal profile. For a study towards these effects in greater detail, three-dimensional modelling or 2DV-modelling are preferred. Also, in case of a study towards application of multiple systems, these are the models of choice.

The modelling results demonstrate that the required heating demand at the Jacob van Lennepkanaal can be met for the considered district. However, it is inevitable that thermal energy is also extracted from surrounding canals through mixing processes and heat conduction. By analyzing the heat fluxes through the water surface, the total average heating power of the atmosphere above the cooled surface water was calculated. Total atmospheric heating power profiles showed that increasing the ΔT_{max} over the heat exchanger did not result in a higher atmospheric energy yield near the SWH system. Results also show that recirculation is inevitable within the dimensions of the considered district in this case study. Recirculation limits the maximum recoverable heat capacity of a SWH system. The scenarios considering multiple SWH systems showed that interference between systems can also become a considerable limiting factor. More research is needed into interference issues to draw further conclusions.

A disadvantage of a case study is that, although useful insights are obtained, the forthcoming results are not generally applicable. To create a more generally applicable and proper research basis, it is recommended to study issues related to interference and installation of multiple systems. An even higher priority is to verify the behaviour of a negatively buoyant plume by initiating a monitoring campaign for a real SWH system with water temperature measurements spatially distributed around system intake, outfall and further away from the system. In this way, future modelling efforts can be validated on this well-monitored SWH system. On the modelling side, it is recommended to improve the modelling of the near-field region around the SWH outfall with a non-hydrostatic model or an expert analytical model could be used combined with a hydrostatic model, as the one in this study, in follow-up research.

Keywords: Surface Water Heat, cold water plume, Delft3D, negative buoyancy, city canal

Contents

List of Abbreviations

C_s	The Smagorinsky coefficient [-]
α_0	Thermal molecular diffusivity [m^2/s]
α_t	Thermal turbulent diffusivity [m^2/s]
ΔQ	Heat flux difference [W/m^2]
ΔT	Temperature Difference [°C]
$\Delta T_{\max}$	Temperature Difference through SWH heat exchanger (maximum) [°C]
ϵ	turbulent kinetic energy dissipation [m^2/s^3]
κ	von Karman constant (=0.41 (-))
$\lambda_f(z)$	Frontal area density [-]
$\nu_{Huniform}$	Uniform or background horizontal eddy viscosity [m^2/s]
ν_V	Vertical eddy viscosity [m^2/s]
σ	Stefan-Boltzmann's constant (= $5.67x10^8 J/m^2 sK^4$)
τ_b	Bottom shear stress [kg/ms^2]
τ_s	Wind shear stress [kg/ms^2]
B_ε	Buoyancy induced turbulent energy dissipation term [m^2/s^2]
B_k	Buoyancy induced turbulence production [m^2/s^2]
c_μ	Closure parameter in Kolmogorov-Prandtl equation (= 0.09 for log law of the wall turbulence development)
C_D	Wind drag coefficient [-]
c_E	Dalton number [-]
$c_{fr.conv}$	Coefficient of free convection, calibrated at 0.14 [-]
c_H	Stanton number [-]
c_p	the specific heat capacity of water (= 4184 J/kgK)
D_ε	Diffusion coefficient for turbulent energy dissipation [m^2/s]
D_k	Diffusion coefficient for kinetic turbulent energy [m^2/s]
F_c	Cloud fraction [-]
h_k	Height of the Urban Boundar Layer [m]
H_{Secchi}	Secchi depth [m]
K	heat exchange coefficient with atmosphere [W/m^2/°C]
k	Turbulent kinetic energy [J/kg]
$l(z)$	Mixing length of wind above building height ($z > z_w$)[m]

$l_c(z)$	Mixing length of wind in urban canopy region [m]
$l_m(z)$	Mixing length of wind in the shear layer ($H < z < z_w$)[m]
M_x	Momentum in x-direction from source/sink [m/s^2]
M_y	Momentum in y-direction from source/sink[m/s^2]
P	Baroclinic pressure [kg/ms^2]
P_ε	Production term for turbulent energy dissipation [m^2/s^2]
P_k	Production term for turbulent kinetic energy [m^2/s^2]
Pr	Prandtl number [-]
Pr_t	Turbulent Prandtl number [-]
Q_{cofree}	Conductive heat flux through free convection [W/m^2]
Q_{evfree}	Evaporative/latent heat flux through free convection [W/m^2]
Q_{co}	Conductive heat flux [W/m^2]
Q_{eb}	Effective long wave back radiation [W/m^2]
Q_{ev}	Evaporative/latent heat flux [W/m^2]
Q_{sn}	Net incident short wave solar radiation [W/m^2]
Q_{tot}	Total heat flux [W/m^2]
r_{hum}	relative humidity [%]
S_T	Heat source term in energy equation [°Cs^{-1}]
u, v, w	Flow velocities in x, y, z direction [m/s]
U_{10}	wind velocity at 10 metres above free water surface [m/s]
ATES	Aquifer Thermal Energy System
ATES+	Aquifer Thermal Energy System combined with a system for well regeneration
BILDE	Bilderdijkgracht
CFD	Computational Fluid Dynamics
CIW	Commission Integral Watermanagement
COP	Coefficient of Performance
DACOS	Da Costagracht
DESA	Distributed Entrainment Sink Approach
DSWC	Direct Surface Water Cooling systems
DUIVV	Duivendrechtse Vaart
EWFD	European Water Framework Directive
HSWHP	Hybrid Surface Water Heat Pump systems
JVLEN	Jacob van Lennepkanaal
KEIZE	Keizersgracht

LMTD	Log Mean Temperature Difference method
MAE	Mean Absolue Error
ME	Mean error
NTU	Number of Transferring Units method
NWHER	Nieuwe Herengracht
ODES	Stiff Ordinary Differential Equation
PSA	Partial Shaded Area [%]
RANS	Reynolds-averaged Navier Stokes
RMSE	Root Mean Square Error
STOWA	Stichting Toegepast Onderzoek Waterbeheer
SVF	Sky View Factor (SVF=0 for entire sky blocked by obstacles) [-]
SWH	Surface Water Heat systems
SWHP	Surface Water Heat Pump systems
T	Temperature [°C]
UBL	Urban Boundary Layer, same as Internal Boundary layer (IBL)

List of Figures

1

Introduction

Increased awareness of the effects of climate change has led to a global search for renewable energy sources. The water cycle has a large potential to represent a key role in finding these renewable energy solutions . Water in the water cycle can either be used as an energy carrier, or internal chemical and thermal energy can be directly extracted from it (Van der Hoek, 2012). The Paris Climate Agreement of 2015 and recent reports by the International Panel on Climate Change (Intergovernmental Panel on Climate Change, 2018) have shown that, in order to stabilize global warming to a preferred 1.5 degrees Celsius, measures to reduce our dependence on greenhouse gas emitting energy sources, thereby initiating a global energy transition, are of utmost importance . Also within the continent of Europe, this has led to the forming of policy initiatives and a green deal by the European Commission (European Commission, 2019). It shows that global ambitions are historically high and the urgency to study the energy collection, storage and recovery capacity of water is increasing accordingly.

A way to retrieve energy from water, is by extracting or supplying thermal energy from and to surface waters. In this way, a surface water, for example a lake, river or canal, functions as a large heat sink. It either stores thermal energy from sunlight, which can be used to provide heat to buildings, or it could be used directly to cool down houses, offices or other commercial buildings by storing the outgoing surplus heat during summer conditions. Although both of these modes are used in practice, this thesis focuses on the first situation: extraction of thermal energy during the summer period for the supply of heat to buildings. In this case, the thermal storage, required to overcome the period between the recovery during summer and when the energy is needed in winter, often occurs in underground aquifers by means of Aquifer Thermal Energy Systems (ATES) , see figure 1.1. ATES systems consist of two water wells; a cold well and a hot well. Both of these wells can be used to provide respectively cooling capacity and heating capacity to the climate system of the connected building(s). The possibility to exchange thermal energy through an extra heat exchanger in connection with nearby surface waters is often used to recharge the wells of an ATES. In this way, long term thermal imbalances between the cold and hot well of the ATES are prevented. The use of ATES for heat storage facilitates indirect use of surface water heat for space heating and for example the production of heated tap water. To upgrade the low temperature heat supplied by the ATES, heat pumps are commonly installed. In 2018, a Dutch study towards the potential on national scale estimated that these type of Surface Water Heat systems , hereafter referred to as SWH, have a theoretical heating potential of 40% of the total heat demand in the built environment of the Netherlands (CE Delft, Deltares, 2018).

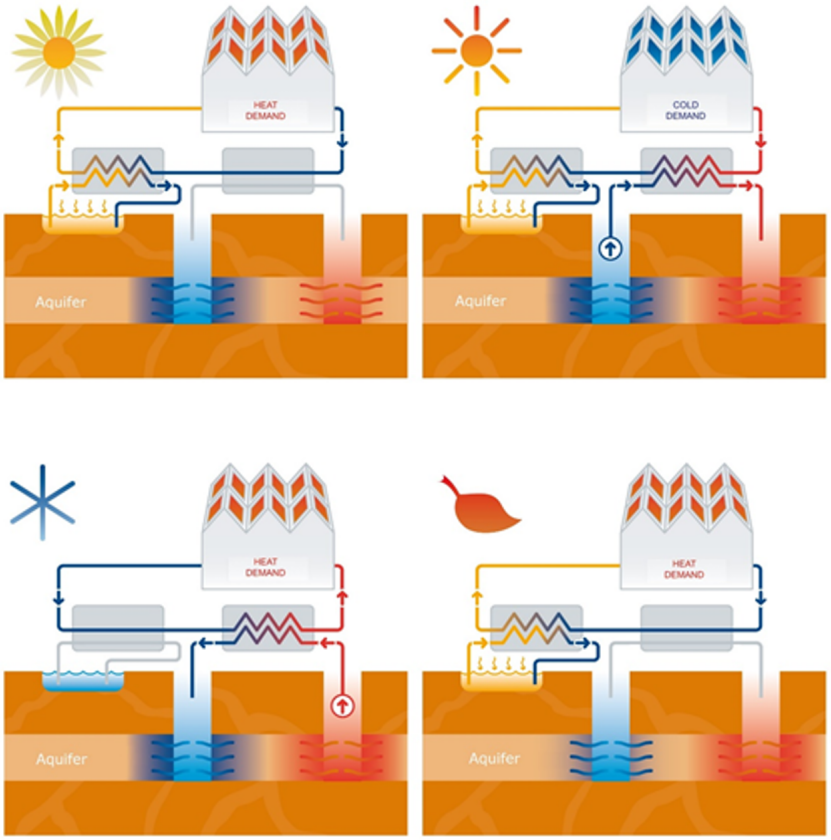

Figure 1.1: Simple representation of working principle of heat recovery from surface waters combined with an ATES system, the so-called ATES+ solution. During summer (upper right) heat from the surface waterbody is used to charge the hot well and optionally cold can be supplied. In winter (lower left), the stored heat is extracted from the hot well. In spring and autumn, heat can be supplied directly from the surface water. Figure retrieved from IF Technology bv (2017).

1.1. Motivation for this research

In the Netherlands, energy for the heating of the built environment is responsible for 40% of total energy consumption and by far the largest component in the national energy balance (de Jong, 2010). Furthermore, provided that worldwide about two-third of total energy is consumed in cities (United Nations, 2020), it is worthwile to conduct research towards sustainable energy sources in an urban context. This study focuses on recovery of heat with SWH in such an urban context: the largest city of the Netherlands, Amsterdam. Amsterdam is rich in surface waters. This provides a promising opportunity in which heat could be extracted from the city's many well known city canals.

This is not a new idea. Already in 1946, a proposal was made for the city of Amsterdam to explore the capacity of the Amsterdam canal system for the heating of buildings (Zanstra, Giesen en Sijmons architectenbureau, 1946). However, until date, no SWH systems have been realised in the city canal system, but merely in the larger waterways and lakes, such as the IJ and Sloterplas (Netwerk Aquathermie, 2020). Currently, the city of Amsterdam is possibly missing out on an unique opportunity where sustainable heat could be retrieved within the city's own highly urbanised borders. The main reason why SWH is still not developed in these types of waters is the lack of knowledge about the thermal effects and heating potential of SWH in smaller urban surface waters such as the city canal network. Although several studies in the Netherlands have already portrayed the thermal, hydrodynamic and ecological effects of SWH for other specific locations (Van Megchelen, 2017) (Aparicio Medrano, 2008) (Boderie and Troost, 2020), a three-dimensional modelling study in which several SWH system design configurations were varied and assessed for their thermal effects on the receiving surface water body, has not been carried out yet. This study is an attempt to provide insight into this knowledge gap, specifically for the urban city canal case.

Apart from the variation in design configurations, the Amsterdam canal system itself also forms a unique and complex water system in an open connection with larger water bodies such as the IJ and Amsterdam Rijnkanaal. This is in contrast with the earlier mentioned studies, which were merely elaborated in separate water bodies in which SWH effects were restricted to the boundaries of the respective surface water. It is this important aspect, together with the hyperlocality of the urban climate in the atmosperic boundary layer (Landsberg, 1981) (van der Hoeven and Wandl, 2013), that gives the city canal system its typical character with changing flow directions, varying bed levels, changing mixing patterns and changing microscale thermal stratification. Particularly these characteristics call for a three-dimensional heat model that is created in this study to provide insight into the thermal effects of SWH on a city canal as a first attempt.

1.2. Study objective and research questions

The objective of this study is to investigate the thermal effects of heat recovery from urban surface waters by SWH systems. The focus lies on a case study in the canals in the inner city of Amsterdam for which a heat model has been created validated with water temperature measurements. In line with this objective definition, it is translated into the following *central research question*:

What are the thermodynamic effects of Surface Water Heat (SWH) applications on a city canal?

1.2.1. Subquestions

To answer this rather broad research question, it is subdivided in several subquestions. Answering the subquestions ultimately leads to an overall insight in the thermodynamic behaviour of SWH systems in a complex city canal network. The subquestions read:

- **S1**: How are SWH systems applied in practice?
- **S2**: What kind of existing regulation and calculations related to the thermodynamic modification by SWH systems are currently used in the Netherlands?
- **S3**: Do the water temperature measurements indicate existence of thermal stratification in a city canal?
- **S4**: Can a 3D city canal model be developed that accurately models daily variations in water temperatures and thermal stratification?
- **S5**: Where is the cold water plume, discharged by SWH systems for heating, located in the water column?
- **S6**: Can the local heating demand for the case study situation be met, considering different distances between SWH intake and outfall and related interference and recirculation issues?

The first two subquestions, S1 and S2, relate to SWH design and provide insight in the practical application of SWH systems. This background information assists in construction of a representation of the SWH systems in the heat model. S3 relates to the existence of thermal stratification in a city canal, which is known to have a considerable effect on the behaviour of thermal discharges such as the cold water discharge by SWH (Jirka et al., 1996). By answering S4, a heat model for the city canal is created and validated with the water temperature measurements. The last two subquestions, S5 and S6, relate to the model outcomes and together provide insight in the main research question.

1.3. Research scope

Since this study is established in close collaboration with Waternet, the governmental body responsible for regulation of the Amsterdam surface waters, this research will form a first step in the assessment and granting of water permits for future SWH projects, based on knowledge of the surface water system. Although for the execution of these legal tasks, ecological effects might be equally or even more important for Waternet, the focus of this study is on thermodynamics and to a lesser extent, local hydrodyanmics. It was decided to exclude ecology in this preliminary research phase. The ecological effects of SWH systems have also been partially covered in previous studies by Van Megchelen (2017) and (Boderie and Troost, 2020). For further analysis of the effects on ecology, as well as economic and administrative analyses, it is strongly advised to elaborate within these study fields in follow-up studies.

1.4. Research approach and report outline

To obtain the described central objective, a theoretical, experimental and modelling approach is followed. The approach and outline for the remainder of this report can be described as follows:

- Chapter 2: Study towards SWH layout, settings and applications. The concept of extracting heat from surface waters is explained and an overview is provided of different settings in which SWH systems are currently implemented.
- Chapter 3: A description of the case study at the van Lennepkanaal in Amsterdam is provided. Additionally, in the second part of chapter 3, the water temperature measurement campaign is explained and results are evaluated. The water temperature measurements are utilized to provide insight in the thermal behaviour of city canals under the current scenario without SWH and they are used to validate the created heat model.
- Chapter 4: This chapter contains a study towards hydrodynamic processes related to intake and discharge of water by SHW systems. In the second part, the thermodynamic processes and heat fluxes at the interface between atmosphere and water surface are further explained.
- Chapter 5: Explanation of the setup of the three-dimensional surface water temperature model. The governing equations behind the chosen computational fluid dynamic (CFD) model, Delft3D, are explained. Data input choices such as typical meteorological conditions determining the model forcing and boundaries are clarified. Finally, the model is validated for different meteorological forcing combinations.
- Chapter 6: Presents an overview and thorough analysis of the modelled results under the chosen scenarios. This chapter also provides insight in thermal effects of different configurations of SWH systems.
- Chapter 7: Discussion
- Chapter 8: Conclusions and recommendations

2

Surface Water Heat systems in an urban district

Surface water heat (SWH) systems utilize surface waters to provide heat to buildings or to store surplus heat from buildings in the case of cooling. In this chapter, an overview of different system configurations and definitions in the field of SWH are further explained. Also an insight is provided into the setting, layout and current applicable law for SWH systems in the Netherlands.

2.1. The SWH concept and system configurations

In this report the abbreviated term SWH is used as an umbrella term for the concept of thermal energy extraction from surface waters. There are however many different possible configurations of SWH that can be categorized. For all types of SWH systems, the heat exchanger that exchanges heat or cold with the surface water is the central component. During the development of SWH over the last decades, several different techniques and configurations have evolved. According to Spitler and Mitchell (2016), SWH system configurations can be categorized in two ways:

- Open-loop or closed-loop. For open-loop systems, water is withdrawn from the surface water body, then passed through a heat exchanger, and finally returned to the surface water body. In closed-loop systems, the heat exchanger is submerged directly into the surface water and water is only circulated within the SWH system connected to the particular building.
- By the degree to which a heat pump is used. For some systems, heat or cold can be provided directly, without a heat pump in between. Other systems, provide all heat with a heat pump and some systems only partially, for example only in autumn or spring when demands are low. The systems can again be catagorized into the following subcategories:
  (a) Direct Surface Water Cooling (DSWC) systems: systems that extract cold from surface water without chillers or heat pumps. Often there are intermediate heat exchangers to seperate fouling-prone surface water from the building's internal heating system.
  (b) Surface Water Heat Pump (SWHP) systems: these systems use heat pumps or chillers to provide heating and/or cooling from the surface water. They can provide heating only, cooling only or a combination of heating and cooling.
  (c) Hybrid Surface Water Heat Pump (HSWHP) systems: these systems also use heat pumps or chillers for heating and/or cooling, but they can also process cold from the surface water directly.

Besides the categorization by Spitler and Mitchell (2016), there is also a third distinction that can be made. In strongly seasonal climates, SWH systems are combined with a storage system to store heat or cold and to use the stored thermal energy in accordance with the seasonal profile. In these systems, water, either heated or chilled by the surface water, is stored in a groundwater aquifer and it is used to regenerate the wells of an Aquifer Thermal Energy Storage (ATES) system. When an ATES is combined with SWH as regeneration technique, in literature these systems are sometimes referred to as ATES+ systems (Miltenburg et al., 2008).

2.2. SWH systems in the Netherlands

This study focusses on the situation in the Netherlands and more specifically the metropolitan area of Amsterdam, where ATES is currently an increasingly accepted technique due to the geohydrological suitability for ATES systems and the seasonality of the climate (Bloemendal et al., 2015). It can therefore also be expected that interest for the combination of ATES with SWH systems will grow in the Amsterdam surface waters. Furthermore, since a lot of the built environment in the Netherlands has a higher heating demand than cooling demand and national policies currently prescribe less dependance on natural gas for heating (Rijksoverheid, 2019), this study only considers the recovery of heat from surface waters during summertime. Following the categorizations described, for the Netherlands this would translate into a study primarily applicable to the ATES+ solution with the SWHP type of SWH.

2.2.1. A matching opportunity: Thermal energy and the replacement of quay walls in Amsterdam

The city of Amsterdam, the capital city of the Netherlands, is well-known for its many canals and open surface waters. Due to this abundance of surface water in the city centre, the city of Amsterdam also contains approximately 600 kilometres of quay walls and canal banks. In July this year, the municipality of Amsterdam reported in their preliminary assessment and research towards the city's key walls that possibly 200 kilometres of quay walls are currently in a poor state (Municipality of Amsterdam, 2019). The municipality forecasts that a large-scale renovation of the city's quay walls is required in the coming 20 years.

The surface waters in Amsterdam are managed by Waternet. Waternet is the public water utility of Amsterdam and surroundings. It is owned by the municipality of Amsterdam and the Regional Water Authority Amstel, Gooi and Vecht. The activities of Waternet comprise not only drinking water supply, but also wastewater collection and treatment, surface water management and control, flood protection and groundwater management. The broad and diverse scope of activities of Waternet makes this governmental company unique within the Netherlands.

Waternet has set internal goals with respect to reduction of greenhouse gas emissions. In 2020, Waternet has the ambition to operate fully climate neutral (Waternet, 2015). Thermal energy from surface water is potentially an important contributor in reaching these goals. In 2011, Waternet reported that SWH could contribute to a reduction of 35% CO2 equivalents emitted by their own activities (Van der Hoek, 2012). In 2018, lower numbers are presented, around 12% (van der Hoek et al., 2018). However, in both papers only the recovery of cooling energy from surface water is considered and the future planned projects in these evaluations are rather limited. Using the thermal energy in surface water for heat extraction and given that future renewable energy projects will develop rapidly due to present-day climate change awareness, these numbers could increase considerably.

The use of surface water as heating energy source is not a new technique. Already in 1946, a proposal was made for the city of Amsterdam to investigate the capacity of the Amsterdam canal system to heat new urban districts (Zanstra, Giesen en Sijmons architectenbureau, 1946). However, an investigation was never made because of an abundance of natural gas at that time (Miltenburg et al., 2008). Renewed interest for SWH came, at the start of the development and pilot years of Aquifer Thermal Energy Storage (ATES) in the Netherlands, roughly between 1985 and 2005 (Snijders, 2005). As part of ATES systems, SWH is commonly used as regeneration technique to balance out thermal inequalities between the hot and cold well. Several of these so-called ATES+ systems have been installed in the years that followed. Examples can be found at Paleiskwartier in Den Bosch (Aparicio Medrano et al., 2009), Hoog Dalem district in Gorinchem (Van Megchelen, 2017), Stadsgracht in Wageningen (IF Technology bv, 2019) and the Ouderkerkerplas in Amsterdam (Van der Hoek, 2012).

Combining the considerations above, a promising matching opportunity appears. While renovating and replacing deteriorated quay walls in Amsterdam city centre in the coming years, SWH systems could be installed synchronically that extract heat from surface water that can be used for heating of the surrounding buildings. This interesting case forms the starting point for this research.

2.2.2. SWH as part of heat networks

The ATES+ solution in combination with SWHP is generally realised or planned as part of local district heating grids (Falkoni et al., 2020) (Kyrou, 2019) (Gemeente Amsterdam, 2019). Also at European level, the EU has implemented the use of heat pumps sourced by renewable energy sources(RES) in future small scale thermal energy grids to achieve energy and climate targets for the years 2030 and 2050 (Sayegh et al., 2018). However, the EU did not account for large scale heat pump implementation, sourced by for example drinking water, sewage water and surface waters, in already existing district heating grids (Bach et al., 2016). Also on a larger scale, SWHP in combination with ATES could be applied to complement future heating demand.

In small-scale heating grids, one SWH installation can be combined with one or multiple ATES systems. An open-loop SWH system roughly consists of a heat exchanger, pump and an intake and outfall construction. Heat from the surface water transferred by the heat exchanger is transported through the neighbourhood's heating network to the ATES wells, where it is stored for the upcoming heating season. Generally, temperatures in heating networks sourced by renewables are low, between 12 and 20 °C. In this way, temperatures match with the temperature of the surface water and heat losses due to conduction to ambient ground are reduced(STOWA, 2017). Also heating networks with higher temperatures are possible with centralised heat pumps installed upgrading the temperature in the pipes of the network to a higher level. Heat stored and transported in the heat network is eventually supplied to the buildings by a combination of a heat exchanger and, for low temperature grids, also extra heat pumps. In practice, these installations connected to the buildings are often referred to as 'substations' or 'energystations'.

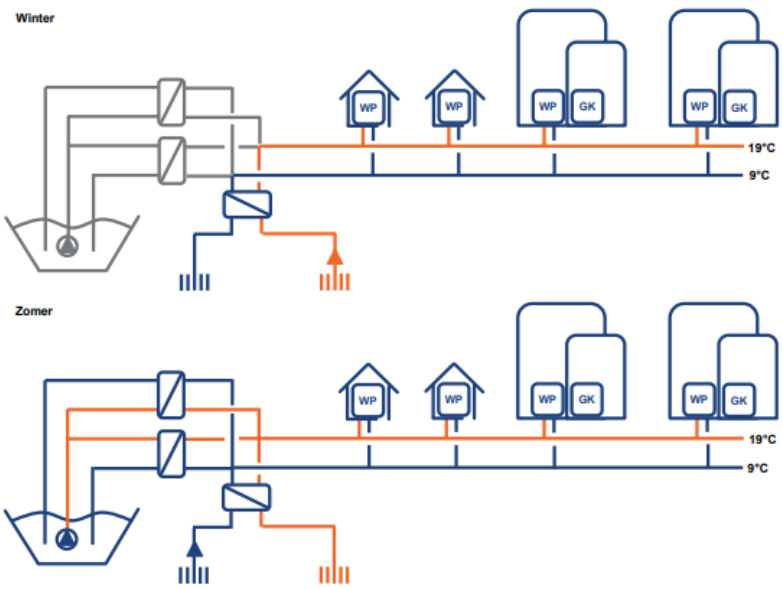

Figure 2.1: SWH installation as part of a low temperature heating network. Here, only one ATES is coupled to the heating network, but multiple ATES systems can be coupled. In the upper image the winter situation is displayed and in the lower image the situation during summer is represented. The 'WP' blocks are the in-building heat pumps and the 'GK' blocks represent additional heating systems running on natural gas. Figure retrieved from STOWA (2017).

In figure 2.1, two modes of a heating system with a SWH installation are presented, during winter and summer. In the winter, heat is extracted from the hot well of the ATES system and supplied to the heating network. Low temperature heat from the network is upgraded with the individual in-building heat exchangers and heat pumps to make sure that buildings can be heated according to their individual heating demand. In the summer season, the direction of flow in the ATES system changes and the cold well is recharged through a heat exchanger with heat from the surface water. Also, when surface water temperature is high enough, the heating network can be heated directly by the SWH installation. During summer or late spring, this direct supply of heat might still be necessary for the production of hot tap water or, in some cases, also space heating.

2.2.3. Layout of a SWH system

Most of the spatial or physical layout of a SWH system as part of a district heating network is invisible at ground level and located in the subsurface or built-in into uitility rooms, i.e. the system of heat network pipes, the ATES system, SWH heat exchangers, pumps and substations or energystations. For this study focussed on the waterside of SWH systems, the layout of a SWH system in the water body is most important. In practice, the system design is quite simple and often consists of two endings of pipelines, the intake and outfall. Radial intake screens are installed at the intake, see figure 2.2, to prevent the system, especially the heat exchanger, from clogging.

(a) Radial intake screen of SWH installation in city canal of Wageningen

(b) Example of layout of a SWH system seen from waterside, Houthavens, Amsterdam.

Figure 2.2: Layout of intake of a SWH system.

2.2.4. Dutch Law and Regulation on the effect of SWH

In current regulation on the effects of SWH on a respective water body, the Dutch Water Act is the most prevalent legal framework. The Dutch Water Act is the national regulatory elaboration of the European Water Framework Directive. From 2021 and on, the Dutch Water Act, and therefore the underlying Water Framework Directive, will dissolve into the Environment and Planning Act.

On European level, The Water Framework Directive (EWFD) prescribes that water and ecological quality of European surface waters is assessed based on a reference situation representing a 'good ecological potential'. A good ecological potential is defined as: "the state where the values of the relevant biological quality elements reflect, as far as possible, those associated with the closest comparable surface water body type, given the physical conditions which result from the artificial or heavily modified characteristics of the water body" (WFD Annex V 1.2.5). The translation of this requirement led to national applicable guidelines and criterions for different types of surface waters.

Regulation structure

The introduction of SWH systems in surface water bodies result in an anthropogenic change to the status of the surface water and therefore it needs to be assessed whether this change is compliant with drawn up criterions. In the Dutch national regulation, the hydro- and thermodynamic criterions have been derived from ecological indicators in accordance with the EWFD. In these national regulations, the overall surface water modification that open-loop SWH systems, used for heating, imply can be seperated in four legally distinctive environmental actions (Netwerk Aquathermie, Universiteit Utrecht, 2019):

1. Withdrawal of surface water
2. Thermal modification, in this case cooling of the surface water
3. Discharge of surface water
4. Possible discharge of substances for system cleaning

For actions 1 and 3 a water permit has to be granted by the competent authority depending on the size of withdrawal and discharge. For most of the surface waters in the metropolitan area of Amsterdam, depending whether the surface water is acknowledged as a national or local water body, this is the regional water board. The water board assesses the permit request based on their locally applicable regulation, the 'Waterschapskeur' and the Water Act. Small size water withdrawals and discharges only require notification of the authority. However, most SWH systems used for the heating of larger areas, exceed these non-permittable sizes.

For actions 2 and 4, the Environmental Management Act determines which governmental body is responsible for the effects of the modification on the environmental quality. In the Environmental Management Act also the so-called precautionary principle, meaning that the best available techniques need to be applied, and the stand still principle, implying that water quality may not deteriorate, are established (Netwerk Aquathermie, Universiteit Utrecht, 2019). For surface waters, the permittance for these actions is again executed with a water permit granted by the local water authority based on the Water Act, more specific regulations in the Water Decree and the locally applicable 'Waterschapskeur'.

Norms for water quality: directives and guidelines

For the assessment of the discharge of possible polluting substances, norms and maximum allowable concentrations in surface waters are required. These norms are established in water guidelines or directives. Norms can either be determined at European level, such as the Water Framework Directive (WFD), or at national level, for example the Water Quality and Monitoring Decree 2009. The WFD has a binding legal status for member states within the EU. In contrast to for example an Act or rules initiated by a governmental body in a Decree, the WFD is not directly applicable and states maintain autonomy to choose the form and methods to achieve the aimed result (Mostert, 2020). They first have to be transposed in binding national law. However, provisions within the directives or guidelines can become directly applicable if they:

1. are generally considered and accepted in a professional working field.
2. are practically workable
3. are specific and not too universal
4. are clear and not too ambiguous

The WFD gives the national authorities leeway to construct policies in cooperation with practice and for example in a development phase where effects and consequences of the chosen policy are not fully known. There is still freedom for common sense and shared responsibility between government and third parties, without pinning everything down in too restrictive laws and regulations. For thermal influence on surface waters, currently there is also one applicable national directive, 'Beoordelingssystematiek Warmtelozingen', initiated by the Commission Integral Watermanagement (CIW) in the Netherlands in 2004. This directive provides an assessment framework for the discharge of hot water to surface waters, for example water discharges originating from cooling installations of power plants. For SWH systems used for heating and resulting in cold water discharges, this directive is not directly applicable. According to Van Megchelen (2017), until 2017 no Dutch regulation or directives on cool water discharge were yet constructed. Van Megchelen (2017) also proposed to follow a methodology for the setup of a future cool water discharge assessment framework in line with the current CIW assessment framework for hot discharges. A brief summary of the current CIW guideline can be found in figure 2.3.

Current assessment framework for SWH system discharges

In the past years, with the increased attention for the energy transition in the Netherlands, the interest for SWH systems also grew, resulting in an exploration for a new assessment framework for cool water discharges by STOWA, the Dutch knowledge center of local waterboards. No official framework has been drafted until date, but a conceptual framework has been created by STOWA. In this new conceptual framework the methodology of the CIW guideline for hot discharges has indeed been incorporated as Van Megchelen (2017) proposed, see figure 2.5. In this conceptual assessment framework, the water temperature of a surface water body is not allowed to become less than 12 °C and the temperature difference with the background water temperature is not allowed to become more than 5 °C, both after fully mixing of the water. Whether these

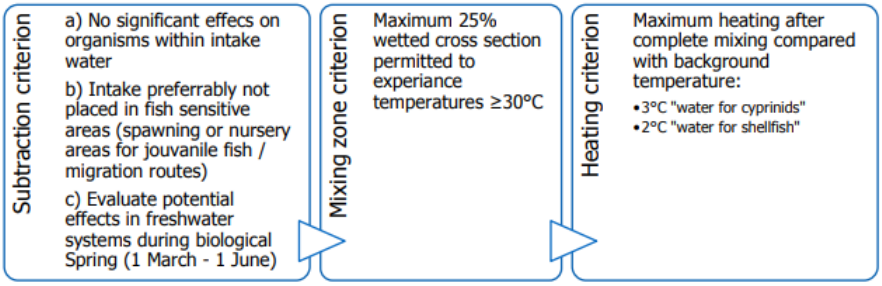

Figure 2.3: Summarized criterions in Dutch CIW guidelines for hot water discharge. Figure retrieved from Baptist et al. (2005)

norms are also applicable in situations where SWH systems would start recovering heat earlier in the season and the related cold water discharges also occur in spring and winter is not described. STOWA indicates that this still remains a knowledge gap (de Lange et al., 2017). However, larger temperature differences than 5 °C and lower absolute water temperatures than 12 °C may be allowed when:

1. they occur within mixing zone which is up to 10 % of the ecohydrological unit;

2. they occur only when background temperature is higher than 25 °C

3. they do not deteriorate the ecological state of the EWFD surface water body.

The conceptual framework is not yet published and therefore exact definitions of terms, such as mixing zone and ecohydrological unit, remain unclear. It is also not clear whether the spatial requirement of the mixing zone is defined volumetrically or in terms of wetted perimeter or surface area.

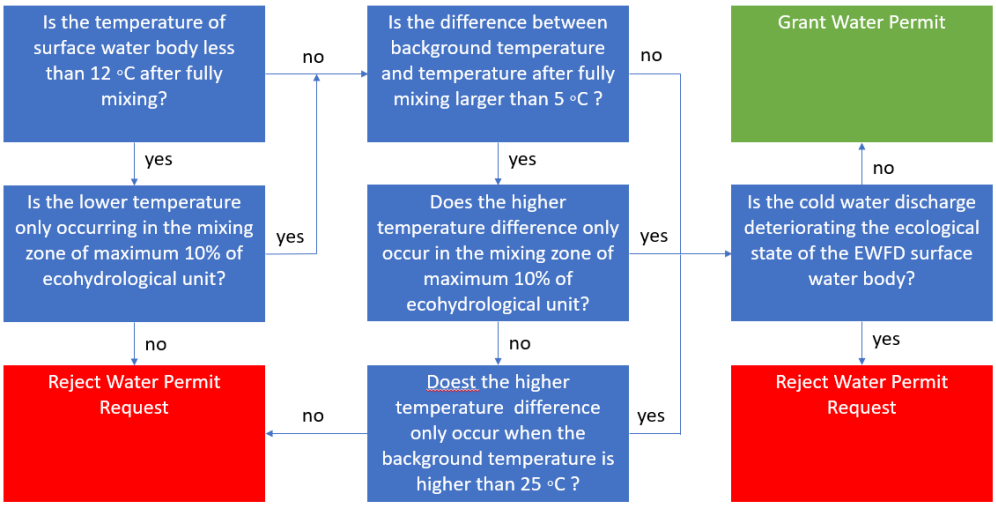

Figure 2.4: Steps from the conceptual assessment framework for cold water discharges in the Netherlands, figure based on Kruitwagen (2019).

2.2.5. Calculations for thermal effects of SWH systems

The local waterboard of Delfland, Hoogheemraadschap Delfland, currently has an assessment method and accompanying model for cold water discharges into surface waters (Ludikhuize et al., 2020). The calculations that form the foundation for this assessment method could possibly explain the chosen norms and limit values in the national conceptual framework by STOWA.

The assessment's foundation: the natural water temperature variations

Hoogheemraadschap Delfland collected measured water temperatures in different water bodies until 2013 and measured water temperatures wer plotted against corresponding day of the year. In this way, insight is gained in the temperature range of the water system during the year, see figure 2.5. The natural variations in daily average water temperatures were utilized to determine an allowable temperature difference with the ambient background water temperature. The underlying assumption is that the artificial change in water temperature induced by for example SWH systems is not allowed to surpass the natural temperature range on a structural basis. From the figure it follows that the range is approximately 10 °C around the average daily water temperatures (red line). It can also be observed that the temperature range is especially higher during spring and summer. This is also the time that SWH systems for heating are usually operable. Furthermore, it can be concluded that when lowering the water temperature with 5 °C with a SWH system for heating, this decrease in average temperature structurally shifts the natural water regime virtually with 1 up to 2 months, see the green line in figure 2.5. When the temperature modification by the SWH system is limited to only 3 °C, the temperature shift becomes half to one month, which is considered to fit reasonably in the natural variation pattern. Following the precautionary principle, considering that in late spring (May/June) a large shift of up to two months can be expected when cooling with 5 °C (see the green line from approximately day 140 up to 190), it is stated that a temperature difference above 5 °C is only allowed to occur restrictively. This is in line with the proposed conceptual national assessment framework on cold water discharges.

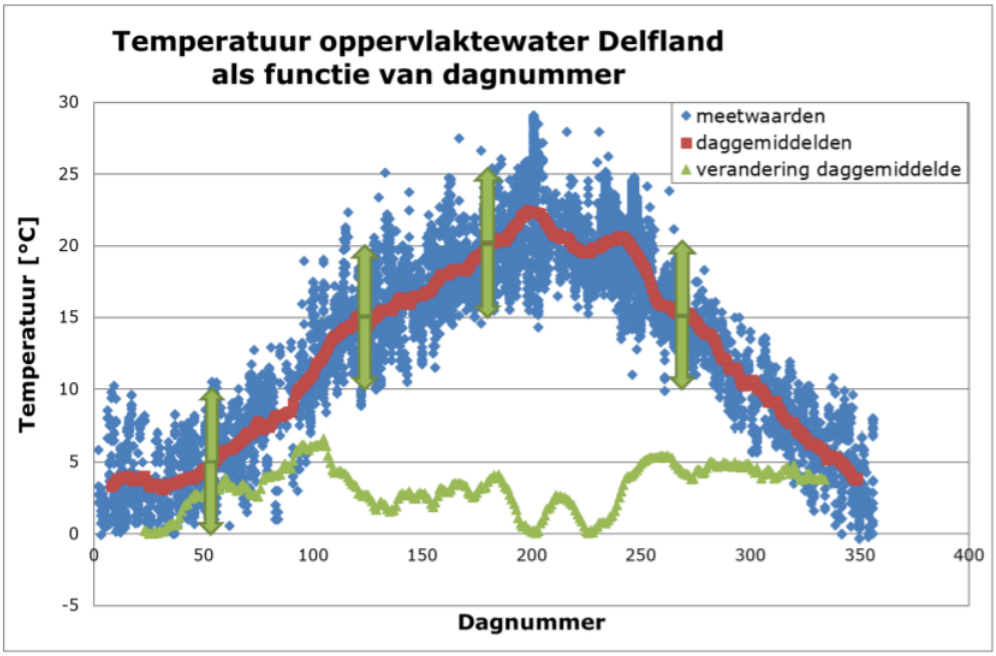

Figure 2.5: Measured natural temperature variations in Delfland until 2013 (blue dots). The red dotted line shows the average daily temperatures. The green dots show the absolute monthly gradient in daily water temperature for the red dots. Figure retrieved from Ludikhuize et al. (2020)

Assessment method Delfland: determining available capacity

When assessing a permit request for a SWH system, Hoogheemraadschap Delfland also performs a capacity check primarily based on recirculation and the mixing zone (Ludikhuize et al., 2020). The most important parameters in this assessment are the water surface area between the intake and outfall of the system, the distance to the edge of the mixing zone and the flow occurring in the respective water body.

Steady state model

Restoring the cooled water to natural water temperatures in a primarily stagnant water body occurs due to heat exchange with the atmosphere. The model that is used for the recirculation and mixing zone assessment of a SWH system is a Delta-T model. In this model the temperature differences with the natural water temperatures are modelled. This model was also described by (Aparicio Medrano, 2008) as a model under steady (time-independent) conditions. The model assumes a fully mixed discharge of cold water. It is assumed that

temperature difference is gradually decreasing from the source point discharge proportional to the natural logarithm. According to Delfland, approximately 90 % of the time their inland waters are primarily stagnant and the other 10 % water is moved by pumping stations in the area. This flow property is captured in the velocity factor of the Delta-T equation. The equations of the Delta-T model read:

$$\Delta T(x) = \Delta T_{\max} * e^{\frac{-(K \cdot x)}{(v * h * \rho_{\text{water}} * C_{\text{water}})}} \tag{2.1}$$

$$v = \frac{Q_{\text{tot}}}{b.h} \tag{2.2}$$

which is a solution of the first order differential equation:

$$\frac{\partial u_x H}{\partial x} = K(\Delta T) \tag{2.3}$$

where $\Delta T(x)$ is the temperature difference (°C) dependent on the distance from outfall point, $\Delta T_{\max}$ is the maximum temperature difference (°C) at the outfall, K is the heat exchange coefficient with atmosphere (W/m^2/°C) , v is the surface water velocity (m/s), Q_{tot} is the total discharge (m^2/s) and h and b are the depth and width of the surface water body respectively.

The Hoogheemraadschap Delfland also coupled criterions for mixing zone and recirculation. For more information on these criterions the reader is referred to appendix A of this report.

3

Case study: SWH energy for a heating district in Amsterdam

Energy from surface waters forms an alternative energy source for the heating of districts in urban areas. In order to get insight in the effects of SWE on surface water, and the effect on a city canal system specifically, a case study location has been chosen in the canals of Amsterdam. Provided that a case study is by definition location-specific, it is also important to gain insight in the properties of the local water system to be able to qualify the forthcoming results. Therefore, a short descriptive evaluation of the entire canal system of Amsterdam is provided and temperature measurements have been elaborated in the case study area and direct surroundings.

3.1. The hydrodynamics of the Amsterdam canal system

3.1.1. Hydrodynamic situation under normal weather conditions

Under normal circumstances, at a normal water level in the city canals and IJ, surplus water from the city and polders upstream of the city flows under gravity through the city canals to the IJ river and Noordzeekanaal. When the water eventually reaches the IJmuiden sea lock, it is discharged into the North Sea, either under gravity through the flushing sluice or it is discharged by the pumping stations in IJmuiden (gemaal IJmuiden and spuigemaal IJmuiden). In this first mode of the water system, discharges in the city canals are directed towards the mouths of the canal system, see figure 3.1. This is the prevailing and most frequently occurring flow pattern in the city canals.

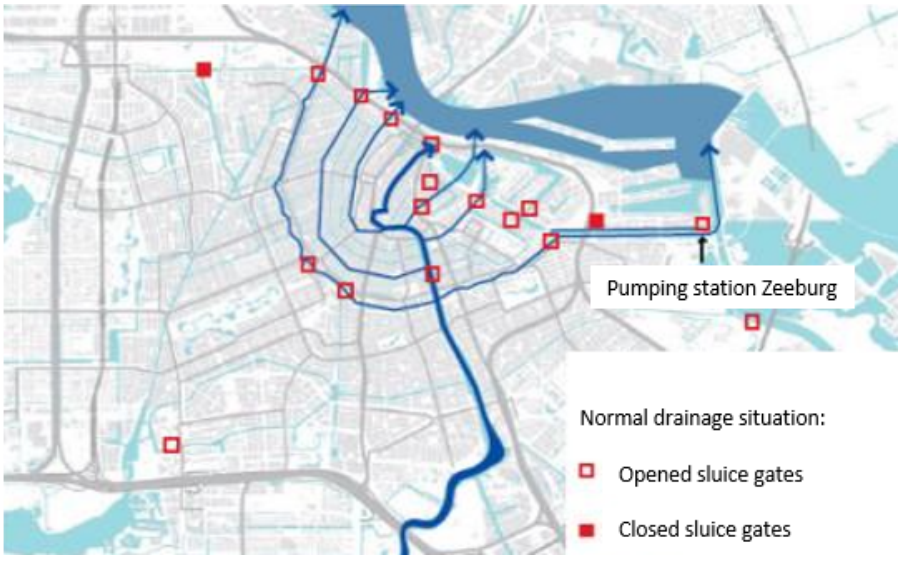

Figure 3.1: Drainage of Amsterdam canal system under normal conditions. Figure retrieved from Noord Hollands Archief (2011).

The situation changes when the water supply to the IJ becomes larger than the discharge capacity in IJmuiden. This situation generally occurs at high tide in the North Sea, when the flushing sluice of IJmuiden is closed. Less water can be discharged into the sea and water coming from upstream is accumulating. In this second mode of the city canal system, especially the water supply of the upstream Amsterdam Rijnkanaal, which discharges significant amounts of water from the Rijn into the IJ, is of importance. Since the discharge of the Amsterdam Rijnkanaal can fluctuate significantly over time, an increase in discharge of the Amsterdam Rijnkanaal combined with high tide in the North Sea can give rise to elevation of water levels in the IJ (Nelen en Schuurmans, 2005). As a result, water from the IJ flows into the city canals and the flow direction in the city canals changes in opposite direction. Therefore, the situation in the Amsterdam city canals is sometimes also called 'pseudo tide', referring to the fluctuations in flow direction.

3.1.2. Hydrodynamic situation under extreme weather conditions

Besides these two main system modes, there are roughly two other situations that could take place in the city canal system. Both these modes are related to more extreme conditions. The first one occurs when the water levels in the Noordzeekanaal and IJ become too high and there is a risk of flooding, especially in the polder areas far upstream of the city. In this case, the sluice gates at the canal mouths are closed to prevent flooding and the canal water is disconnected from the Amsterdam Rijnkanaal, IJ and Noordzeekanaal system. In this situation, the tidal flow pattern is no longer prevailing in the city canals. Until the high water levels are returned to their normal levels, surplus water from the canals and upstream polders can be drained by the Zeeburg pumping station to the IJmeer, northeast of the city. The second situation could occur in a long period of drought or when oxygen levels in the canals are low. In these cases, it might be needed to flush the canals with fresh water. In this situation, the Zeeburg pumping station can also introduce fresh water from the IJmeer into the city canal system. Until 2010, it was common practice to flush the city canals with the Zeeburg pumping station a few times per week. Nowadays, flushing activities with fresh water from the IJmeer are only executed in case of water quality problems.

3.1.3. Incorporation of hydrodynamics in the surface water model

In the Delft3D model presented in this report, the hydrodynamics of the year 2015 have been used. Although hydrodynamics between years can fluctuate, it was chosen to limit the analysis on the effects of SWH to a time scale of half a year in line with the scope of this research. The lateral discharge values adopted at the boundaries of the model, have been reproduced from earlier research towards the Noorzeekanaal, IJ and Amsterdam Rijnkanaal hydrodynamics by Deltares (Verbruggen et al., 2019). In this research led by Deltares, the two most important hydrodynamic features; the flow regime through the Amsterdam Rijnkanaal and the flushing and pumping data of IJmuiden lock complex, were based on discharge measurements by Rijkswaterstaat at Weesp and day reports generated by Rijkswaterstaat of the pumping stations in the locks respectively, both in the year 2015. The lock day reports contain parameters such as:

- Flushing time
- The amount of deployed pumps and flushing chambers (in Dutch: spuikokers)
- The total discharged water volume within the given flushing time
- The measured water slope over the different installations

Furthermore, since the study by Deltares was originally conducted to model salt intrusion at the locks in IJmuiden, the inland discharges induced by the passing of ships are also incorporated in the model. As described in the research, there is a preference for ship passing and operation of the locks at high tide, leading to a net inland discharge from the North Sea into the Noordzeekanaal. For more information on the hydrodynamics and the choices that were made for the boundary conditions of the Delft3D model, the reader is referred to section 5.3 of this report.

3.2. The case study location: Van Lennepkanaal in Amsterdam

The location that will form the basis for the case study is the Van Lennepkanaal in Amsterdam, see figure 3.2. At this location, a citizen' initiative has led to the foundation of an energy cooperation for the Wilhelmina Gasthuis district, an area with approximately 1440 building equivalents. The energy cooperation, which is called Ketelhuis WG, has the goal to lead the energy transition towards renewable and sustainable energy sources for this particular district. Guiding principles and requirements are that future solutions are affordable, comfortable, cost-effective and decided upon by mutual agreement among the inhabitants. In the exploratory research, performed by consultanty agencies Tauw and Atrivé, a SWH installation similar to the situation described in section 2.2.1 turned out to be most promising for the supply of renewable heat (Ketelhuis WG, 2019). In this proposal, a SWH heat exchanger in the Van Lennepkanaal is combined with multiple ATES systems in a centralised heating network supplying heat to the district for hot tap water and space heating.

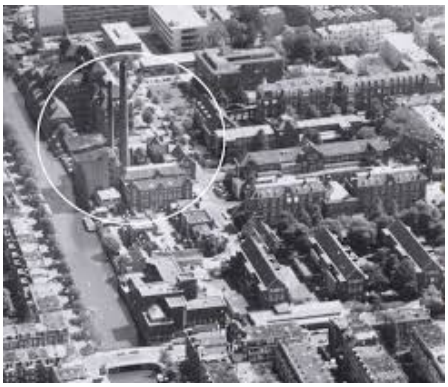

(a) The old ketelhuis (English: boiler room) at the Van Lennepkanaal (in 1973). Heat was provided to the Wilhelmina Gasthuis district by burning coal that was transported over the water. The building was demolished in 1983. (Source: beeldbank Amsterdam).

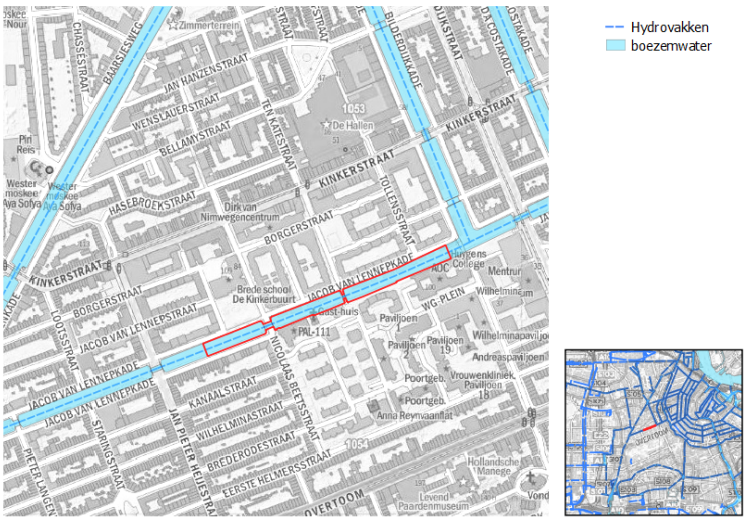

(b) Map of the Van Lennepkanaal and its location.

Figure 3.2: The van Lennepkanaal, canal along the Wilhemina Gasthuis district.

3.3. Heat demand in the Wilhelmina Gasthuis district

The Wilhelmina Gasthuis district exists of 2500 building units, for the largest part organized in large apartment buildings, with a wide spread in year of construction, varying from 1884 up to 2011 (Kadaster, 2020). This large construction year variety implies large insulation quality differences and therefore it provides a heterogenous picture of heat demand for the buildings in this area, differing . Each building has its own specific

heat demand and needs its own specific renovation plan to become suitable for heating by a heat network. A survey under local inhabitants of the neighbourhood in which the inhabitants kept track of their own energy use, combined with known key figures for energy use in the building environment, has led to a first estimation of the total heat demand in the area. The overall outcomes and applied heat demand characteristics of the Wilhelmina Gasthuis district are summarized in table 3.1.

District specific data		
Housing equivalents	1,443	#
Number of buildings	29	#
Total gross floor area	100,471	m^2
Current heat energy density range	58 - 266	kWh/m^2
70 Celsius ready heat energy density range	33 - 70	kWh/m^s
Total current yearly heat demand + 10% uncertainty/pipe heat loss	40,981	GJ
Total yearly heat demand in case of a 70 °C heat network + 15% uncertainty/pipe heat loss	29,301	GJ
Assumed overall Coefficient of Performance (COP) [16 to 70 Celsius]	3.0	[-]
Required current heat demand from surface waters	27,320	GJ
Required 70 Celsius heat demand from surface waters	19,534	GJ
Heat energy density for hot water	20	kWh/m^2
Total heat demand for hot water	7,234	GJ

Table 3.1: Heat demand data for the Wilhelmina Gasthuis district.

The above described total yearly heat demand in case of a 70 °C heat network is an ambition of the Ketelhuis WG. By insulating the building envelopes in the near future, dwellings in the district save energy and a lower heating water temperature can be supplied by the heating network. With lower delivering water temperatures the heat pumps within the entire system will also work more efficiently.

3.4. SWH system design

The next step is to translate the district heat demand into a open-loop SWH system design that is able to meet the specified heat demand. In the design of an open-loop SWH system, there are several key design choices together determining the eventual influence on the connected surface water body. Examples of such parameters are:

- The maximum ΔT or maximum temperature difference for heat extraction through the heat exchanger
- The minimum allowable modified surface water temperature at the outfall
- The water temperature when the SWH system starts working
- The aimed number of days that the system is operable
- The flow/discharge through the system
- The distance between intake and outfall
- Size of the intake and outfall and chosen structures
- Vertical position of intake and outfall in the surface water body

These choices are not to be taken independently and they should be approached as interrelated. For the van Lennepkanaal case considered in this report, choices for the SWH design were made representing a possible system installation in the future. Also, for some scenarios that will be discussed in chapter 6, variation in design choices were modelled by applying two different systems. The chosen properties of both systems are summarized in table 3.2.

System design parameters	system 1	system 2	
Minimum water temperature for operation	16	19.5	°C
Number of operable days	97	72	days
Required heating power of heat exchanger	3539	4767	kW
Maximum ΔT through heat exchanger	5	7.5	°C
Minimum water temperature at outfall	12	12	°C
Discharge through the system	610	547	m^3/h
Maximal distance between inlet and outfall	350	350	m
Average modelled water temperature during operation	20	20.5	°C
Applied heat transfer coefficient (k) of heat exchanger	2400	2400	W/m2K
Calculated average Log Mean Temperature Difference (LMTD)	5.4	4.7	°C
Indication of heat exchanging surface area	270	420	m^2

Table 3.2: System design parameters for both modelled systems in Van Lennepkanaal.

3.4.1. Creating SWH time series for discharge and heat extraction

Based on the presented design decisions, time series were created describing the hourly discharge and temperature difference ΔT through the heat exchanger of the SWH system. The result of the created time series is visualized in figure 3.3. On average, the extracted heat in the heat exchanger was equivalent to the cooling of the surface water with a ΔT of -5.0 °C. However, some fluctuation can be observed. This fluctuation is partially caused by a lower cooling rate at a surface water temperature of 16 °C to 17 °C, since the canal is not allowed to be cooled beneath 12 °C by human intervention.

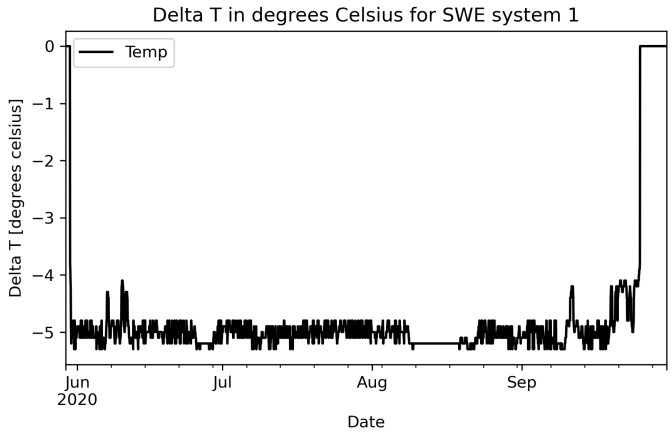

Figure 3.3: Graph of time series for ΔT for SWH system 1 with an average ΔT of 5.0 °C

Another reason for the fluctuation in ΔT is the method used to compute the cooling of the surface water. Water temperatures through the heat exchanger were computed by a combination of two heat exchanger calculation methods: the Log Mean Temperature Difference (LMTD) method and Number of Transferring Units (NTU) method. For the computation of water temperatures at the outlet of the heat exchanger, 7 operational levels were determined, each for an incoming surface water temperature increment of 1.0 °C, thus from 16 °C and onwards. These 7 levels were needed to mimic the different modes of a real SWH system, where ΔT can be regulated by adjusting the heat capacity rate at the system side of the heat exchanger, i.e. the flow at the system side. Regulation at the system side is necessary, since the size of the heat exchanger or the heat exchanging area (m^2) is designed for one particular combination of flows on the surface water side and system side of the heat exchanger. Since the 7 pumping levels were determined for an interval in surface water temperature of 1.0 °C, there is still some leeway for the ΔT to fluctuate within that interval. This explains the small variation (between -4.7 °C and -5.3 °C) in ΔT in the time series in figure 3.3. Acknowledging that this variation is primarily caused by the chosen way of modelling of the SWH system and not based on for example real data, it is assumed that these time series represent the heat exchanger functioning within the surface water system sufficiently. In reality, it could be possible to design a system that maintains a ΔT of

−5.0 °C perfectly with frequency controlled pumping for example, but even then, the system would still need time to react to changes in surface water temperature in the canal. In this case, this would still lead to some temporarily variation in ΔT.

Similar time series were created for system 2, but with a higher ΔT around −7.5 °C. For the second system, the ΔT was given some leeway at surface water temperatures higher than 23.0 °C, leading to higher ΔT values, especially during the heat wave in August 2020. This design and modelling choice was made to evaluate the thermal effects of a more flexible system which is able to extract more heat during high surface water temperatures. Also from an ecological point of view, this system choice could be interesting in fighting eutrophication and the development of 'blue-green algae', which both accelerate at high water temperatures above 25 °C (Nazari-Sharabian et al., 2018).

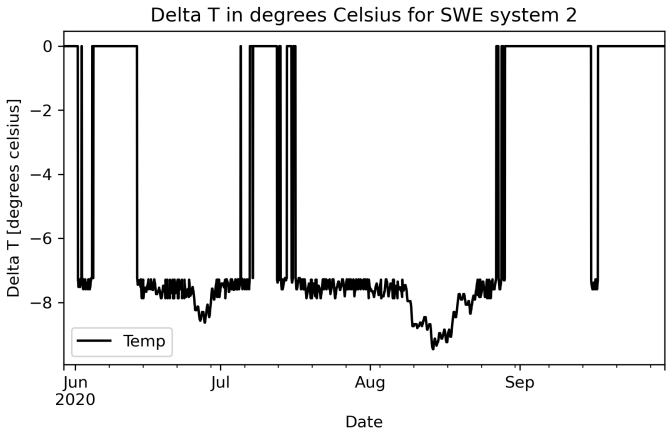

Figure 3.4: Graph of time series for ΔT for SWH system 2 with an average ΔT of −7.5 °C

3.5. Water temperature measurements in the city canals

3.5.1. The measurement setup

At 17 locations in the Amsterdam canal system, water temperature measurements were executed from the 9th of June till 4th of November, see figure 3.6. For each measurement location, water temperatures at different depths in the water column were measured with multiple HOBO Pendant MX water temperature data loggers with a accuracy of 0.5 °C (HOBO, 2019), see figure 3.5 for a schematisation of the equipment setup.

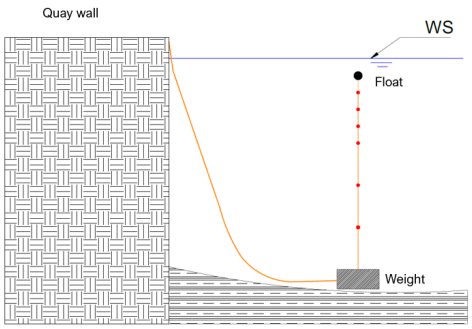

(a) Schematisation of the measurement equipment.

(b) HOBO Pendant MX water temperature logger.

Figure 3.5: Setup of the measurement equipment

Additionally, for each of the 17 measurement locations, light intensity (lux) was measured at the highest position in the water column. During the deployment of the measurement equipment, also measurements were performed with a Secchi disk as an indication for the degree of turbidity at each location. Both these optical factors could be of use in a further analysis towards the influence of incident sunlight and eventual

studies towards the influence of shading on water temperature. In the end, only the Secchi depth measurements have been used in the modelling of this study in order to determine the vertical spreading of incoming solar radiation in the water, see section 4.4.1.

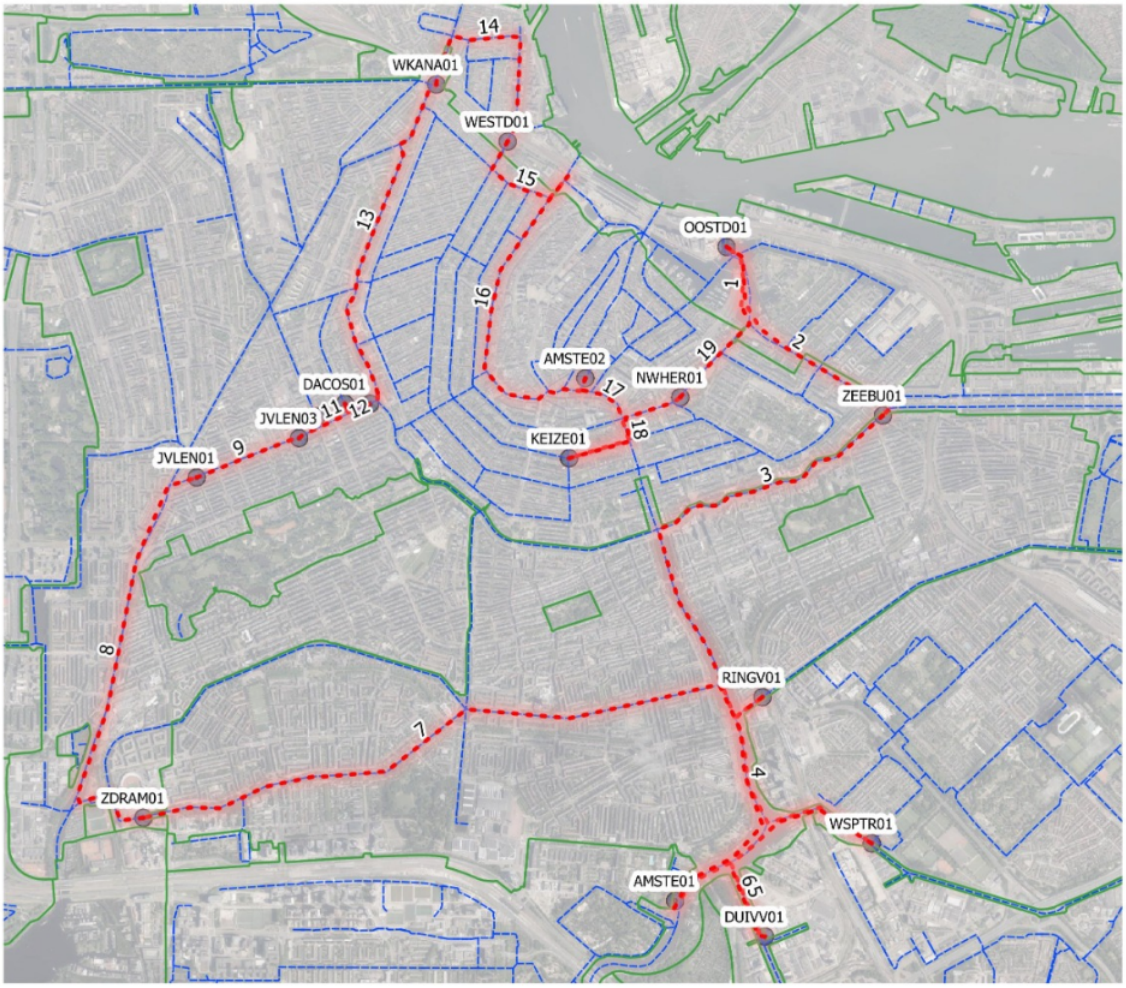

Figure 3.6: Water temperature sensor locations (red points) in Amsterdam city canals.

Generally, measurements were taken at standard depths in relation to the local surface water level at the time of deployment of the equipment. These depths were approximately -0.2 m, -0.4 m, -0.6 m, -1.0 m and -2.0 m and an additional measurement at the bottom of the canal depending on the local water depth. The general water level in the canals is regulated by Waternet at -0.4 m NAP and can be assumed to be almost constant. Furthermore, since the largest part of the canal area has a bed level in between 2 and 4 metres, this resulted in 5 or 6 water temperature measurements for each location. The idea behind measuring temperatures at different depths in the canal is to get insight in the existence and degree of thermal stratification in the canals.

The temperature data loggers were mounted to a steel cable with an anchor and a float at both cable ends, see figure 3.7. In this way, the cable was able to maintain its vertical position in the water column and the measurements were easy to be deployed and removed during the measurement campaign. The reading out and cleaning of the measurement equipment was executed periodically and eventual damages were fixed.

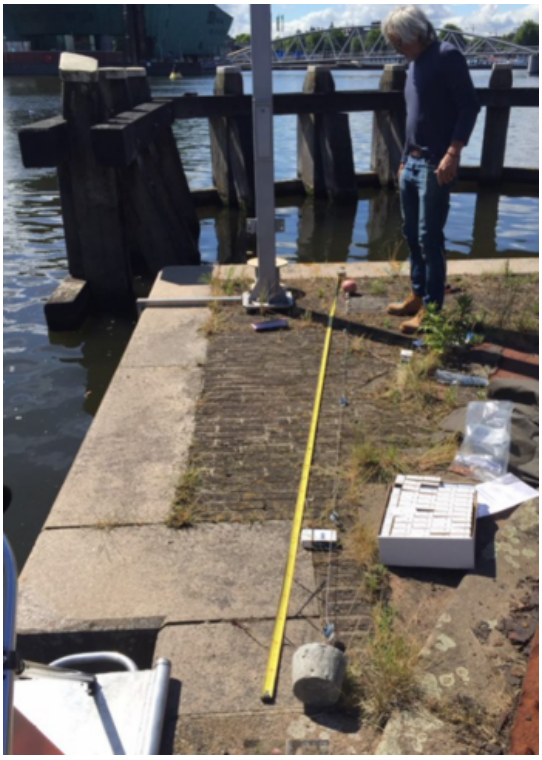

(a) Installation of the measurement equipment: the mounting of the sensors to the steel cable.

(b) Reading the measurements after two months of water temperature logging. A considerable amount of algae deposition and attachment of small shellfish was observed.

Figure 3.7: An impression of the measurement campaign.

4

Physical processes for surface water heat extraction

In order to be able to capture thermal energy from surface water efficiently and to determine the capacity of SWH, it is wise to study the processes behind the heating of surface water and the source of this energy; sunlight. In this chapter the thermal processes occurring in a water body are described. Firstly, the hydrodynamic processes are described and in the second part of this chapter the different factors in the heat balance, such as the net solar radiation, net atmospheric radiation, sensible heat flux and the latent heat flux are further explained.

4.1. Hydrodynamic processes

When assessing the impact of SWH systems on a surface water body, there are a bunch of hydrodynamic transport processes that govern the eventual outcome generated by the three-dimensional modelling. A list of definitions with most important involved processes was presented by Baptist et al. (2005) based on Fischer et al. (2013) and gives a rough overview of the hydrodynamic mixing processes that come into play. The list with definitions reads:

1. *Advection.* Transport by an imposed current.
2. *Diffusion (molecular).* The scattering of particles by random molecular motions.
3. *Diffusion (turbulent).* The scattering of particles by turbulent motion, considered rougly analogous to molecular diffusion, but with "eddy" diffusion coefficients, which are much larger than molecular diffusion coefficients and not of equal size in all directions.
4. *Shear.* The advection of fluid at different velocities at different positions; this may be the simple normal velocity profile for a turbulent flow where the water flows faster with increasing elevation from the bed; or shear may be a result of changes in both magnitude and direction of the velocity vector in complex flows such as in estuaries or coastal waters. Furthermore, shear also develops in the upper layers of surface waters because of the impact of wind on the water surface.
5. *Dispersion.* The scattering of particles or a cloud of contaminants by the combined effect of shear and transverse diffusion.
6. *Mixing.* Diffusion or dispersion as described above; turbulent diffusion in buoyant jets and plumes; any process which causes one parcel of water to be mingled with or diluted by another.

A state in which only one of these hydrodynamic processes is completely determining the model results is not existent in the real world. For real streams or open channels, the hydrodynamics are always a result of a heterogenous and continuously changing combination of the processes described above. Their magnitude and mutual proportions depend on, for example, channel or surface water body geometry, local meteorology, water temperature, salinity and upstream and downstream flow conditions. In the following sections the modelling approach to capture these processes and their dependencies in a Delft3D model are further clarified.

4.2. Modelling a SWH system: density driven flow and negatively buoyant jets

An open-loop SWH system, used for district heating, withdraws water, cools the water by extracting heat and then discharges the same water into the surface water body. When water is cooled, the temperature dependent density of the water increases. In other words, the density changes due to the induced temperature changes by the SWH system. This has important implications for the behaviour of the system' surrounding hydrodynamics.

4.2.1. Equation of state

When water is assumed to be incompressible ($\partial\rho/\partial p = 0$) and assuming that the density of the water is not increased by adding substances or sediment, the water temperature and salinity dominate the change in water density following a so-called equation of state, in the modelling of this thesis the UNESCO formulation is used (Joint Panel on Oceanographic Tables and Centre interuniversitaire d'études européennes and International Council of Scientific Unions. Scientific Committee on Oceanic Research and International Association for the Physical Sciences of the Ocean, 1981):

$$\rho = \rho_0 + As + Bs^{3/2} + Cs^2 \tag{4.1}$$

Where:

$$\begin{aligned}
\rho_0 =& 999.842594 + 6.793952\times10^{-2}T - 9.095290\times10^{-3}T^2 + \\
&+ 1.001685\times10^{-4}T^3 - 1.120083\times10^{-6}T^4 + 6.536332\times10^{-9}T^5 \\
A =& 8.24493\times10^{-1} - 4.0899\times10^{-3}T + 7.643\times10^{-5}T^2 + \\
&- 8.2467\times10^{-7}T^3 + 5.3875\times10^{-9}T^4 \\
B =& -5.72466\times10^{-3} + 1.0227\times10^{-4}T - 1.6546\times10^{-6}T^2 \\
C =& 4.8314\times10^{-4}
\end{aligned} \tag{4.2}$$

with salinity s in [ppt] and the water temperature T in [°C].

It is assumed that no chemicals are added during operation and the salinity of the surface water is therefore not adjusted by the SWH system. This is a reasonable assumption since in practice to prevent a heat exchanger from bio-fouling, in-situ generation of chlorine through electrochlorination, chemicals consisting of only hydrocarbons and physical treatment such as flushing and UV radiation are available techniques **??**. These techniques have no immediate effect on salt concentration. From the equation of state, it follows that in this case only the temperature difference through the SWH heat exchanger has an influence on the density of the discharged water. In other words, since colder water has a higher density, the discharge of the SWH after cooling results in a downward or negative buoyancy force that induces a density driven flow.

However, buoyancy is not the only important factor. Besides the negative buoyancy, the SWH outfall also introduces a local increase in momentum depending on the design of the outfall and velocities at the mouth of the outfall construction. Thus, the overall hydrodynamic effect of outfalls, such as found in standard open-loop heating SWH systems, can be summarized as a combination of introduced local momentum and buoyancy effects due to temperature differences. It therefore behaves either as a negatively buoyant jet or, depending on its dimensions and magnitude, the discharged water at the outfall becomes a negatively buoyant plume, as referred to in literature (Baptist et al., 2005) (Addad et al., 2004) and further described in sections 4.2.2 and 6.4.1.

The SWH intake, either installed upstream or downstream, also has an influence on the hydrodynamics and the temperature distribution of the receiving water body. By attracting water, the intake can possibly give rise to recirculation problems. However, generally spoken, the hydrodynamical impact of an intake is less than the impact originated by outfalls, provided that the intake is designed well and is able to let the water in smoothly. It was therefore chosen to give more attention to the hydrodynamics around the outfall of a SWH system in this chapter.

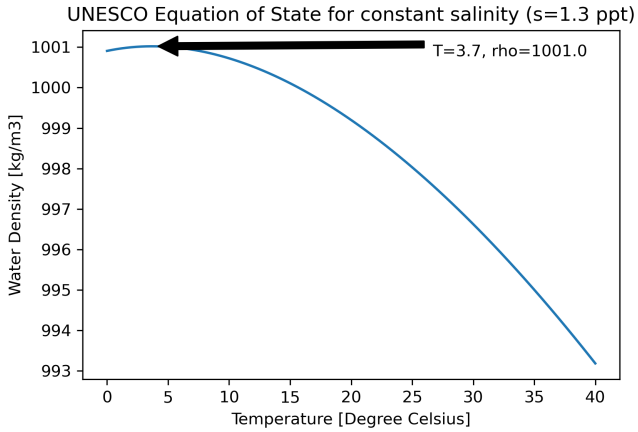

Figure 4.1: Plot of UNESCO equation of state for water and seawater at a constant salinity. The chosen salinity of 1.3 ppt (parts per thousand) is based on average salinity values measured in the Amsterdam city canals (Source: Parool (2011)). A maximum water density is found at 3.7 °C, which is lower than the fresh water temperature of max density (= 4 °C) . This can be accounted to the brackish nature of the city canal water.

4.2.2. Negatively buoyant jets

For positively buoyant jets, a lot of research has been performed in the past. Mostly, because positively buoyant jets are researched for the assessment of cooling water discharges by power plants which have been applied widely. For negatively buoyant jets, where water with a higher density is discharged, less research has been performed until now. However, lots of the characteristics, definitions and processes are the same for both situations.

When considering jets and plumes, there are a few useful definitions that need clarification. In literature, an outfall behaves like a jet when the hydrodynamics around the outfall are dominated by the momentum introduced by the outfall. At further distances from the jet, buoyancy forces start to dominate and the behaviour changes towards a plume-like situation, see figure 4.2.

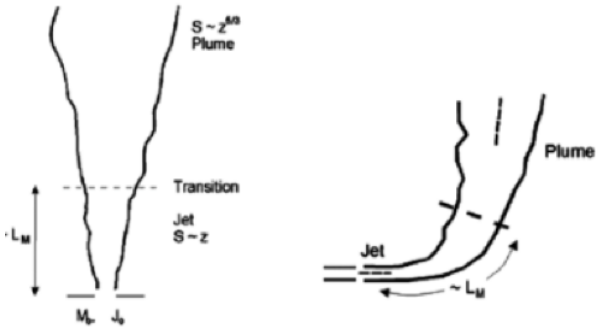

Figure 4.2: Jet to plume transition length scale L_M for a single jet. This length scale allows for a distinction between jet like and plume like behavior. The left image represents a jet with free outflow and the right image a situation with ambient flow. Figure retrieved from Jirka et al. (1996).

The mutual interaction between outfall flow from the jet or plume and the ambient flow is spatially classified in terms of near field and far field behaviour. The distinction between near and far field can be described as:

1. *Near field*: Advection and diffusion are governed by the characteristics of the incoming jet or plume.
2. *Far field*: Advection and diffusion are governed by the properties of the ambient flow.
3. *Mid field*: Transition between near field and far field behaviour. Here, processes like buoyant spreading are dominating.

4.2.3. Jet length scales

As also indicated by figure 4.2, a jet to plume transition length scale can be determined for a particular outfall. Within this length scale, the momentum introduced by the outfall is larger than the buoyancy flux. The flow is then characterised as a jet. Beyond this length scale, buoyancy is the dominant process. To determine the size of the jet to plume transition length scale, a specific momentum flux (eq. 6.3) and buoyancy flux (eq. (6.4) are calculated based on general outfall specifics (Baptist et al., 2005):

$$M = \frac{Q^2}{A} \tag{4.3}$$

$$B = gQ\frac{\Delta\rho}{\rho} \tag{4.4}$$

Where Q is the discharge or volume flux released by the SWH jet (m^3/s), A is the cross-sectional area (m^2), g is the gravitational constant (= 9.81 m/s^2) and $\Delta\rho$ is the difference in density causing the buoyancy flux.

With the momentum and buoyancy flux it is possible to define a jet to plume transition length scale with (Fisher et al., 1979):

$$L_M = \frac{M^{3/4}}{B^{1/2}} \tag{4.5}$$

Or when there is a cross-flow with velocity u_a, the progression of the jet can be expressed in a cross-flow length scale:

$$L_m = \frac{M^{1/2}}{u_a} \tag{4.6}$$

and for buoyancy governed plumes:

$$L_b = \frac{B}{u_a^3} \tag{4.7}$$

4.3. Mixing processes

Sudden velocity changes imposed by jets or plumes, lead to the formation of shear stresses. In other words, a turbulent flow develops. Further away from the outfall, the width of the high turbulence zone increases in the flow direction and the turbulence intensity decreases by a process called 'entrainment'. Less turbulent fluid is entrapped, see figure 4.3, and the shear stresses are transferred by the formation of eddies. Fluid momentum, but also dissolved concentrations (e.g. salt or contaminants) or temperature differences induced by the outfall, are diffused until finally an equilibrium with the ambient fluid is reached. This is the main mixing process for turbulent jets. This section qualitatively describes the different configurations in which these mixing processes occur in the near and far field, focused on negatively buoyant jets installed near walls, the SWH situation in a city canal.

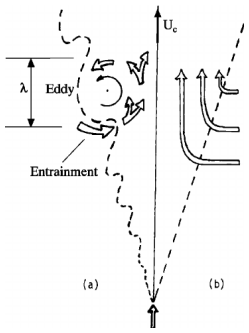

Figure 4.3: Entrainment of ambient fluid by a turbulent jet. Vortex structures (eddies) are formed that roll around each other and entrap irrotational ambient fluid and thereby incorporating it in the turbulent flow. Figure retrieved from Sreenivas and Prasad (2000).

4.3.1. Near-field mixing processes

Although the Delft3D model utilized in this thesis is not suitable for the accurate modelling of subgrid processes in the near-field of a turbulent jet, in this section the processes are described to gain insight in the hydro- and thermodynamics around an outfall. Knowledge of processes in the near-field might also assist in the assessment of far-field representations, since near-field and far-field are also related.

Mixing processes in the near-field are dominated by the momentum flux produced by the outfall. Therefore, closest to the outfall structure, outfall geometry and the magnitude of the momentum predominantly determine the flow. Further in the near-field, density stratification and current in the ambient flow become more important. The ambient current deflects the jet and generates additional turbulent mixing. The ambient density stratification can damp vertical accelerations in the water by exerting buoyancy forces, see figure 4.4 b and c respectively for a visualization of these processes.

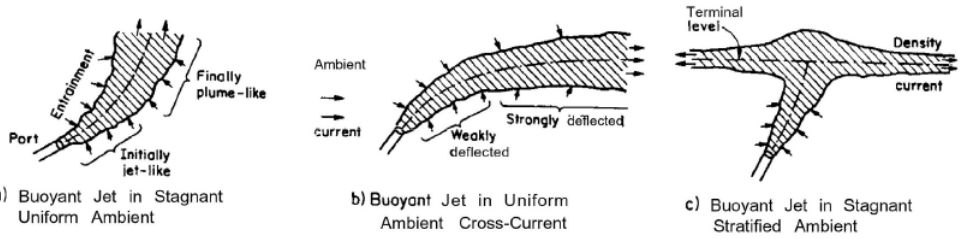

Figure 4.4: Buoyant jet mixing flow patterns under different ambient conditions. Figure retrieved from Zijl (2002).

When an outfall is installed near the bottom or a wall, additional interaction processes come into play. The velocity accelerations caused by the outfall, will result in extra turbulence due to friction with the wall or bottom. At an even smaller scale, a wake can develop near the outfall due to reattachment of the jet to the wall, see figure 4.5.

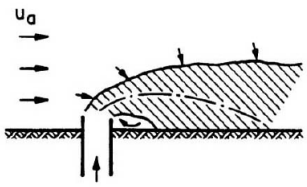

Figure 4.5: Wake attachment for a jet near a wall. Figure retrieved from Zijl (2002).

4.3.2. Far-field mixing processes

Further away from the source, the initial momentum and geometry of the jet become less important. The mixing processes will be governed by the ambient conditions. Processes that determine the far field are buoyant spreading and passive ambient diffusion.

Buoyant spreading

Buoyant spreading is the horizontal tranverse transport of the jet or plume, while the ambient current is advecting it further downstream, see figure 4.6. This type of spreading is caused by density differences between the jet fluid and the ambient fluid. For positively buoyant jets, this process occurs at the water surface and for negatively buoyant jets this process occurs at the bottom of the particular water body (Zijl, 2002). Another possibility is that buoyant spreading develops in the layer with largest density gradient, the so-called pycnocline, in a fluid with a strong density stratification. The process of buoyant spreading can take place at a rappid pace in the direction perpendicular to the jet trajectory, depending on the magnitude of the buoyancy effect.

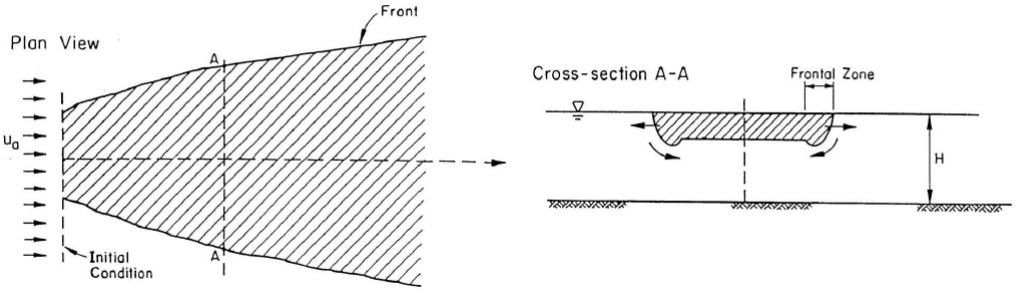

Figure 4.6: Representation of the buoyant spreading process at the water surface. Notice that this process might also occur at the bottom or in the pycnocline of a water body. Figure retrieved from Zijl (2002).

Passive ambient diffusion

Further in the far-field, passive ambient diffusion becomes the most important mixing process, see figure 4.7. In this region, buoyant spreading decreases and passive ambient diffusion takes over. Passive ambient diffusion is induced by the existing turbulence in the ambient fluid. Therefore, the extent to which this process is accomplished depends largely on the ambient conditions and water body geometry. According to Jirka et al. (1996), in case of bounded flow such as in canals, rivers or estuaries, the spreading process can be described by constant diffusivity in vertical and horizontal directions. In this case, the plume will grow until it finally reaches the boundaries of the particular water body. In unbounded ambient conditions, the growth of the plume accelerates in the direction of the plume or jet trajectory.

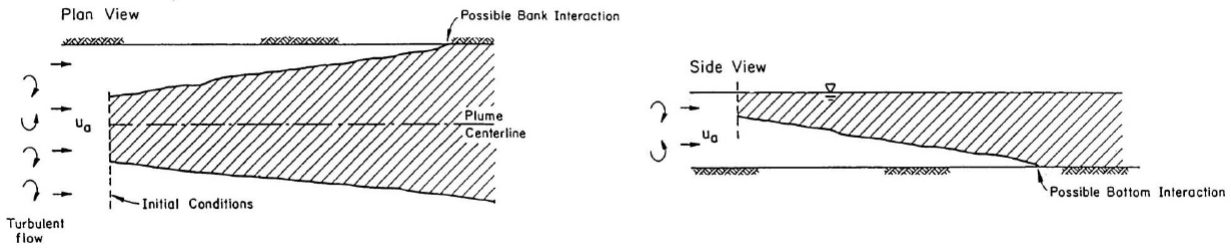

Figure 4.7: Representation of bounded passive ambient diffusion process at the water surface with advection. Figure retrieved from Zijl (2002).

4.4. Thermal processes: the sun as energy source and the surface water heat balance

In this section the heat module within Delft3D and the theoretical background are described. Starting point for this section is the manual of Delft3D by Deltares (Deltares, 2020). Extra explanation on theory is provided for the bulk coefficients, the Dalton and Stanton numbers.

The heat balance starts with sunlight. Sunlight penetrating the water body causes surface waters to be heated. Sunlight reaches the earth's surface in the form of electromagnetic waves in a spectrum of wavelengths between around 250 and 2500 nm, see figure 4.9. When travelling through the earth's atmosphere, these waves can be absorbed, reflected or scattered by air, clouds, dust or particles. Almost all of the solar radiation on the earth's atmosphere is emitted back again in the form of long wave radiation with wavelengths between approximately 4000 and 50 000 nm. This is due to the lower temperature of the earth compared to the sun, which can be easily derived from the Stefan-Boltzmann law. The several heat fluxes for the atmosphere of the earth are shown in figure 4.8.

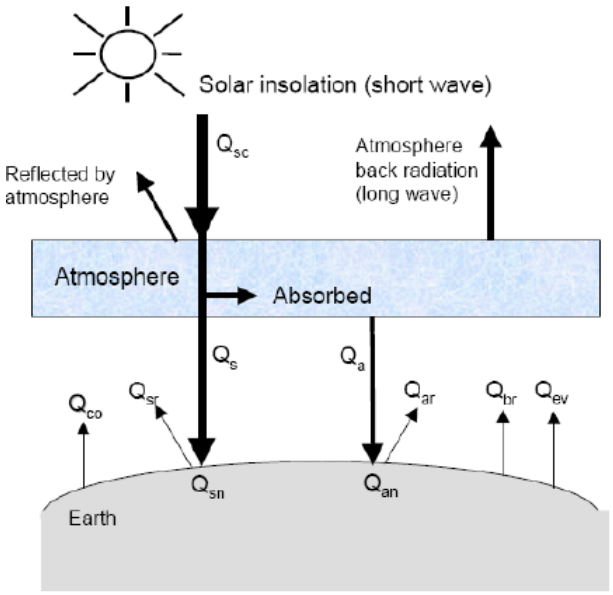

Figure 4.8: Heat balance and heat fluxes of the Earth's atmosphere, figure retrieved from Deltares (2020)

Translating the figure 4.8 into a heat flux balance for a surface water on Earth, the following equation is retrieved:

$$Q_{tot} = Q_{sn} + Q_{an} - Q_{br} - Q_{ev} - Q_{co} - Q_{\text{evfree}} - Q_{\text{cofree}} \tag{4.8}$$

where Q_{tot} is the total heat flux , Q_{sn} is the net incident short wave solar radiation ($Q_s - Q_{sr}$), Q_{an} is the net incident long wave atmospheric radiation , Q_{br} is the long wave back radiation from the surface water , Q_{ev} is the evaporative or latent heat flux, Q_{co} the heat flux through conduction or sometimes referred to as sensible heat , Q_{evfree} is the evaporative heat flux through free convection and Q_{cofree} the conductive heat flux through free convection, all expressed in (W/m^2).

Except for the incident short wave solar radiation which penetrates deeper into the surface water, the total heat flux is computationally considered as a boundary condition at the water surface of the energy equation. This energy boundary condition can be described by:

$$\frac{\partial T_s}{\partial t} = \frac{Q_{tot}}{\rho_w c_p \Delta z_s} \tag{4.9}$$

where ρ_w is the specific density of water (kg/m^3), c_p the specific heat capacity of water (= 4184 J/kgK) and Δz_s the thickness of the toplayer (m).

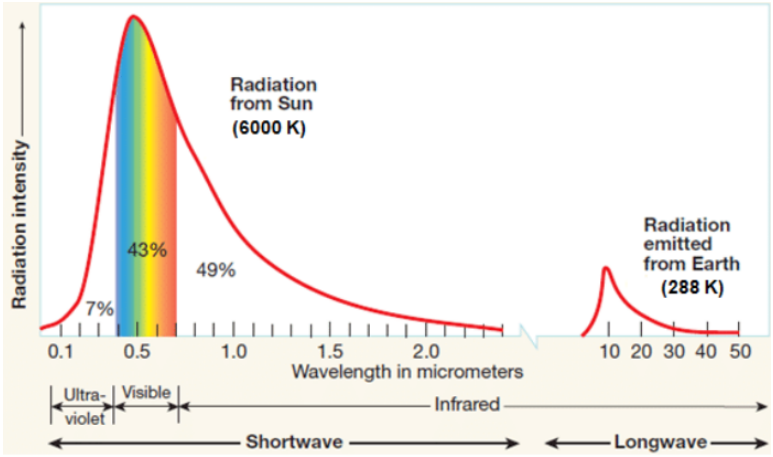

Figure 4.9: Spectra of short and long wave radiation directly from the sun (left) and reflected from the earth/atmosphere (right) respectively.

4.4.1. Solar radiation (short wave)

Solar radiation at the top of the atmosphere can be determined by applying the Stefan-Boltzmann law for a black body:

$$Q = \sigma \bar{T}^4 \tag{4.10}$$

where σ is the Stefan-Boltzmann's constant ($= 5.67x10^8 J/m^2 sK^4$) and $\bar{T}$ the absolute temperature (K).

According to Gill (1982), the incident solar flux for clear sky conditions at the earth's surface is proportional to 76% of the solar flux at the top of the atmosphere. Together with the solar constant S = 1 386 W/m^2 and the solar elevation angle γ (rad) for the specific time of the year, the solar radiation at the Earth's surface for clear sky conditions (Q_{sc}) can be determined by:

$$Q_{sc} = \begin{cases} 0.76S\sin(\gamma), & \sin(\gamma) \geq 0 \\ 0.0, & \sin(\gamma) < 0 \end{cases} \tag{4.11}$$

Radiation of the sun reaching the Earth's surface can be reflected or scattered at the surface. Also cloud cover in the atmosphere prevents sunlight from reaching the Earth's surface or the surface water body. The amount of clouds in the air is expressed as a cloud cover fraction F_c, representing the fraction of the sky covered by clouds. According to Gill (1982), the net downward solar heat flux (Q_{sn}) at the top of the surface water body can be expressed as:

$$Q_{sn} = (1-\alpha)Q_{sc}\left(1.0 - 0.4F_c - 0.38F_c^2\right) \tag{4.12}$$

where α is the albedo or reflection coefficient ($= 0.06$(-)).

Short wave radiation can penetrate over longer depths in water than long wave radiation (Talley, 2011). Incoming long wave radiation is absorbed in the top millimetres of the water column, while short waves can penetrate over distance of 3 to 30 metres, depending on the turbidity or clarity of the particular surface water body. The absorption of light under-water can be described by the Lambert-Beer Law, which is derived from the following first-order ordinary differential equation (ODE):

$$\frac{dQ_{sn}}{dz} = -\gamma Q_{sn} \tag{4.13}$$

$$\gamma = \frac{1.7}{H_{\text{Secchi}}} \tag{4.14}$$

where γ is the extinction coefficient (1/m) and H_{Secchi} the Secchi depth (m).

The extinction coefficient γ can be described by measuring the Secchi depth. The Secchi depth describes the under-water distance at which a Secchi disk is still visible. A Secchi disk is a universal tool used to measure water clarity, see figure 4.10. It is also a representation of the extinction coefficient of light and with a

factor of 1.7, an approximation of the extinction coefficient can be estimated from Secchi disk measurements. Subsequently, the ODE following from the Lambert-Beer law can be rewritten into a function of depth z. In this case, an exponential function develops which reads:

$$Q_{sn}(z) = e^{-\gamma z} Q^0_{sn} \tag{4.15}$$

where Q^0_{sn} is the net incoming solar radiation at the water surface (W/m^2).

This solution of the ODE can be solved for each vertical z-layer in the computational model. In this case, the total short wave solar energy absorbed in one layer is determined by computing the difference of incoming net solar radiation fractions between the upper boundary and lower boundary of the specific layer.

Figure 4.10: Secchi disk placed into surface water.

4.4.2. Atmospheric radiation (long wave)

Besides the direct solar heat flux, there is also atmospheric radiation absorbed at the water surface. The atmospheric radiation is long wave radiation emitted by the atmosphere. It is primarily caused by the emission of refracted and reflected solar radiation by particles in the atmosphere, such as water vapour, carbon dioxide and ozone. Again, the Stefan-Boltzmann law can be utilized to determine the magnitude of the radiation emitted by the atmosphere. At the same time, the surface water itself also emits long wave radiation as an almost black body. These two long wave radiation parts of the heat balance can be grouped into one equation and together they describe the so-called effective back radiation Q_{eb} (Octavio et al., 1977):

$$Q_{eb} = Q_{br} - Q_{an} \tag{4.16}$$

$$Q_{eb} = \varepsilon\sigma \bar{T}_s^4 \left(0.39 - 0.05\sqrt{e_a}\right)\left(1.0 - 0.6F_c^2\right) \tag{4.17}$$

where Q_{eb} is the effective back radiation (W/m^2), Q_{an} is the net incident long wave atmospheric radiation (W/m^2), Q_{br} is the long wave back radiation from the surface water (W/m^2), ε is the emissivity coefficient of a water body (=0.985), σ is the Stefan-Boltzmann's constant (= $5.67x10^8 J/m^2 sK^4$), $\bar{T}_s$ is the absolute water surface temperature (K), e_a is the actual vapour pressure at 10 metres above the water body (Pa) (see equation 4.21) and F_c the cloudiness factor (-).

4.4.3. Evaporative or latent heat flux

The evaporative heat flux is an exchange process of heat between the surface water and the vapour in the atmosphere above it. For the phase transition of water from liquid to vapour energy is required. In other words, a negative heat flux from the respective surface water is related to the evaporation of water. There are two variations of evaporative or latent heat flux: forced convection of latent heat (Q_{ev}) and free convection of latent heat (Q_{evfree}). Forced convection of latent heat is driven by wind forces and free convection is driven by atmospheric instabilities in situations with no wind or low wind speeds.

Forced convection of latent heat

Forced convection of latent heat is driven by wind blowing above the surface water and thereby constantly affecting the vapour pressure of the air above the water. In the Delft3D model used within this thesis forced convection is expressed as:

$$Q_{ev,\,\text{forced}} = L_V \rho_a f(U_{10}) \{q_s(T_s) - q_a(T_a)\} \tag{4.18}$$

with:

$$L_v = 2.510^6 - 2.310^3 T_s \tag{4.19}$$

$$f(U_{10}) = c_E U_{10} \tag{4.20}$$

where L_V is the latent heat of vaporisation (J/kg) dependent on the water temperature, ρ_a is the density of air (kg/m^3), $f(U_{10})$ is the wind speed as function of wind speed at 10 metres (m/s), c_E is the Dalton number (equal to the C_d coefficient used for computation of wind stresses, see section below on Dalton number) and lastly q_s and q_a are the specific humidities for saturated and air at 10 m above water level [kg/kg].

Specific humidity levels for saturated air just above the water surface and remote air at 10 metres above the water surface, are computed based on saturated and remote vapour pressures, according to:

$$\begin{aligned} e_s &= 10^{\frac{0.7859+0.03477 T_s}{1.0+0.00412 T_s}} \\ e_a &= r_{hum} 10^{\frac{0.7859+0.03477 Ta}{1.0+0.00412 Ta}} \end{aligned} \tag{4.21}$$

$$\begin{aligned} q_s(T_s) &= \frac{0.62 e_s}{P_{atm} - 0.38 e_s} \\ q_a(T_a) &= \frac{0.62 e_a}{P_{atm} - 0.38 e_a} \end{aligned} \tag{4.22}$$

where r_{hum} is the relative humidity [%] .

Turbulent bulk coefficient: the Dalton number

The Dalton number c_E is a dimensionless bulk coefficient denoting the ratio of heat transferred into the fluid relative to the thermal capacity of the fluid ($\rho u c_p$) due to forced convection. It is a transfer coefficient lumping the turbulent processes at the interface between water surface and atmosphere for the exchange of latent heat. The Dalton number forms the link between the changes in atmospheric properties, such as local humidity levels and wind speed, and the latent heat exchange at the water surface forced by these same changes. Following from the Delft3D manual (Deltares, 2020), the Dalton number in the heat flux module was calibrated at the North Sea to be equal to c_e = 0.0015 (-). Since the exchange coefficients of latent heat and momentum are closely related (Hicks, 1975), the Dalton number and the wind drag coefficient C_d are assumed to be equal in this report.

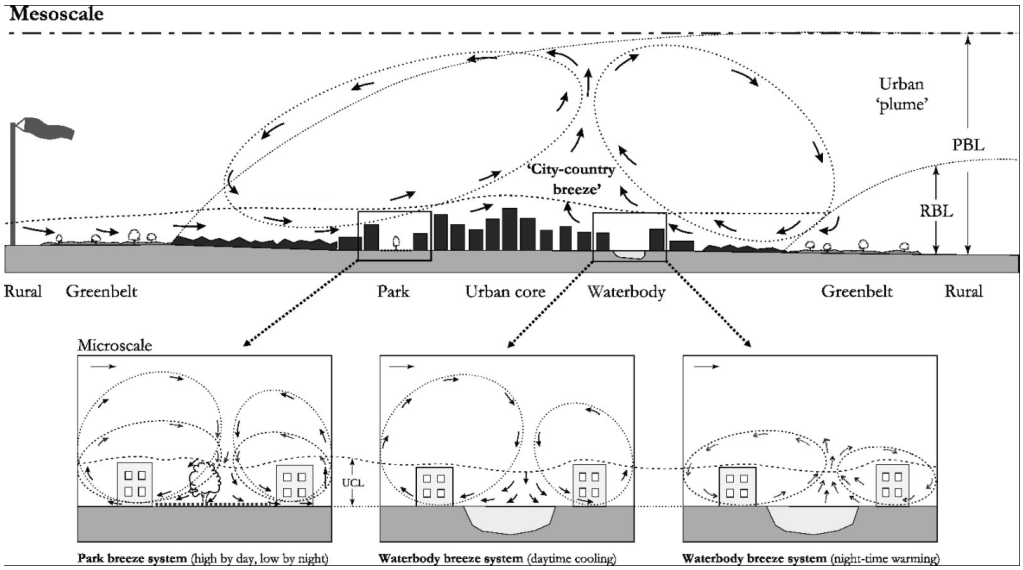

Figure 4.11: Convectional wind patterns at meso- and microscale in the city boundary-layer, figure retrieved from Gunawardena et al. (2017).

Free convection of latent heat

Besides latent heat exchange at the water surface through wind-driven forced convection, so-called free convection also induces heat loss from the water body through latent heat. Free convenction is the process in which buoyancy forces result in vertical transportation of air and water vapour. The density differences in the atmosphere, driving the free convection process, create unstable conditions in the atmospheric boundary layer. Under these unstable conditions and when wind speed is low, light moist and heated air near the Earth surface or water surface tends to rise, transporting water vapour and enhancing the latent heat exchange.

Without including the effect of free convection, the heat loss from the water body through latent heat is underestimated. Particularly in cities, which is of special interest in this study, the free convection process can play an important role, especially during summer nights with no wind or almost no wind. On such nights, the city and its structures are heated up during the day and remain heated during the night. This effect is also referred to as the Urban Heat Island (UHI) effect (see section 5.4.2), referring to higher average air temperatures found in cities compared to rural surroundings. The effect is strongest during nights. During a hot summer night, heated air near the urban surface starts to ascent and moist air from the rural surroundings is attracted towards the city, see figure 4.11. From the figure it follows that convection of air also occurs on urban microscale above e.g. a street canyon or a canal. It stipulates the importance of including the free convection processes in the urban heat balance.

The free convection latent heat flux above a surface water body has been described by Ryan et al. (1974). Ryan et al. (1974) prescribed a calculation method for free convection as a correction to the wind function $f(U_{10})$. The equation reads:

$$Q_{ev,\,\text{free}} = k_s L_V \bar{\rho}_a \left(q_s - q_a\right) \tag{4.23}$$

with k_s the heat transfer coefficient for free convection, which is a rewritten version of the so-called dimensionless Nusselt number denoting the ratio of convective to conductive heat transfer, described as:

$$k_s = \begin{cases} 0 & \text{if } \rho_{a10} - \rho_{a0} \leq 0 \\ c_{fr.conv} \left\{ \frac{g\alpha^2}{\nu_{air}\bar{\rho}_a} \left(\rho_{a10} - \rho_{a0}\right) \right\}^{1/3} & \text{if } \rho_{a10} - \rho_{a0} > 0 \end{cases} \tag{4.24}$$

$$\bar{\rho}_a = \frac{\rho_{a0} + \rho_{a10}}{2} \tag{4.25}$$

$$\alpha = \frac{\nu_{air}}{\sigma} \tag{4.26}$$

where $c_{fr.conv}$ is the coefficient of free convection (-) (calibrated at 0.14 by Ryan et al. (1974)), ν_{air} is the viscosity of air (m^2/s) assumed at a constant value of $16.0 \times 10^{-6} m^2/s$, α is the molecular diffusivity of air (m^2/s), σ is the Prandtl number, relating momentum diffusivity or viscosity to thermal diffusivity, which is 0.7 for air, ρ_{a10}, ρ_{a0} and $\bar{\rho}$ are the remote air density, saturated air density and average air density respectively (kg/m^3).

The saturated and remote air density are used to decide whether the local atmosphere is stable or unstable. Consequently, the correct relation for the heat transfer coefficient for free convection k_s can be used. Their respective formulations can be described by the following equations:

$$\rho_{a0} = \frac{\frac{100P_{atm} - 100e_s}{R_{dry}} + \frac{100e_s}{R_{vap}}}{T_s + 273.15} \tag{4.27}$$

$$\rho_{a10} = \frac{\frac{100P_{atm} - 100e_a}{R_{dry}} + \frac{100e_a}{R_{vap}}}{T_{air} + 273.15} \tag{4.28}$$

where R_{dry} is the gas constant for dry air (287.05 J/kgK) and R_{va_p} is the gas constant for water vapour (461.495 J/kgK). Specific humidities and vapour pressures can be calculated by equations 4.21 and 4.22.

4.4.4. Sensible heat flux

The sensible heat flux is related to the exchange of heat through differences in temperature between the water surface and the air above it. Near the surface, at molecular scale, the heat transfer between water and air is induced by conduction. Further from the water surface, heat transfer is primarily caused by turbulent mixing in the air. Considering daily variations, since air temperatures are generally higher during day and lower during night, the sensible heat term forms a heat source at daytime and a heat sink at night in the total heat balance. In other words, sensible heat is either absorbed by the water body (mostly during day) or released (mostly during nighttime).

Forced convection of sensible heat

The exchange of heat at the water surface by the sensible heat flux, or sometimes also referred to as convective heat flux, can be described with the help of another bulk coefficient, the Stanton number c_H. This leads to the following set of equations for free convection of sensible heat:

$$Q_{co,\,\text{forced}} = \rho_a c_p g\,(U_{10})\,(T_s - T_a) \tag{4.29}$$

$$g\,(U_{10}) = c_H U_{10} \tag{4.30}$$

where c_p is the specific heat capacity of air, which is considered constant at 1004 J/kgK and c_H is the Stanton number which is considered equal to the wind drag coefficient C_d in analogy with the Dalton number for latent heat.

Turbulent bulk coefficient: The Stanton number

Comparable to the Dalton number for the transport of latent heat, the Stanton number c_H is transfer coefficient representing the turbulent mixing processes between water surface and air for sensible heat. In the literature study performed by Aparicio Medrano (2008), it was found that during extensive measuring campaigns to calibrate energy budget models for oceans in the 70s and 80s, the Stanton number was slightly higher than values found for Dalton numbers. Isemer and Hasse (1987) found a ratio between Stanton and Dalton numbers of $c_E/c_H = 0.94$, including free convection processes. This discrepancy was also found to be highest for low wind speeds and under unstable conditions, supporting the existence of free convection of sensible heat, see the next section. When the wind speeds increased or with higher turbulency, the two bulk transport coefficients were found to be the same. In the created Delft3D model, for forced convection or under turbulent conditions, the two turbulent transport coefficients are assumed to be the same and equal to the wind drag coefficient ($c_E = c_H = C_D$). The effect of free convection is included in seperate equations. Without the effect of free convection, the Stanton number for the North Sea was calibrated by Deltares at 0.00145, even slightly lower than the prevailing Dalton number of 0.0015, see section 4.4.3. But again, this value was not used, the Stanton number was assumed to be equal to the wind drag coefficient instead.

Free convection of sensible heat

Besides free convection of latent heat, also free convection exchange of sensible heat occurs. The free convection term can be expressed as:

$$Q_{co,\,\text{free}} = k_s \bar{\rho}_a c_p\,(T_s - T_a) \tag{4.31}$$

where k_s is the heat transfer coefficient (m/s) provided by equation 4.24.

5

3D water temperature modelling

For the three-dimensional modelling of water temperature a Deltares Delft3D model has been utilized. In this chapter, the relevant model parameters and underlying assumptions are explained.

5.1. Model setup

The setup of a computational model, such as Delft3D, for a city canal requires a translation from the conditions of the real physical world to a discretized computable form. The physical domain or water body geometry is roughly determined by defining three model features: a computational grid, the corresponding bed level height and other geographical features such as land boundaries and sources or sinks. In this section, these model features will be briefly discussed.

5.1.1. Grid generation

In the field of computational fluid dynamics (CFD), water quantity and water quality parameters are calculated in a grid consisting of multiple grid cells. For each individual grid cell, the Reynolds-averaged Navier Stokes are solved, which will be further explained in section 5.2.2. Figure 5.1 shows the several grids of the Amsterdam canal system that have been implemented into this study. First, a large unstructured grid of the entire canal system including the Noordzeekanaal and Amsterdam Rijnkanaal, which was made by Deltares and Arcadis in cooperation with Waternet and Rijkswaterstaat, has been applied as a starting point in this study. In order to reduce computation time, the grid was then clipped to the city canal system only. At the boundaries of the city canal grid, modelled discharge and water temperature time series of the large grid model runs were implemented as boundary conditions. Results of this intermediate city canal grid model have primarily been used to evaluate the accuracy of the model compared to the executed temperature measurements in this study. Last of all, a grid was generated specifically for the van Lennep case study. The grid was again clipped to the extents of the case study area and again model results of earlier runs were imposed as time series boundaries.

Figure 5.1: Computational grids of the canal system of Amsterdam. From left to right the grid is further clipped to the particular case study site, the van Lennepkanaal. On the left image, the entire canal system attached to Noordzeekanaal and Amsterdam Rijnkanaal is displayed. The middle image shows the grid of the city canal system and the picture on the right side illustrates the grid used for the van Lennepkanaal case.

5.1.2. Bed level

Since the original grid by Arcadis and Deltares was applied for a larger area and purposed for another research aim and level of detail, corresponding grid bed levels were interpolated over larger areas. For an analysis on smaller scale, such as this study, this would impose an error in the model results. For some canals, a large area interpolation did even lead to a uniform cross-sectional bed level. The bed levels were therefore updated with the latest known bathymetry database measured by Waternet. In this way, also the typical trapezoid shape of a city canal cross section is respected in the created model. The bed level and grid dimensions together describe the water body geometry.

Figure 5.2: Updated bed level values (m NAP) for the van Lennep case study.

5.1.3. SWH installation as coupled source/sink

As mentioned earlier, it is also possible to include geographical structures to the water body geometry in Delft3D. For the modelling and study of outfalls and intakes, such as in the case of an open SWH installations, the coupled source and sink is the most important feature. A coupled source and sink system is created by defining the locations of the intake and outfall in the grid coordinate system together with a set of time series defining the discharges and the corresponding constituents: salinity and water temperature difference (ΔT).

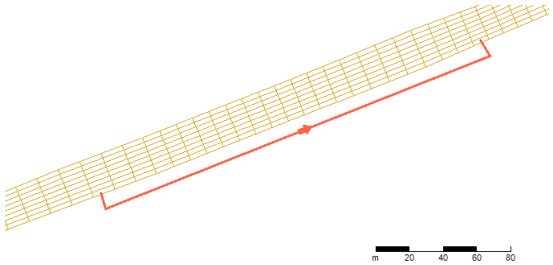

Figure 5.3: Visual representation of a SWH system modelled as a coupled source sink system along a canal in Delft3D.

5.2. Model hydrodynamics

When modelling temperature in a Delft3D model, the Reynolds-averaged Navier-Stokes (RANS) equations are solved for each grid cell along with a heat transport equation. For the closure of momentum, a $\kappa - \epsilon$ turbulence model modified for buoyancy effects is included. Following the formal application of Delft3D in shallow waters, variations in vertical momentum are reduced to the hydrostatic assumption, also known as the shallow water equation. Another important simplification compared to the full compressible formulation of the RANS equations is the Boussinesq approximation. It assumes that density is constant in the time-dependent and convective terms of the RANS equations. Therefore, the density differences and thus the temperature differences need to be relatively small allowing the Boussinesq approximation to be valid (Abbasi, 2016). According to White and Corfield (2006) and Ferziger et al. (2002) the Boussinesq approximation introduces errors of less than 1% for temperature variations of 2 K for water.

5.2.1. Hydrostatic pressure assumption

The shallow water assumption in Delft3D dictates a reduction of the vertical momentum equation to a hydrostatic pressure equation. This means that vertical accelerations due to immediate buoyancy effects and sudden variations in bed topography are assumed to be small compared to the gravitational acceleration and are therefore not taken into account (Deltares, 2020). Vertical water displacements are only described by the continuity equation. With the hydrostatic pressure assumption, the vertical momentum equation reduces to:

$$\frac{\partial P}{\partial z} = -\rho g h \tag{5.1}$$

where $\partial P \partial z$) is the vertical pressure gradient (N/m^2), ρ is the water density (kgm^-3) and h the water depth .

This is an important limititation of the Delft3D model when considering for example SWH installations modelled as jets. Here, immediate buoyancy effects could alter the flow pattern, especially in the near-field of a SWH outfall. In such a case, the hydrostatic assumption might lead to inaccurencies in the model results (Baptist et al., 2005). However, the vertical density differences are considered in the horizontal pressure gradients and in the vertical turbulent exchange coefficients. Delft3D is therefore suitable to be used in the study towards mid-field and far-field dispersion simulations of, for example, an outfall study.

5.2.2. The simplified Reynolds-averaged Navier Stokes equations

Combining the mentioned simplifications, the full Reynolds-averaged Navier Stokes equations can be rewritten in a simpler form. For the hydrodynamic part, the continuity equation (5.2) and the momentum equations in both horizontal directions (5.3 and 5.4) can be expressed as:

$$\frac{\partial u}{\partial x} + \frac{\partial v}{\partial y} + \frac{\partial w}{\partial z} = 0 \tag{5.2}$$

$$\frac{\partial u}{\partial t} + u\frac{\partial u}{\partial x} + v\frac{\partial u}{\partial y} + w\frac{\partial u}{\partial z} - fv = -\frac{1}{\rho_0}\frac{\partial P}{\partial x} + F_x + \frac{\partial}{\partial z}\left(\nu_V \frac{\partial u}{\partial z}\right) + M_x \tag{5.3}$$

$$\frac{\partial v}{\partial t} + u\frac{\partial v}{\partial x} + v\frac{\partial v}{\partial y} + w\frac{\partial v}{\partial z} + fu = -\frac{1}{\rho_0}\frac{\partial P}{\partial y} + F_y + \frac{\partial}{\partial z}\left(\nu_V \frac{\partial v}{\partial z}\right) + M_y \tag{5.4}$$

where u, v, w are velocities (m/s) in directions x, y and z respectively , t is the time vector (s), f represents a Coriolis parameter which depends on latitude and the angular speed of rotation of the earth (s^{-1}), ρ_0 is the water density at reference temperature (kgm^{-3}), P is the baroclinic pressure (N/m^2) , F_x and F_y represent the unbalance due to horizontal Reynolds stresses (m/s^2), ν_V is the vertical eddy viscosity coefficient (m^2/s) and M_x and M_y represent the momentum (m/s^2) in both directions induced by external sources and sinks, or for this particular study; the intake and outfall of a SWH installation.

Next to these hydrodynamic equations, an energy equation or a scalar field can be solved for the computational grid. Since water temperature is of main interest within this study, the following heat transport equation derived from the energy equation has been written in terms of total temperature:

$$\frac{\partial T}{\partial t} + u\frac{\partial T}{\partial x} + v\frac{\partial T}{\partial y} + w\frac{\partial T}{\partial z} - \alpha\frac{\partial}{\partial z}\left(\frac{\partial T}{\partial z}\right) = S_T(t,z) \tag{5.5}$$

where T is the water temperature (K), α is the thermal conductivity parameter or diffusivity parameter ($m^2 s^{-1}$) and $S_T(t,z)$ is the heat source term ($K s^{-1}$) .

Together, these equations (5.1, 5.2, 5.3, 5.4 and 5.5) define the hydrodynamics and water temperature for the entire flow field within the computational grid. It needs to be stipulated that the velocity, pressure and temperature values in the equations are Reynolds averaged, see next section 5.2.3. For a complete derivation and theoretical basis of the continuity and momentum equations of the Navier-Stokes equations, the reader is referred to the thesis of Aparicio Medrano (2008).

5.2.3. Reynolds averaging

Solving the exact solution of the Navier-Stokes equations would describe all the details of the flow on all length scales. This would mean that even at the smallest scale of turbulent flow, i.e. representing the smallest eddies in the flow, which can have an order of 10^{-3} smaller than the typical length scale of the flow, the full equations need to be solved. This would require intensive computations that are not desirable for the model size of most civil engineering problems. Usually, the grid is too coarse and time step too large to resolve all turbulent scales. These processes are "sub-grid". Therefore, a method is needed to lump these small scales and average them proportional to the chosen grid step size and/or time step size.

The Reynolds averaging method is a statistical approach and splits the velocity, pressure and temperature components in a mean part and a fluctuating part according to the following procedure:

$$u_i = \langle u_i \rangle + u_i' \tag{5.6}$$

$$P = \langle P \rangle + P' \tag{5.7}$$

$$T = \langle T \rangle + T' \tag{5.8}$$

where $\langle u_i \rangle$ is the mean or averaged velocity in i-direction and u_i' are the fluctuations from the mean of u_i. The same principle holds for the pressure and temperature terms.

Substitution of the Reynolds decomposition terms (5.6, 5.7 and 5.8) into the general Navier Stokes equations and taking the ensemble average leads to the Reynolds-Averaged Navier-Stokes equations incorporating so-called Reynolds stresses, accounted for in the F_x and F_y terms in 5.3 and 5.4 respectively. Reynold stresses are sometimes also referred to as turbulence stresses. They represent the transport of momentum by turbulent fluctuations in the fluid. Substitution and ensemble averaging of the Reynolds decomposition leads to the following formulation of the horizontal momentum equations and energy equation in the Navier Stokes equations:

$$\frac{\partial \langle u \rangle}{\partial t} + \langle u \rangle \frac{\partial \langle u \rangle}{\partial x} + \langle v \rangle \frac{\partial \langle u \rangle}{\partial y} + \langle w \rangle \frac{\partial \langle u \rangle}{\partial z} - f\langle v \rangle = -\frac{1}{\rho_0}\frac{\partial \langle P \rangle}{\partial x} - \frac{\partial \langle u'v' \rangle}{\partial x} + \frac{\partial}{\partial z}\left(\nu_V \frac{\partial \langle u \rangle}{\partial z}\right) + M_x \tag{5.9}$$

$$\frac{\partial \langle u \rangle}{\partial t} + \langle u \rangle \frac{\partial \langle v \rangle}{\partial x} + \langle v \rangle \frac{\partial \langle v \rangle}{\partial y} + \langle w \rangle \frac{\partial \langle v \rangle}{\partial z} - f\langle v \rangle = -\frac{1}{\rho_0}\frac{\partial \langle P \rangle}{\partial y} - \frac{\partial \langle v'u' \rangle}{\partial y} + \frac{\partial}{\partial z}\left(\nu_V \frac{\partial \langle v \rangle}{\partial z}\right) + M_y \tag{5.10}$$

$$\frac{\partial \langle T \rangle}{\partial t} + \langle u \rangle \frac{\partial \langle T \rangle}{\partial x} + \langle v \rangle \frac{\partial \langle T \rangle}{\partial y} + \langle w \rangle \frac{\partial \langle T \rangle}{\partial z} + \frac{\partial \langle w'T' \rangle}{\partial z} - \alpha_0 \frac{\partial}{\partial z}\left(\frac{\partial \langle T \rangle}{\partial z}\right) = S_T(t,z) \tag{5.11}$$

where α_0 is the thermal molecular diffusivity (m^2/s) .

The second terms on the right hand side of both the horizontal momentum equations 5.9 and 5.10 are the Reynolds or turbulence stresses representing momentum transport due to turbulent movements in the fluid. In the energy equation 5.11 the fifth term on the left hand side represents the transport of heat by

turbulence. In equation 5.5 this term is merged together with the sixth term in equation 5.11, which describes the spreading of heat by molecular diffusivity, into a general thermal conductivity parameter α:

$$\alpha = \alpha_t + \alpha_0 = \frac{\nu_V}{Pr_t} + \frac{\nu_0}{Pr} \tag{5.12}$$

where ν_0 and ν_V are the molecular kinematic viscosity and vertical eddy viscosity respectively (m^2/s), Pr is the Prandtl number which is defined as the ratio of molecular momentum diffusivity to thermal diffusivity ($Pr = \frac{\nu_0}{\alpha_0}$) (-) and Pr_t is the turbulent Prandtl number (-) defined as the ratio of diffusivity of turbulent shear stress $-\langle u'v' \rangle$ to diffusivity of turbulent heat flux $-\langle w'T' \rangle$. For the transport of heat, the turbulent Prandtl number is $Pr_t = 0.7$ (-). For the general Prandtl number, describing the thermal conduction by molecular diffusion, the value is set to $Pr = 7.07$ (-) at a water temperature of 20 °C.

5.2.4. Turbulence closure model

Due to the development of Reynolds stresses created by the Reynolds decomposition and the ensemble averaging process, the RANS equations consist of more unknowns than available equations. Finding a proper description for the subgrid turbulence terms closes this underdetermined problem. Such a turbulence closure model estimates the turbulence parameters, i.e. the Reynolds stresses, based on closure relations and known hydrodynamic parameters such as velocity and pressure gradients.

Horizontal turbulence: The Smagorinksy model

In Delft3D, different turbulence conceptualizations are used for horizontal and vertical turbulence. In the horizontal, the Smagorinsky turbulence model is used. This model is based on the Boussinesq concept, which assumes that turbulent shear stresses or Reynolds stresses are proportional to the eddy viscosity (m^2/s) and the velocity gradients according to:

$$\begin{aligned} -\langle u'v' \rangle &= \nu_t \left(\tfrac{\partial \langle u \rangle}{\partial y} + \tfrac{\partial \langle v \rangle}{\partial x} \right) - \tfrac{2}{3} k \delta_{ij} \\ k &= \tfrac{1}{2} \langle u'w' \rangle \end{aligned} \tag{5.13}$$

where k is the turbulent kinetic energy [J/kg] or [m^2/s^2] and δ_{ij} is the Kronecker delta function. The second term on the right hand side is absorbed in the pressure term of the RANS equations.

The Boussinesq approximation prescribes that turbulent fluctuations are dissipated into the mean flow. Mathematically, this means that the Boussinesq approximation simplifies the influence of turbulence in the RANS equations towards an adjusted molecular diffusion equation (Garnier et al., 2009). The Smagorinsky model adds a subgrid-scale eddy viscosity $\nu_r = C_s\Delta$ (m^2/s) representing the turbulent fluctuations to the chosen uniform horizontal eddy viscosity. This simple horizontal turbulence model was implemented into Delft3D to be able to cope with grid spacing variations, it reads:

$$\nu_t = \nu_H = \nu_{Huniform} + (C_s\Delta)^2 \left(\frac{\partial \langle u \rangle}{\partial y} + \frac{\partial \langle v \rangle}{\partial x} \right) \tag{5.14}$$

where $\nu_{Huniform}$ is the defined uniform or background horizontal eddy viscosity , C_s is the Smagorinsky coefficient (-) and Δ the filter width or the chosen grid spacing (m). The Smagorinksy coefficient C_s is an a priori input parameter defined by the user. For the modelling purposes of this thesis a value of $C_s = 0.2$ is proposed which has been validated by Deltares in former researches (Verbruggen et al., 2019).

Vertical turbulence: $k-\epsilon$ turbulence model

The vertical turbulence is modelled with a two equation turbulence model, the $\kappa - \epsilon$ model. Two equation models describe turbulent fluctuations in the flow based on transport equations. In the $k-\epsilon$ model, two equations for two turbulent parameters k (J/kg) or (m^2/s^2), denoting the turbulent kinetic energy, and ϵ (J/kgs) or (m^2/s^3), representing the dissipation rate of turbulent kinetic energy, are solved to model the production and transport of vertical turbulence.

Also for the vertical turbulence, an expression to model the turbulent kinetic viscosity or eddy viscosity is required. From the two turbulent parameters k and ϵ following from the transport equations, the vertical eddy viscosity can be calculated with the Kolmogorov-Prandtl equation:

$$\nu_V = c_\mu \frac{k^2}{\varepsilon} \tag{5.15}$$

where c_μ is a closure parameter with a value of 0.09 (-) corresponding to turbulence development in a logarithmic velocity profile along a wall.

In the transport equations the production of turbulence, buoyancy-induced turbulence and dissipation of turbulence are the dominant processes. The transport equations for k and ϵ read:

$$\begin{aligned} \frac{\partial k}{\partial t} + u\frac{\partial k}{\partial x} + v\frac{\partial k}{\partial y} + w\frac{\partial k}{\partial z} = \\ + \frac{\partial}{\partial z}\left(D_k \frac{\partial k}{\partial z}\right) + P_k + B_k - \varepsilon \end{aligned} \tag{5.16}$$

$$\begin{aligned} \frac{\partial \varepsilon}{\partial t} + u\frac{\partial \varepsilon}{\partial x} + v\frac{\partial \varepsilon}{\partial y} + w\frac{\partial \varepsilon}{\partial z} = \\ \frac{\partial}{\partial z}\left(D_\varepsilon \frac{\partial \varepsilon}{\partial z}\right) + P_\varepsilon + B_\varepsilon - c_{2\varepsilon}\frac{\varepsilon^2}{k} \end{aligned} \tag{5.17}$$

with the diffusion coefficients (m^2/s) defined as:

$$D_k = \frac{\nu_0}{Pr} + \frac{\nu_V}{Pr_k} \tag{5.18}$$

$$D_\varepsilon = \frac{\nu_V}{\mathrm{Pr}_\varepsilon} \tag{5.19}$$

In the turbulent production term P_k (m^2/s^2) of the Delft3D model, the vertical velocity gradients are neglected. The production term is based on horizontal velocity gradients with respect to the vertical and extra turbulence is produced by the side walls of the water body. For the computation of turbulence caused by the side walls, a second term with fully horizontal velocity gradients is added in equation 6.20. The production terms for kinetic turbulent energy (P_k) and energy dissipation (P_ε) are described by:

$$\begin{aligned} P_k = 2\nu_V \left[\frac{1}{2}\left\{\left(\frac{\partial u}{\partial z}\right)^2 + \left(\frac{\partial v}{\partial z}\right)^2\right\}\right] + \\ + 2\nu_V \left[\left(\frac{\partial u}{\partial x}\right)^2 + \frac{1}{2}\left(\frac{\partial u}{\partial y} + \frac{\partial v}{\partial x}\right)^2 + \left(\frac{\partial v}{\partial y}\right)^2\right] \end{aligned} \tag{5.20}$$

$$P_\varepsilon = c_{1\varepsilon}\frac{\varepsilon}{k}P_k \tag{5.21}$$

When density gradients in the water column occur, turbulent kinetic energy can be converted into potential energy. Buoyancy effects on surface water turbulence are described by the following set of equations:

$$B_k = \frac{\nu_V}{\rho Pr_t}\frac{g}{h}\frac{\partial \rho}{\partial z} \tag{5.22}$$

$$B_\varepsilon = c_{1\varepsilon}\frac{\varepsilon}{k}(1 - c_{3\varepsilon})B_k \tag{5.23}$$

It can be observed that most terms in the ε-equations are scaled with a factor of $(\frac{\varepsilon}{k})$. The turbulence dissipation factor ε is treated as a constituent similarly to the turbulent kinetic energy k, which explains the similarity in the two transport equations and justifies the use of this scaling factor. Besides this scaling factor, also calibration coefficients are introduced. From experiments and experience in calibration, $k-\varepsilon$ models have been proven to work well when these constants are defined as (Rodi, 1984) (Shih et al., 1995):

$$\begin{aligned} c_{1\varepsilon} &= 1.44 \\ c_{2\varepsilon} &= 1.92 \\ c_{3\varepsilon} &= \begin{cases} 0.0 & \text{unstable stratification} \\ 1.0 & \text{stable stratification} \end{cases} \end{aligned} \tag{5.24}$$

In the ε-equation for buoyancy-induced turbulence, the dissipation of buoyant turbulence is switched off when a stable stratification is observed in the water column. When the stratification becomes unstable, the dissipation of buoyant turbulence is turned on again.

5.3. Boundary conditions

At the boundaries of the model area, boundary conditions need to be specified. Therefore, at the outer boundaries of the model area, boundary conditions containing time series have been applied for temperature as well as water flow. Furthermore, in order to represent the flow close to canal walls and beds, generally applicable boundary conditions are implemented in Delft3D. Both types of boundary conditions will be further discussed in this section.

5.3.1. Bed and wall friction

Friction between the water flow and the bed and side walls of the water body result in viscous shear stresses in the water column. Knowing that these shear stresses are proportional to the vertical eddy viscosity ν_V and velocity gradients as described in section 5.2.4, this results in the following set of fixed boundary conditions or so-called Dirichlet boundary conditions near the bed:

$$\nu_V \frac{\partial u}{\partial z}\bigg|_{z=0} = \frac{1}{\rho_0}\tau_{bx} \tag{5.25}$$

$$\nu_V \frac{\partial v}{\partial z}\bigg|_{z=0} = \frac{1}{\rho_0}\tau_{by} \tag{5.26}$$

where ν_V is the vertical eddy viscosity (m^2/s) , ρ_0 is the reference water density only dependent on water temperature (see eq. 3.2) (kg/m^3) and τ_{bx} and τ_{by} are the components of bed shear stress in x- and y-direction.

For wall friction, similar boundary conditions are implemented but then in x- and z-direction, parallel to the water body walls. The shear stress τ_b can be computed as result of several roughness formulations, such as Chézy, Manning, logarithmic law of the wall, White-Colebrook or Strickler. For the city canal model in Amsterdam, bed shear stresses were mostly calculated using White-Colebrook's formulation with Nikuradse roughness k ranging between 0.05 m for muddy banks and harbours and 0.15 m as a standard value for river and canal beds.

Through the k-ϵ turbulence model, the vertical eddy viscosity near the bed is calculated by the Kolmogorov-Prandtl equation (see equation 5.15). To determine vertical eddy viscosity and the production of turbulence by the wall and bed friction, boundary conditions in the k-ϵ model need to be defined. A Dirichlet boundary condition and a Neumann boundary condition can be defined in the k-ϵ model for the bed, which read respectively:

$$k|_{z=0} = \frac{u_{*b}^2}{\sqrt{c_\mu}} \tag{5.27}$$

$$\frac{\partial \varepsilon}{\partial z} = \frac{(\varepsilon_{b+1} - \varepsilon_b)}{\Delta z_b} = \frac{u_{*b}^3}{\kappa\left(\frac{\Delta z_b}{2} + 9z_0\right)^2} \tag{5.28}$$

where u_{*b} is the bed or wall friction velocity (m/s), c_μ is the closure parameter with a value of 0.09 (-), corresponding to turbulence development in logarithmic velocity profile along a wall, Δz_b is the height of the grid cell above the bed (m), κ is the von Karman constant with a value of 0.41 (-) and z_0 is the roughness height (m) where velocities tend to go to zero, proportional to the Nikuradse roughness $k_n = 30z_0$ in case of hydraulically rough flow.

In Delft3D, the logarithmic law of the wall is applied for turbulence development as a result of bed and wall friction. The law of the wall prescribes that the average velocity of a point in the turbulent flow is proportional to the logarithm of the distance of this point to the wall. For the boundary conditions (5.27 and 5.28) the friction velocity u_* is computed according to the law of the wall. According to Schlichting and Gersten (2016) the logarithmic law of the wall can be rewritten as:

$$u = \frac{u_*}{\kappa} \ln \frac{z}{z_0} \tag{5.29}$$

or, in Delft3D, rewritten in terms of a Chézy coefficient C_{2D} ($m^{1/2}/s$):

$$C_{2D} = \frac{\sqrt{g}}{\kappa} \ln\left(1 + \frac{30R}{ek_n}\right) \tag{5.30}$$

$$\tau_b = \frac{\rho_0 g u|u|}{C_{2D}^2} \tag{5.31}$$

$$u_* = \sqrt{\frac{\tau_b}{\rho_0}} \tag{5.32}$$

Where R is the hydraulic radius [m] and k_n is the Nikuradse roughness (m).

5.3.2. Time series boundaries of discharge and water temperature

In the process of producing nested grids, as described by section 5.1.1, time series boundaries were generated to represent the hydrodynamics and exchange of heat flux from the larger grid into the smaller clipped grid. The generated time series consisted of stratified temperature profiles with 4 up to 6 temperature values over the vertical, depending on the local depth, and discharge values for the entire cross-section of the water column. Plots of one of the applied time series boundaries, at the Oostertoegang, are provided in figures 5.4 and 5.5.

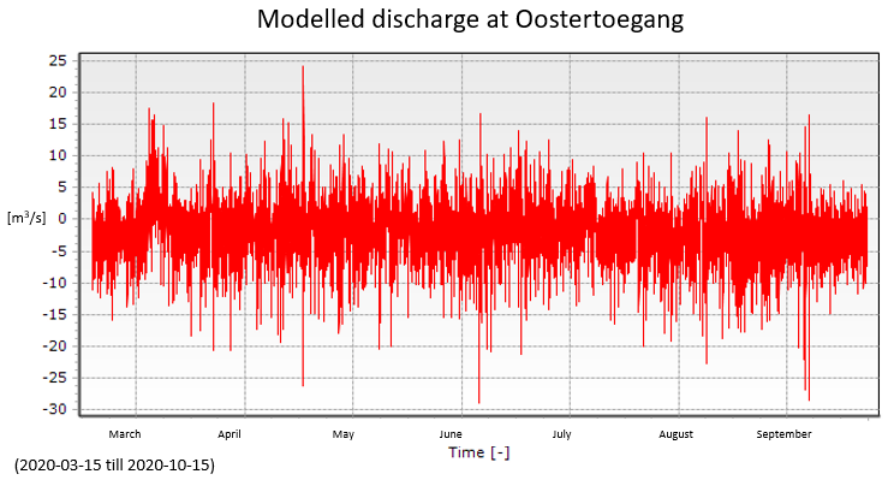

Figure 5.4: Modelled discharges at Oostertoegang, an entrance to the city canal system, applied for the grid nesting process.

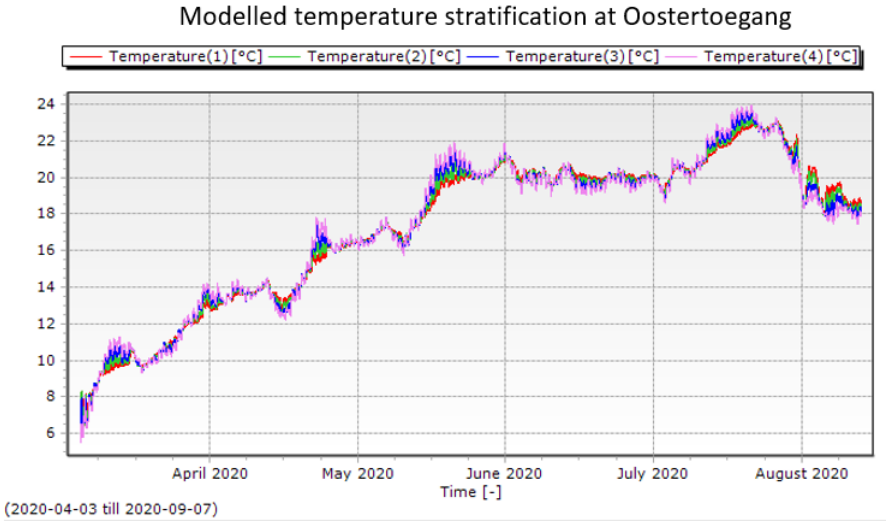

Figure 5.5: Modelled water temperature stratification at Oostertoegang, an entrance to the city canal system, applied for the grid nesting process. Temperature 1 is the temperature at the bottom and temperature 4 at the water surface

5.3.3. Model laterals

Since the water system of Amsterdam consists of many different water bodies varying in magnitude, from small side channels to large channels such as Amsterdam Rijnkanaal. For simplicity and to reduce computation time, it was chosen to model only the larger surface water bodies. The discharge and heat flux exchange at intersections between the large water system with smaller water bodies was modelled by so-called laterals. From a modelling point of view, these laterals were modelled as momentumless 1D point sources or sinks, depending on the direction of flow. These point sources or sinks discharge at one specified grid cell and mixing of the incoming water occurs within the model grid, partly by continuity and partly through turbulence caused by increase in local velocities. For each lateral, both measured water temperature and discharge time series, corresponding with the years 2020 and 2015 respectively, were provided. An overview of the locations of the modelled is given in figure 5.6.

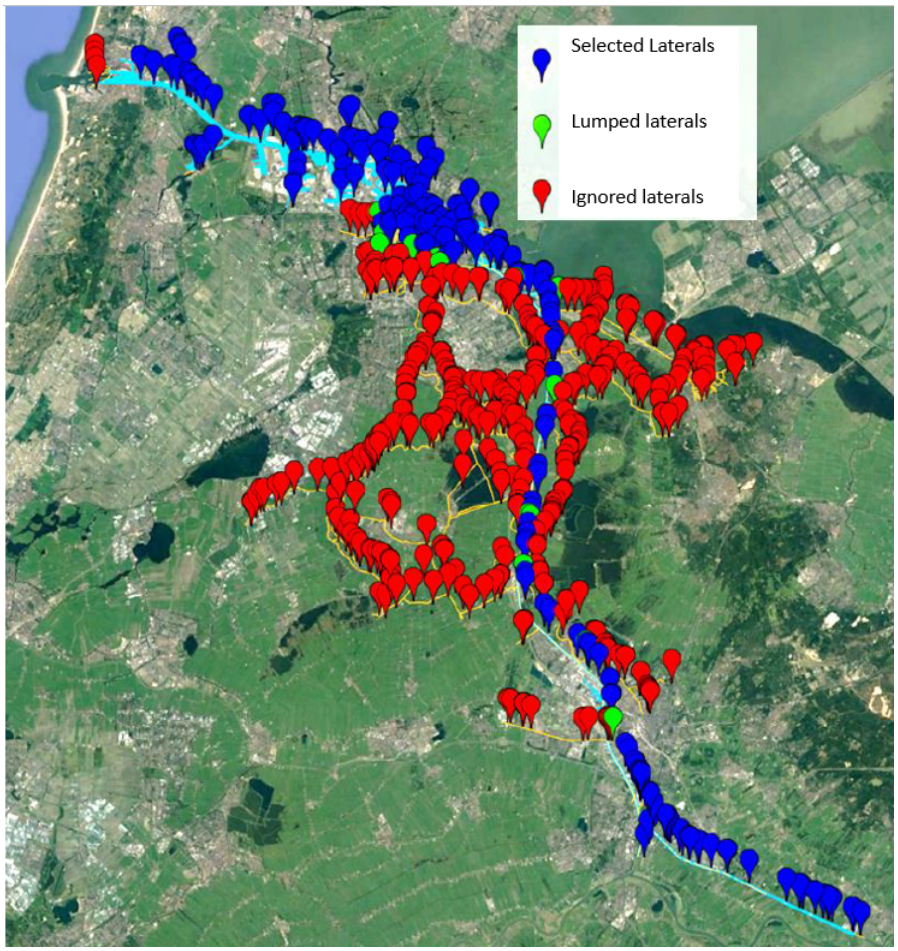

Figure 5.6: Overview of laterals used in the Delft3D-FM model, figure retrieved from Verbruggen et al. (2019). Only the blue points were implemented directly and the red locations are implicitly modelled by lumping them in the green lateral locations.

At the edges of the model, including the IJ, Noordzeekanaal and Amsterdam Rijnkanaal, laterals with high discharges were also implemented. The entire model reaches from the sluices and lock system at IJmuiden all the way up to the Prinses Irene locks in Wijk bij Duurstede and the Beatrix locks in Nieuwegein, upstream in the Amsterdam Rijnkanaal. For these points at the boundaries of the model, time series laterals were created. Also, as indicated in figure 5.6, the so-called lumped laterals have been applied in the model of Arcadis and Deltares (Verbruggen et al., 2019). These laterals represent the laterals marked in red and therefore represent the flow from the upstream polder system into the city canal system. Time series for all laterals were retrieved from model results of the Boezemmodel by Waternet Together, all laterals and especially the high discharge laterals at the edges of the model determine the major hydrodynamics and the prevailing hydrodynamic mode of the system, as described in the model system description in section 3.1.

5.4. Model forcing

This section describes the external forcing applied on the modelled water body at the van Lennepkanaal. The external forcing exists of meteorolocial forcing, wind forcing and external forcing induced by the modelled SWH systems. An emphasis is placed on the complexity of finding representative values for the different kinds of model forcing in the hyper local and hetereogeneous urban landscape.

5.4.1. Meteorological forcing

In first instance, meteorological data was retrieved from the KNMI airport weather station in Schiphol. As described in section 3.2, explaining the thermal processes within an urban water body, the meteorological input parameters for Delft3D are relative humidity [%], air temperature [°C] and cloudiness as a percentage of a completely cloudy sky [%]. When these three forcing parameters are defined, the water temperature of any water body can be determined with the described composite heat flux model in section 4.4. This section describes the chosen data sources for the meteorological input and describes the derivation of representative urban meteorological model input.

MODIS cloudiness

Since relative humidity and air temperature are common parameters for weather stations, time series for both parameters were retrieved from the weather station directly. However, the measuring procedure for cloudiness or cloud coverage in standard weather stations is considered less precise for application in Delft3D. Although Dutch weather and climate institute KNMI measures cloudiness continuously based on LIDAR equipment reporting accurate time series of detected clouds and cloud base height, the cloudiness values are averaged and reported in eighths or octas (Wauben, 2002). This implies that KNMI cloudiness values have a substantial bandwith of 12.5 % in which the cloudiness values can still vary. Since the cloudiness is important parameter for determining the incoming short wave radiation of the sun, which in turn is the dominating thermal heat flux for the heating of surface waters, a higher precision was required. Therefore, hourly cloudiness values were retrieved from MODIS satellite data used in the NASA MERRA 2 atmospheric reanalysis with a resolution of 0.5 x 0.625 degrees, corresponding to a spatial resolution of approximately 55 x 42 km at given latitude and longitude.

Meteorological forcing under urban conditions

The Schiphol airport weather station is located outside the city of Amsterdam, approximately 7.5 km away from the area of interest, the Wilhelmina Gasthuis district. The Schiphol airport station is situated in the middle of a grass lawn along the airport runaways, with no buildings in the direct vicinity. The meteorological conditions at the airport weather station can be characterized as less urban compared to Wilhelmina Gasthuis situation and more of a rural type. Still the Schiphol weather station experiences some urban effects from the nearby airport, comparable to a small city. Considering , the Schiphol airport weather data might be less representative for the actual weather conditions occuring in the Van Lennepkanaal.

5.4.2. Meteorological forcing: the Urban Heat Island Effect

In cities and especially in the high urbanized areas, the well known urban heat island (UHI) effect can be observed, implying that air temperatures in cities are on average higher than observed air temperatures in more rural areas (Oke, 1973) (Deilami et al., 2018). According to van der Hoeven and Wandl (2015), also the city of Amsterdam experiences this so-called UHI effect. Further analysis of figure 5.7 provides yearly averaged UHI values expressed in degrees Celsius for the Schiphol weather station, which is approximately 0.6 °C. It can also be observed that at the Van Lennepkanaal the yearly average UHI effect is approximately 1.7 °C. Due to this substantial diffence in air temperature, it was chosen to also incorporate meteorological data from a local citizen weather station from the WOW-NL database at approximately 500 meters from the area, the Oud-West Wiegbrug station. The weather station is an Automatic Weather Station (AWS) of the Davis Vantage Pro series. The air temperature sensor is protected from radiation by a Stevenson screen and installed at 18 metres above ground level mounted on an elevated surface of a rooftop. The metadata of the weather station in the WOW-NL database reports that the location of the Oud-West Wiegbrug station can be classified in category 1 out of classes 0 to 5. This class corresponds to a sheltered location where obstacles such as heated buildings are within a radius of 1H (H = the obstacle height). Presumed that the measurement equipment is of sufficient quality, air temperature measurements of weather stations in this class are representative for the

direct surroundings, which justifies the use of this weather station for the van Lennepkanaal. Furthermore, the location is ranked with a rating of 2 stars out of 5 in the WOW-NL database. A comparative study between citizen weather stations in the WOW-NL database and official KNMI stations, showed that WOW-NL weather stations with location class 2 deviate between +2.5 °C and -2.0 °C with a confidence interval of 95% (Koole, 2016). For this urban weather station, according to figure 5.7 the UHI effect amounts to approximately 2.0 °C. This means that in terms of air temperature, the Oud-West Wiegbrug weather data would represent the city weather conditions better. The locations of both weather stations are displayed in figure 5.7 as well.

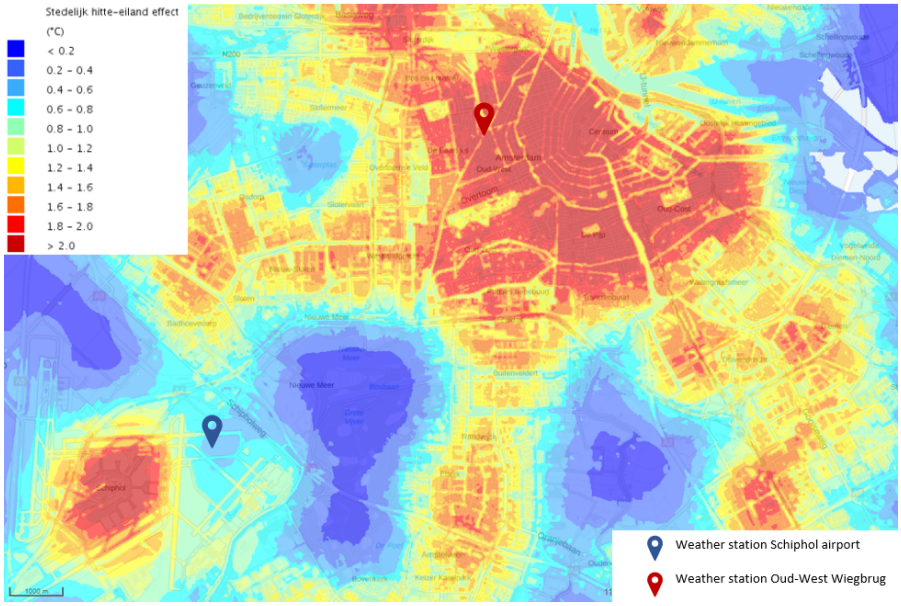

Figure 5.7: Yearly mean Urban Heat Island (UHI) effect in Amsterdam in degrees Celsius, figure retrieved from Atlas Natuurlijk Kapitaal developed by RIVM (2017).

Relative Humidity in cities

Besides the modification in air temperature induced by urban areas, also relative humidity values in urban areas are different from rural conditions. In cities, the high imperviousness of the urban surfaces results in less average evaporation and, in turn, this could result in lower local relative humidity levels. This effect was indeed noticed in the research for the city Beijing and the literature study towards urban-rural humidity relations performed by Liu et al. (2009). The urban relative humidity difference was also found to have a positive relationship with the UHI effect. Especially during nighttime, when the UHI effect is strongest, relative humidity levels in rural areas were significantly higher than relative humidity (RH) levels in the city (Holmer and Eliasson, 1999). Since a higher air temperature in the city enables the air to contain more moisture. This process increases the maximum vapor pressure of the city air and RH levels decrease accordingly. On the contrary, according to Hage (1975) and Lee (1991), absolute humidity levels were discovered to be higher in urban areas. Possible explanations are anthropogenic emmissions and enhanced vertical mixing patterns over the rough city texture, thereby capturing moisture from higher atmospheric layers and increasing the urban moisture content.

Differences in RH between the two weather stations can be found in figure 5.8. The graphs show that indeed the relative humidity is on average higher for the more rural weather station Schiphol, especially during nighttime (up to 10-15%). During daytime, a reverse effect is visible. Daytime RH levels are comparable, but tend to be higher in the city (up to 5-10%). However, it needs to be noted that the positioning of the citizen weather station Oud-West Wiegbrug might not be ideal and could be biased. Since RH levels can vary significantly on a small scale, installation of the amateur weather station in the city near airconditioning systems, chimneys or other exhaust sources could significantly alter the local measured RH.

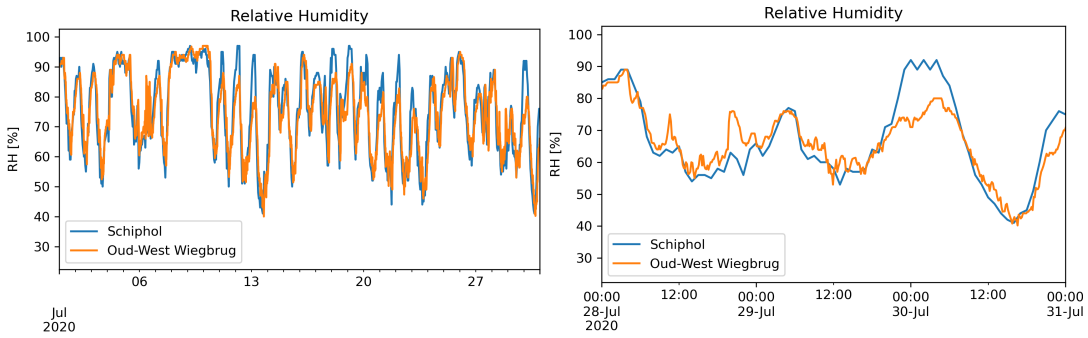

(a) Relative Humidity for Schiphol and Oud-West Wiegbrug in July 2020.

(b) Relative Humditiy for Schiphol and Oud-West Wiegbrug from July 28 to 31.

Figure 5.8: Relative Humidity for both meteo stations.

5.4.3. Meteorological forcing: shadow effects by buildings

Another typical urban aspect that needs consideration are the shadow effects from buildings adjacent or near the canal. Shadow reduces the incident solar radiation that falls on the canal water body. The reduction in solar radiation is quantified with a simple straightforward shadow model. In this model, that has been applied before by Shashua-Bar and Hoffman (2003) and Aparicio Medrano (2008), the incident solar radiation corrected by a factor called "Partial Shaded Area" (PSA) . In the van Lennepkanaal case, the PSA represents the width of the city canal that is shaded by adjacent buildings. In order to determine the PSA, the azimuth and elevation angle of the sun during the computation period are required. The PSA and corrected solar radiation are described by the following set of relations:

$$W_s = H \left| \frac{\cos(\psi - \psi_s)}{\tan\gamma} \right| \tag{5.33}$$

$$PSA = \frac{W_s}{W_p} \tag{5.34}$$

$$\mathrm{Q_{tot}} = \mathrm{Q_{dir}}\,(1 - PSA) + \mathrm{Q_{diff}} \tag{5.35}$$

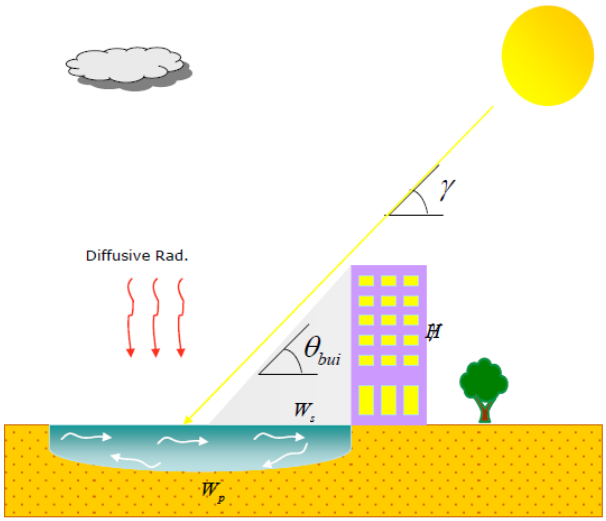

Figure 5.9: Visualization of the shadow model situation. Figure retrieved from Aparicio Medrano (2008).

where W_s is the shaded width of the pond (m), W_p is the total pond with (m), ψ is the direction of the canal with respect to North (rad), ψ_s is the azimuth of the sun (rad), γ is the solar elevation angle (rad), H is the height of surrounding buildings, Q_{dir} is the direct solar radiation (W/m^2) and Q_{diff} is the diffusive radiation (W/m^2). See figure 5.9 for a schematisation of the model situation.

The shadow relations above are the same as applied by Aparicio Medrano (2008), except for the modulus that was applied to the goniometric part in the shaded width calculation. This modulus is applied because buildings exist on both sides of the van Lennepkanaal, as opposed to the visualisation in figure 5.9.

5.4.4. Meteorological forcing: the urban wind model

In Delft3D wind stresses at the free surface of the water body are modelled as velocity boundary conditions (for u and v) in the momentum equation and as a turbulent kinetic energy (k) boundary condition in the $k-\epsilon$ turbulence closure model, similar to the bed and wall friction as described in section 5.3.1, leading to the following boundary equations for the horizontal momentum equations:

$$\nu_V \frac{\partial u}{\partial z}\bigg|_{z=z_{top}} = \frac{1}{\rho_0}\tau_{sx} \tag{5.36}$$

$$\nu_V \frac{\partial v}{\partial z}\bigg|_{z=z_{top}} = \frac{1}{\rho_0}\tau_{sy} \tag{5.37}$$

with:

$$\begin{aligned} \tau_{sx} &= \rho_a C_D U_{x10}\sqrt{U_{x10}^2 + U_{y10}^2} \\ \tau_{sy} &= \rho_a C_D U_{y10}\sqrt{U_{x10}^2 + U_{y10}^2} \end{aligned} \tag{5.38}$$

where τ_{sx} and τ_{sy} are the wind shear stresses in x and y direction respectively , the ρ_a is the density of air (kg/m^3), C_D is the wind drag coefficient which is dependent on the wind velocity at 10 meters above the free water surface U_{10} (m/s) , which is subsequently splitted in a x and y component (U_{x10} and U_{y10}).

In the $k-\epsilon$ turbulence closure model, wind impact is modelled as a boundary condition in the turbulent kinetic energy equation (k). Also for the top layer or water surface layer, the lograthimic law of the wall is applied, similar to bed and wall friction, see equation 3.29. In analogy with bed and wall friction, the boundary is of the Dirichlet type and reads:

$$k|_{z=z_{top}} = \frac{u_{*s}^2}{\sqrt{c_\mu}} \tag{5.39}$$

where u_{*s} is the wind friction velocity (m/s) which can be derived from the wind shear stresses ($u_{*s} = \sqrt{\frac{\tau_s}{\rho_a}}$) and c_μ is the closure parameter with a value of 0.09 (-) corresponding to turbulence development in logarithmic velocity profile along a wall.

Wind effects on a small-scale

Wind-induced turbulence at the water surface is caused by friction of wind with the water surface, pressure fluctuations (waves) and currents related to wind drift and waves (Wang et al., 2013). Below the surface layers affected by waves, the vertical profile of horizontal water velocities is assumed to follow the law of the wall. As acknowledged by Wüest and Lorke (2003) and Abbasi (2016), in small inland water bodies and especially urban water bodies, the wave field at the surface is not fully developed due to small wind fetches and wind shielding which are typical for the urban landscape. This results in a small wave-affected layers and justifies excluding these wave effects.

For the determination of the wind drag coefficient (C_D), which is the unknown in the above wind relations, the wind model proposed by Wüest and Lorke (2003) is applied. The proposed representation of wind speeds by Wüest and Lorke (2003) is specifically developed for use at a small scale and was applied to small lakes. From model experience with Delft3D it was found that this wind model provides accurate results for modelling of water temperature (Verbruggen et al., 2019). The model utilizes the wind speed measured at 10 meters above the surface water as wind input parameter and distinguishes two wind modes; high wind speed

($U_{10} > 5m/s$) and low wind speeds ($U_{10} < 5m/s$). For the two wind modes, two different wind relations are used to compute the wind drag coefficient:

For strong winds ($U_{10} > 5m/s$), a variation of the Charnock's law is used:

$$C_{D,10} = \left[\kappa^{-1} \ln \left(\frac{10g}{C_{D,10} U_{10}^2} \right) + 11.3 \right]^{-2} \tag{5.40}$$

For small and shielded urban water bodies, wind speeds are typically low. For these lower wind speeds ($U_{10} < 5m/s$), the drag coefficient C_D seems to follow a different relation with the wind velocities. In accordance, Wüest and Lorke (2003) proposed a least square fit of C_D for the lower wind speeds based on previous research data. This relation reads:

$$C_{D,10} = 0.0044 \times U_{10}^{-1.15} \tag{5.41}$$

Wind velocities in the city

To determine the wind velocity at 10 meters above the surface water (U_{10}), wind velocities within the urban canopy layer need to be modelled. The urban canopy layer can be described as the near surface air layer in between the city's buildings. The height of the canopy layer is therefore dependent on the local building height, see figure 5.10.

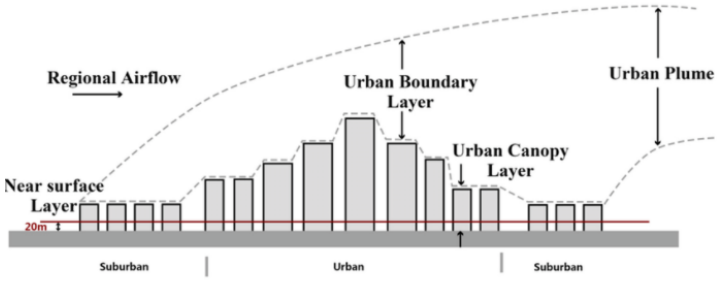

Figure 5.10: Visualization of the Urban Boundary Layer (UBL) and urban canopy layer.. Figure retrieved from Yang et al. (2020).

The modelling of wind velocities in urban areas, and especially in the urban canopy, is difficult. In cities, high variability in surface roughness and building canopy heights result in location specific and heterogeneous wind patterns. Therefore, the wind speed in urban areas is merely a location specific parameter which in principle cannot be modelled based on generalized characteristics of the urban texture (Mertens, 2003). Acknowledging the locality of urban wind, urban wind was mainly studied for limited areas in computational models, which are able to capture local variabilities in the urban landscape (Van Hooff and Blocken, 2010) (Blocken et al., 2012) (Barlow, 2014). Others have studied these variabilities in simplified scale models tested in wind tunnels and derived relations for determining wind speed in obstacle rich environments such as cities (Macdonald et al., 2000) (Macdonald, 2000). Despite the heterogeneity of the urban surface, this section attempts to describe the method used within these thesis based on the work of Mertens (2003) and Di Sabatino et al. (2008) to calculate urban wind velocities at 10 meters height (U_{10}) based on wind speed measurements at the more rural or suburban Schiphol airport weather station.

Wind velocities in the Urban Boundary Layer (UBL)

When wind from more rural areas blows towards a city, a change in surface roughness results in a change of the wind speed profile above the different land cover type, see figure 5.11. In this case, a new boundary layer develops; the Urban Boundary Layer (UBL) which is the same as the Internal Boundary Layer (IBL) displayed in figure 5.11. Above this layer, the wind profile is nearly undisturbed by the change in roughness and equal to the wind velocities upwind of the change in roughness, the External Boundary layer. Being a part of the UBL, the first step in computing the wind velocities at 10 meters (U_{10}) is calculating the spatial extent of the UBL. Mertens (2003) proposes the use of a relation for boundary layer growth over a smooth plate, which was first suggested by Wood (1982) for neutral atmospheric conditions. The relation reads:

$$h_k(x) = 0.28 z_{0,\max} \left(\frac{x}{z_{0,\max}} \right)^{0.8} \tag{5.42}$$

Where h_k is the UBL height (m) , x is the distance downstream of the change in roughness (m) and $z_{0,\max}$ is the larger surface roughness (m).

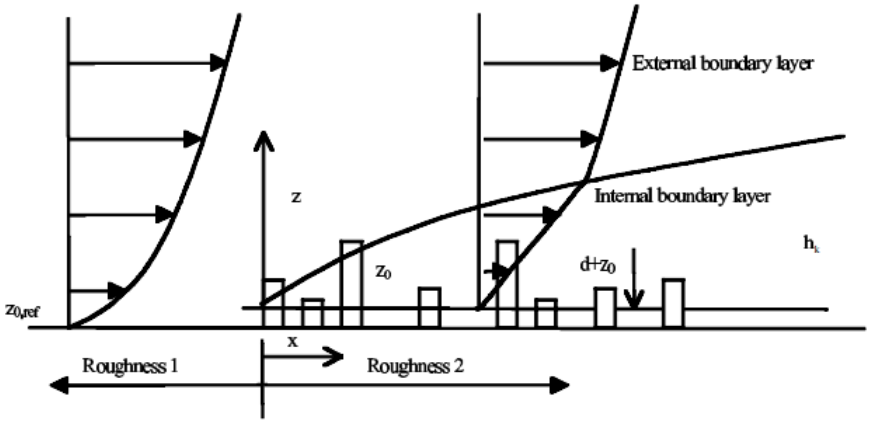

Figure 5.11: Difference in wind speed profiles due to change in surface roughness from rural (left) to urban (right). Figure retrieved from Mertens (2003).

Far downwind of the rural-urban interface, the UBL is in equilibrium with the External boundary layer shear force and the new surface roughness. In this case, the wind speed profile becomes logarithmic. Mertens (2003) calculates the far downwind wind speed with the following logarithmic formulation:

$$u_0(z) = \frac{\ln\left(\frac{h_k(x)}{z_{0,ref}}\right)}{\ln\left(\frac{h_{ref}}{z_{0,ref}}\right)} \frac{\ln\left(\frac{z-d}{z_0}\right)}{\ln\left(\frac{h_k(x)-d}{z_0}\right)} u_{ref} \tag{5.43}$$

with:

$$d = 0.67 \bar{h}_b \tag{5.44}$$

where z is the height (m) at which u_0 is computed, d is the zero displacement height (m), z_0 and $z_{0,ref}$ are the surface roughness at location of interest and reference location respectively (m) and u_{ref} is the wind velocity at reference location (m/s).

This logarithmic profile is only valid in the UBL for heights that comply with the following criterion (Wieringa and Rijkoort, 1983):

$$z \geq 20 z_0 + d \tag{5.45}$$

The proposed UBL wind model of Mertens (2003) was applied to calculate wind speeds at a height of 250 meters above the city. The model was also used to compute the wind speed derivative at this altitude. The derivative at 250 meters is one of the boundary conditions used in the urban canopy model that is described in the next section. Table 5.1 summarizes the parameter values that were adopted in the UBL model.

Wind model parameters		
Urban roughness length z_0	1.5	m
Schiphol (rural) roughness length $z_{0,ref}$	0.3	m
Schiphol measure height h_{ref}	10	m
Urban zero displacement height d	10.7	m
Assumed average building height H	16	m
Min distance Jacob van Lennepkanaal x downstream of roughness change corresponding to wind from South East direction	3500	m
Max distance Jacob van Lennepkanaal x downstream of roughness change corresponding to wind from South direction	9700	m

Table 5.1: Wind parameters used in the UBL wind model. For the computation of the boundary layer size h_k, the distance downstream of the step in roughness x was estimated from satellite images for 8 wind directions in total.

Wind velocities within the urban canopy layer

Wind velocity values based on the model of Mertens (2003) were used as boundary conditions in the model developed by Di Sabatino et al. (2008). Di Sabatino et al. (2008) tried to create a simple model based on existing knowlegde of wind patterns in the urban boundary layer. A vegetation canopy wind model was extended with results from scale model measurements by Macdonald et al. (2000). Di Sabatino et al. (2008) used a mixing length closure model to close the force balance between wind shear forces above and around the city buildings and drag forces. This balance reads:

$$\frac{d}{dz}\left(l(z)\frac{dU}{dz}\right)^2 = \frac{1}{2}C_D U^2(z)\frac{\lambda_f(z)}{H} \tag{5.46}$$

where $l(z)$ is the mixing length dependent on height (z) (m), U is the wind velocity (m/s), C_D is the average drag coefficient of the obstacles (-), H is the average building height (m) and $\lambda_f(z)$ is the height dependent frontal area density (-).

For the determination of the mixing length of a respective atmospheric layer $l(z)$, three different regions are distinguished; the logarithmic region, the shear layer region and canopy region. For the logarithmic region above the average building height ($z > z_w$), the mixing length is defined as:

$$l(z) = \kappa(z-d) \tag{5.47}$$

In the shear layer region just above and around the city's buildings ($H < z < z_w$), transmission of shear forces to drag forces takes place through the forming of vortices in air (turbulence). For this region Macdonald et al. (2000) suggested an analytical method for the calculation of the mixing length profile over height :

$$l_m(z) = l_c + \left(\frac{z-H}{z_w-H}\right)(\kappa(z_w-d) - l_c) \tag{5.48}$$

In the urban canopy region ($z < H$), mixing length is assumed to be independent of height z and constant according to:

$$l_c(z) = \kappa(H-d) \tag{5.49}$$

where κ is the von Karman constant (= 0.41 (-)) and z_w is the height at the top of the shear layer (m).

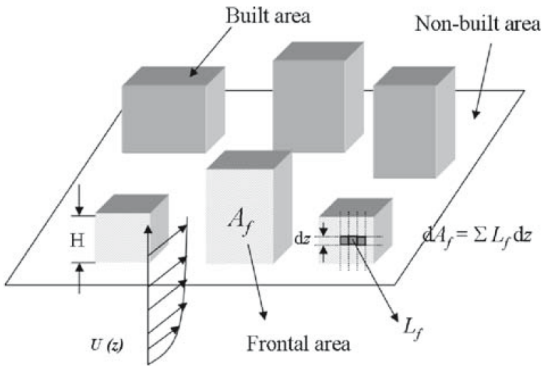

Figure 5.12: Frontal area density visualization within an urban area. Figure retrieved from Di Sabatino et al. (2008).

The frontal area density $\lambda_f(z)$ is assumed to be constant at 0.4 for $0 < z < 10m$ and to decrease exponentially to $\lambda_f(z) = 0$ at $z = 25m$. The frontal area density can be described as the fractional width of the buildings at a specific height of the considered wind domain, see figure 5.12 for a visual representation of $\lambda_f(z)$. For the van Lennep case study, values for the city of Amsterdam were estimated based on visual inspection of the Algemeen Hoogtebestand Nederland (AHN) and comparison with values found for other cities by Ratti et al. (2006). For higher accuracy, $\lambda_f(z)$ values could be computed through several spatial computation steps with a Digital Elevation Model (DEM) of the urban texture in the considered domain. This has not yet been done in this thesis.

It is possible to rewrite equation 5.46 in the form of a stiff ordinary differential equation (ODES), which can be solved numerically for the vertical profile (see figure) of wind speed U:

$$\frac{du_2}{dz} = \frac{-l(z)\frac{dl}{dz}u_2^2 + \frac{1}{4}u_1^2\frac{\lambda_f(z)}{H}C_D}{l^2(z)u_2} \tag{5.50}$$

The two boundary equations necessary to solve this ODES are completed with the boundary conditions following from the UBL model by Mertens (2003) described in the previous section:

$$U = u_1 \tag{5.51}$$

$$\frac{dU}{dz} = u_2 \tag{5.52}$$

Furthermore, an estimation for shear layer height z_w needs to be made. Based on the work of Macdonald et al. (2000) and confirmed by Di Sabatino et al. (2008) a value between $1.3H$ and $2.0H$ was chosen: $1.8H$. As indicated by Di Sabatino et al. (2008), the proposed model performs worst within this shear layer region. This is due to the simple nature of the model trying to represent complex processes especially within this layer. The estimation of z_w and the description of mixing length in the shear layer are therefore the weakest spots in this model.

Urban canopy model parameters		
Height of shear layer top z_w	$1.8H$	m
Assumed average building height H	16	m
Frontal area density range $\lambda_f(z)$	0 to 0.4	-
von Karman constant	0.41	-
Assumed average drag coefficient of built environment C_D	1.2	-

Table 5.2: Model parameters for the urban canopy model by Di Sabatino et al. (2008).

The assumed parameters in the wind model are summarized in table 5.2 and an example of a vertical wind profile is provided in figure 5.13. From the velocity profile, it can be noticed that the logaritmic profile above the urban canopy reshapes into an exponential profile within the urban canopy. This typical form of

the velocity profile is in good agreement with the findings in the small scale wind tunnel measurements of wind blowing around square and staggered positioned cubes, representing an urban canopy Macdonald et al. (2000). The Di Sabatino et al. (2008) is therefore assumed to be a good approximation for the wind velocity within the urban canopy at 10 meters height (U_{10}).

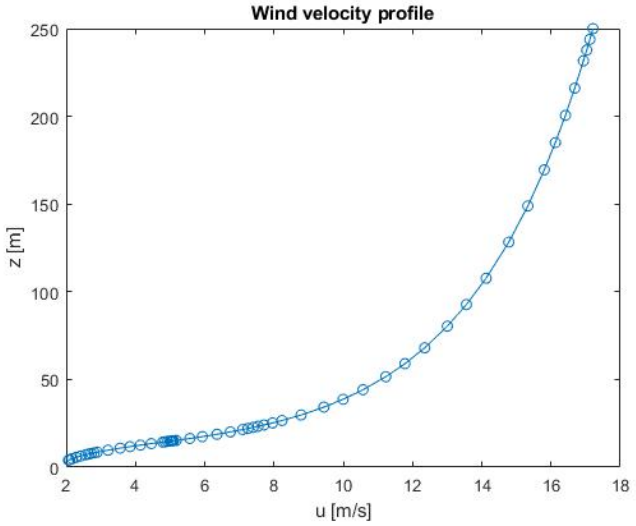

Figure 5.13: An instance of a vertical wind speed profile under urban conditions calculated with the ODES of the Di Sabatino et al. (2008) model. The wind speed at 250 meters is approximately 17.2 m/s and approximately 3.3 m/s at 10 meters height (U_{10}).

5.5. Model scenarios

The two created SWH system time series, see section 3.4.1, were applied in several model scenarios that were constructed to get insight in the effect of future SWH application in the van Lennepkanaal. The starting point in the creation of the scenarios were the SWH system design parameters of primary interest for this study; the distance between intake and outfall, the influence of higher ΔT and accumulation of multiple systems in the canal.

Scenario	**Scenario ID**	**# of systems**	**Intake/outfall distance**
System 1 (ΔT = 5 °C)	1.50	1	50 m
	1.100	1	100 m
	1.150	1	150 m
	1.200	1	200 m
	1.250	1	250 m
	1.300	1	300 m
	1.350	1	350 m
Multiple systems (system 1)	2.300	2	300 m
	3.300	3	300 m
System 2 (ΔT = 7.5 °C)	1.75.100	1	100 m
	1.75.200	1	200 m
	1.75.300	1	300 m

Table 5.3: Overview of the modelled scenarios.

An overview of the modelled scenarios is provided in table 5.3. To assess the influence of varying distance between the intake and outfall of a SWH system, scenarios with distance increments of 50 metres were created. Differences in temperature and heat flux distributions were analyzed with application of system 1 (ΔT = 5 °C) and system 2 (ΔT = 7.5 °C) to provide insight in the effect of variation in ΔT. Finally, the accumulation of multiple systems in the van Lennepkanaal was simulated with the application of respectively 2 and 3 identical systems, each with a distance between intake and outfall of 300 metres. The installation of these systems was assumed to be strategically, meaning that intake and outfall of different systems were placed as far as

possible from each other. Practically, this translates into installation of two intakes and two outfalls near each other and one intake and outfall further away.

6

Results

This chapter contains the results of the measurement campaign, the results of the validation efforts on meteorological forcing and the temperature modelling results respectively.

6.1. Water Temperature measurement results

The figure 6.1 shows water temperatures at one location, the Nieuwe Herengracht, for two different depths in the canal. The measured water temperatures were corrected for outliers by a Hampel filter that applies the median value to outliers within a data window of 24 consecutive measurements. Considerable temperature differences are visible between the water temperature at the bottom and the surface of the canal. Especially during the heat wave in the beginning of August, differences in water temperature were measured up to 2.2 °C between bottom and surface. During the cooling of the water in late summer and autumn, it can be observed that water temperatures at the canal bottom tend to be less reactive to the change in meteorological conditions. This can be explained by the fact that deeper water has a higher thermal inertia, leading to delayed response in water temperature to changes in the atmosphere above it.

Another interesting observation is that during the cooling process at the end of the year, the daily amplitude or daily variation seems to be higher for deeper water in the Nieuwe Herengracht. A possible explanation for this higher amplitude during cooling of the surface water can be found in the mixing by ships in the canal. During daytime, cold water cooled by the atmosphere is mixed with the deeper layers of the canal, leading to an almost unifrom vertical temperature distribution. During nighttime, when there is less water displacement by ships and less mixing of the canal water, a reverse stratification is able to grow. Heat is released from the canal bed and heat from canals in the inner city is transported through the Nieuwe Herengracht to the IJ. These processes especially heat up the deeper water layers, while the less inert top layers of the canals are still cooled by the atmosphere. In this way, considerable differences in water temperature in vertical direction can be observed and, according to figure 6.1, water temperatures can vary up to 1.5 °C between deep and shallow water layers in this period.

In figure 6.2, the water temperature profile for another location, the Duivendrechtsevaart, is plotted. Although this location is merely a canal of an inner harbor, it is also connected to the Amstel and surrounded by urbanized environment. It is however more shallow, approximately 1.9 meters deep, and the depth retardation effect that was described for the Nieuwe Herengracht is not as clearly visible at this location. A reason for this could be the smaller depth or other possible local differences in hydrodynamics, meteorological conditions or different bed characteristics.

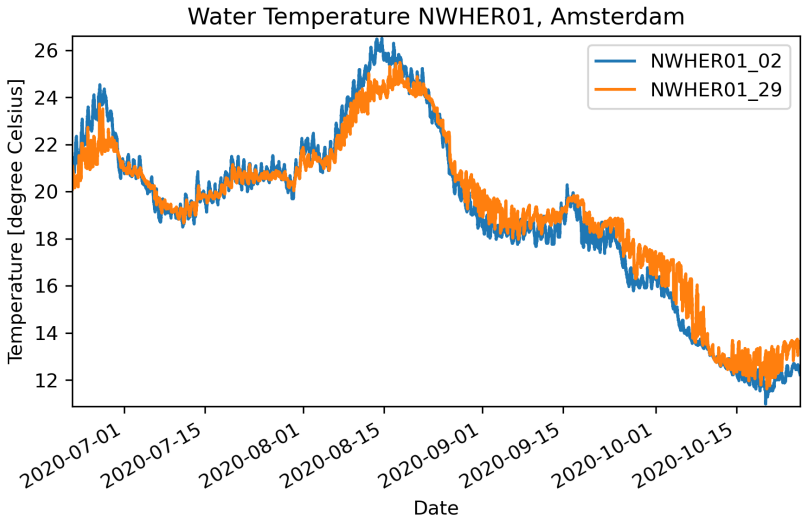

Figure 6.1: Water temperatures at 20 cm below water surface (NWHER01_02) and at approximately 2.9 m below water surface (NWHER01_29) of the Nieuwe Herengracht, the bottom of the canal, during summer of 2020.

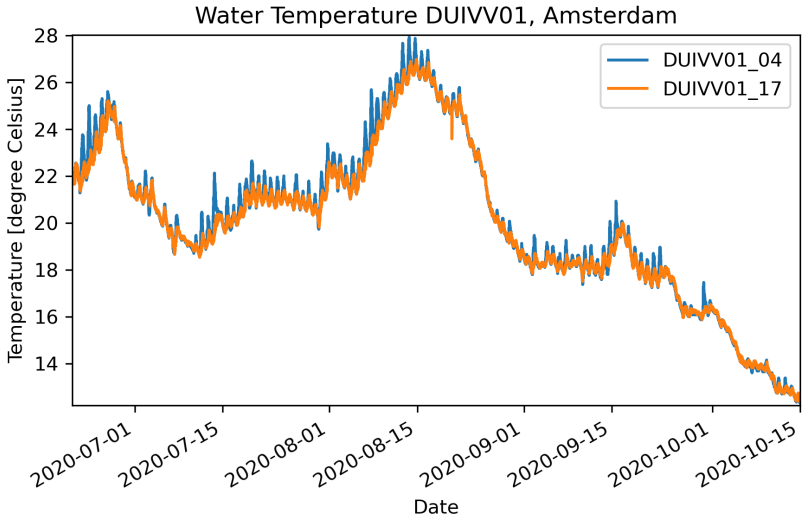

Figure 6.2: Water temperatures in the Duivendrechtsevaart at 40 cm below water surface (DUIV01_04) and at approximately 1.7 m below water surface (DUIV01_17), near the bottom of the canal, during summer of 2020.

6.1.1. Measurements in van Lennepkanaal

In the Jacob van Lennepkanaal, temperature differences between toplayer and surface layer at the two measurement locations in the canal are less pronounced, see figures 6.3 and 6.4. Temperature differences between top and bottom layer are 0.4 °C at maximum. These smaller temperature differences can be accounted to the increased shading of surrounding buildings and smaller depths in the canal. For the same reasons, also the absolute water temperatures tend to be lower in the van Lennepkanaal. From the sharper peaks at measurement point JVLEN03 , it can also be observed that measurement point JVLEN01 has more shadow during the day compared to JVLEN03. These outcomes are in line with expectations, since the measurement assembly at JVLEN01 receives additional shadow from a nearby bridge and houseboat and JVLEN03 is situated at a more open location with a more clear sky view.

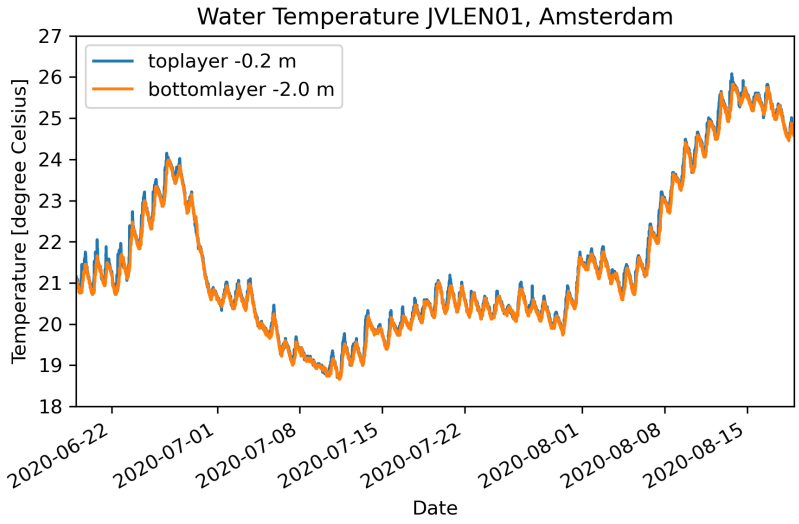

Figure 6.3: Water temperatures at approximately 20 cm below water surface and at 2.2 m below water surface (bottom) of the van Lennepkanaal, during summer of 2020.

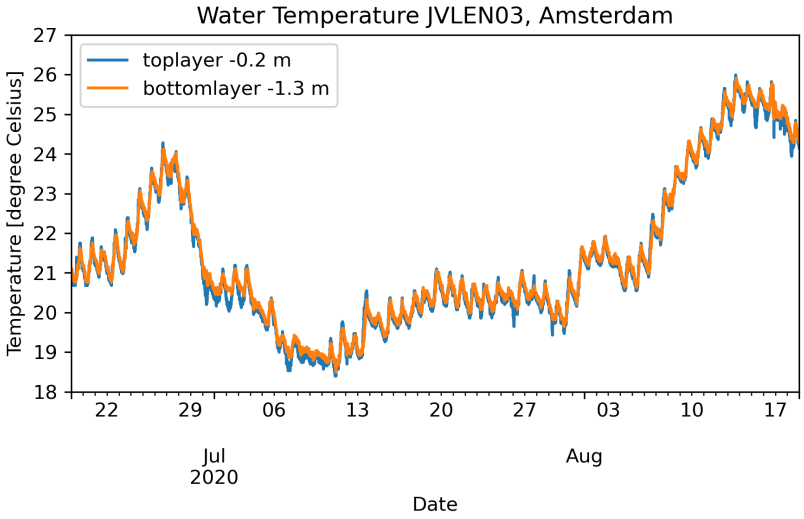

Figure 6.4: Water temperatures at approximately 20 cm below water surface and at 1.5 m below water surface (bottom) of the van Lennepkanaal, during summer of 2020.

6.1.2. Comparison of measurement results

In table 6.1, a short summary of the most important water temperature data from the measurement campaign is provided. As indicated by Boderie and Dardengo (2003), an important parameter when assessing water temperature variation and its relation to the distribution of incoming and outgoing heat fluxes, is the daily amplitude. Boderie and Dardengo (2003) proposed the use of an equilibrium amplitude, meaning the daily amplitude in water temperatures after the respective water body reached a thermal equilibrium. Although the surface water in the city canals never reaches a thermal equilibrium within the timeframe of the measurements, a depth-averaged daily amplitude according to the following calculation:

$$\text{Average Daily Temperature Amplitude} = \frac{\sum_{i=1}^{n} \left(T_{max_i} - T_{min_i}\right)}{2n_d} \tag{6.1}$$

where T_{max} and T_{min} are the maximum and minimum daily temperatures and n_d is the number of measured days.

	NWHER01	KEIZE01	DUIVV01	JVLEN01	JVLEN03	DACOS01	BILDE01
Mean Temperature [°C]	21.7	22.0	21.9	21.6	21.5	21.5	21.5
Maximum Temperature [°C]	26.5	26.8	27.9	26.1	26.0	26.6	26.6
Minimum Temperature [°C]	18.5	18.6	17.2	18.7	18.4	18.3	18.4
Average daily amplitude [°C]	0.49	0.44	0.62	0.38	0.45	0.49	0.47
Approximate local depth	3.2 m	2.9 m	1.9 m	2.3 m	1.5 m	2.1 m	2.1 m
Measured Secchi depth (at 20th of August 2020)	0.9 m	0.8 m	1.1 m	1.0 m	0.9 m	1.0 m	1.0 m
Modelled local flow velocity range (2015)	0 - 0.19 m/s	0 - 0.07 m/s	0 - 0.04 m/s	0 - 0.14 m/s	0 - 0.14 m/s	0 - 0.04 m/s	0 - 0.03 m/s

Table 6.1: Table of measured temperature data at several locations between 17th of June and 20th of August (NWHER01 = Nieuwe Herengracht, KEIZE01 = Keizersgracht, DUIVV01 = Duivendrechtse Vaart, JVLEN01 = van Lennepkanaal, JVLEN03 = van Lennepkanaal, DACOS01 = Da Costagracht and BILDE01 = Bilderdijkgracht)

It can be observed from the daily amplitude values in table 6.3 that the JVLEN01 location is indeed shaded for the largest part of the daytime, resulting in a low average daily amplitude. The JVLEN03 location, about 500 metres further in the canal, is less shaded by surrounding objects translating into higher daily variation and amplitudes. It can also be observed that at the more stagnant locations, DACOS01 , BILDE01 and DUIVV01 , average low flow velocities (weak dynamics) result in higher daily temperature amplitudes. Considering the other two weakly dynamic locations, KEIZE01 and DUIVV01, it can be found that the local water depth has a dampening effect on the daily amplitude in water temperatures. This dampening effect was also noticed by Boderie and Dardengo (2003), who studied the dampening effect of depth and bed on water temperature, see table 6.2. Especially the daily amplitudes found at KEIZE01 and DUIVV01, which are comparable hydrodynamically, are in good agreement with the values found in this table.

Water depth (m)	**0.3**	**0.6**	**1.2**	**2.4**	**4.8**
Non-conductive bed	2.9	1.5	0.8	0.4	0.2
Conductive bed	2.2	1.3	0.7	0.4	0.2

Table 6.2: Values for equilibrium surface water temperature amplitudes (depth-averaged) for different water depths without thermal exchange (non-conductive) and with thermal exchange (conductive) through the bed. The assumed equilibrium amplitude of air temperature (difference between day and night) above the water body is 6.5 °C. For shallow waters, thermal exchange through the bed is a significant factor determining the local water temperature. For deeper waters (above 1.2 metres deep), the dampening effect of the bed reduces considerably and becomes almost negligible. Table retrieved from Boderie and Dardengo (2003).

An exception is the Nieuwe Herengracht (NWHER01) location, which is the highest dynamic location in terms of flow. Here, despite the higher flow dynamics and larger depth, a relatively high average daily amplitude is found. A reason for this can be found in the location specific processes mentioned earlier, which induce higher temperature variation, especially at the deeper layers of the Nieuwe Herengracht.

6.1.3. Thermal stratification in city canals

Vertical measurements were performed to gain insight in thermal stratification in the city canals. Apart from analyzing the absolute temperatures, it is interesting to provide insight in the temperature differences between layers. Figure 6.5 provides an oversight of the measured water temperature differences at the bottom and the first layer measured above the bottom in relation to measured water temperature in the top layer. This was done for four locations in total. Apart from the two measurement locations in the van Lennepkanaal (a and b), the other two measurement locations have different hydrodynamic profiles to verify the influence of flow velocity on the development of thermal stratification in the city canals.

Generally, flow velocities in the entire city canal system are low and flow conditions are weak dynamic for almost every location in the city canals. However, from the figure 6.5, it can be noticed that even small differences in flow velocity have an effect on the development of thermal stratification in the canals. At the Da Costagracht for example (figure c in 6.5), where conditions are merely stagnant, temperature differences at the bottom can become 2.2 °C lower than the top layer, while under more dynamic conditions, in the van Lennepkanaal (a and b) temperature differences amount to 1.0 °C at maximum. At the Keizersgracht , where flow conditions are classified as weak dynamic, the degree of thermal stratification can be found in between the three other locations.

Another important difference determining the degree of thermal stratification, is the amount of incident sunlight or shortwave radiation penetrating the respective canal water body. The blue line in the graph of the first measurement location in the van Lennepkanaal (JVLEN01) shows that for locations with a high amount of shadow during daytime, water layers higher in the vertical water column are more uniform in relation to the top layer. The second location in the van Lennepkanaal (JVLEN03) has less shadow, which translates into larger water temperature differences also higher in the water column. The same can be observed from the blue lines of other two locations, which are both also sunnier. The shadow effect on the canal water body, can also be observed from the moments in time where the bottom layer is warmer than the top layer. This situation occurs when the atmosphere is cooling the top layers and water near the bottom stays warmer and slowly exchanges heat with the higher vertical water layers. For the sunny locations, this situation occurs more often and the positive temperature differences are also higher in magnitude.

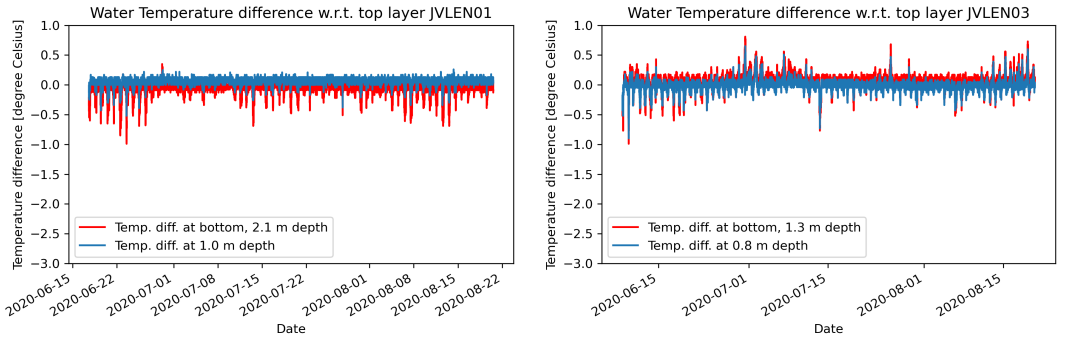

(a) Water temperature differences at van Lennepkanaal (JVLEN01), moderately weak dynamic (0-0.14 m/s)

(b) Water temperature differences at van Lennepkanaal (JVLEN03), moderately weak dynamic (0-0.14 m/s)

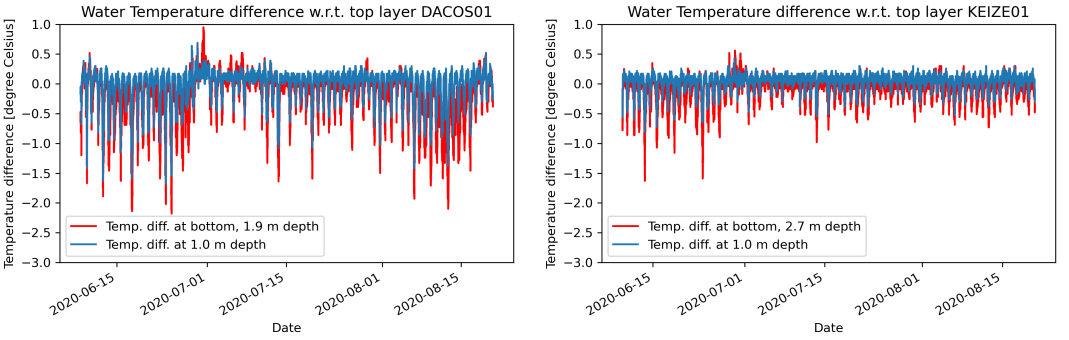

(c) Water temperature differences at Da Costagracht (DACOS01), stagnant conditions (0 - 0.04 m/s)

(d) Water temperature differences at Keizersgracht (KEIZE01), weak dynamic (0 - 0.07 m/s)

Figure 6.5: Measured temperature differences of two layers in relation to the top layer water temperature for four measurement locations with different hydrodynamics.

A last visible aspect that plays a role in the vertical temperature distribution is the local depth of the city canal. At the shallowest location, JVLEN03, water temperatures at the bottom (the red line) are generally higher than the water temperature in the top layer. This effect can be attributed to the sunlight that is able to penetrate into the bed and heats up the bed material. For deeper locations such as the Keizersgracht (KEIZE01), the sunlight or shortwave radiation is attenuated in the water body itself before reaching the bed, resulting in a bed that is less heated and lower temperatures in water layers nearby the bottom.

6.2. Model validation on meteorological conditions

In the process of building a representative heat model for the city canals in Amsterdam, the model was validated for different metereological model forcings and compared with the water temperature measurements taken in the canals of Amsterdam (see section 3.5). The validation of the model was executed based on three meteorological forcing combinations. The composition for each of these three meteorological forcing combinations is further described in table 6.3. For each of the validation steps, the model simulation were run for the entire summer period of 2020, from April 23 to September 7.

Validation step	Application domain	Meteorological forcing combination
1. Rural	City canal grid + model boundaries from validation step 1	1. Cloud fraction F_c: MODIS 2. Air temperature T_a: Schiphol weather station 3. Wind speed U_{10}: Schiphol weather station 4. Shadow model: no shadow effects (PSA = 0)
2. Urban	City canal grid + model boundaries from validation step 1	1. Cloud fraction F_c : MODIS 2. Air temperature T_a: Oud-West Wiegbrug weather station 3. Wind speed U_{10}: Schiphol weather station corrected with urban wind model (di Sabatino (2009) and Mertens (2003)) 4. Shadow model: no shadow effects (PSA=0)
3. Urban with shadow effects	City canal grid + model boundaries from validation step 1	1. Cloud fraction F_c: MODIS 2. Air temperature T_a: Oud-West Wiegbrug weather station 3. Wind speed U_{10}: Schiphol weather station corrected with urban wind model (di Sabatino (2009) and Mertens (2003)) 4. Shadow model: Partial Shaded Area (PSA) model by Shashua-Bar and Hoffman (2003)

Table 6.3: Combinations of meteorological model forcing used for the validation process.

To get insight in the accuracy of the created Delft3D temperature model, modelled water temperatures were compared with measured water temperatures at multiple depths and for each of the three meteorological forcing combinations. In figure 6.6 water temperatures in top and bottom layers are plotted at the shallow depth measurement location JVLEN03 in the van Lennepkanaal, where the canal is approximately 1.6 meters deep.

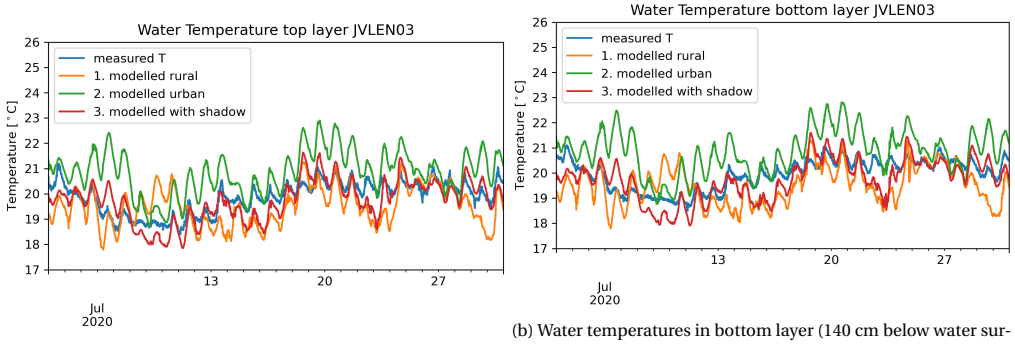

(a) Water temperatures in top layer (20 cm below water surface).

(b) Water temperatures in bottom layer (140 cm below water surface).

Figure 6.6: Measured (blue) and modelled water temperatures in top and bottom layers for the month July 2020 at Jacob van Lennepkanaal (measurement location JVLEN03).

To validate the model, spatially varying water temperatures in the vertical, and at different locations in the city canal system, were compared with observed water temperatures. For every measured depth, basic statistic values were computed such as the mean error ($ME = T_{mod} - T_{meas}$), root mean square error ($RMSE = \left(\sum_{i=1}^{n}\left(T_{mod_i} - T_{meas_i}\right)^2 / n\right)^{1/2}$), mean absolute error ($MAE = \frac{1}{n}\sum_{i=1}^{n}\left|T_{mod_i} - T_{meas_i}\right|$) and the R-squared value as a measure for comparing variations between measurements and modelled water temperature values ($R^2 = \frac{\sum\left(\hat{T}_{mod_i} - \bar{T}_{mod_i}\right)^2}{\sum\left(T_{mod_i} - \bar{T}_{mod_i}\right)^2}$). For all of the validation steps, the results of this analysis are summarized in figure 6.7, again for measurement location JVLEN03.

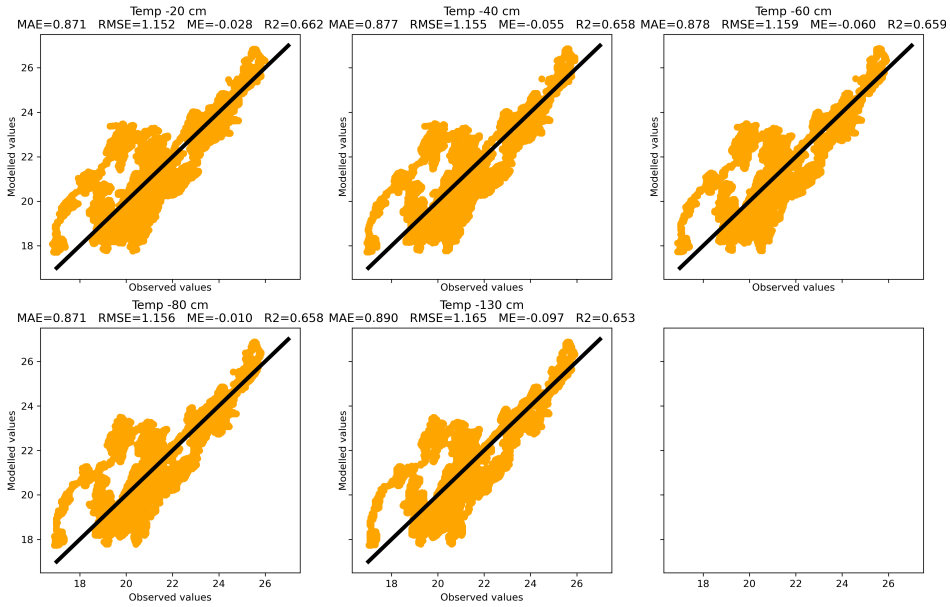

(a) Results validation step 1: Rural (Schiphol meteorology).

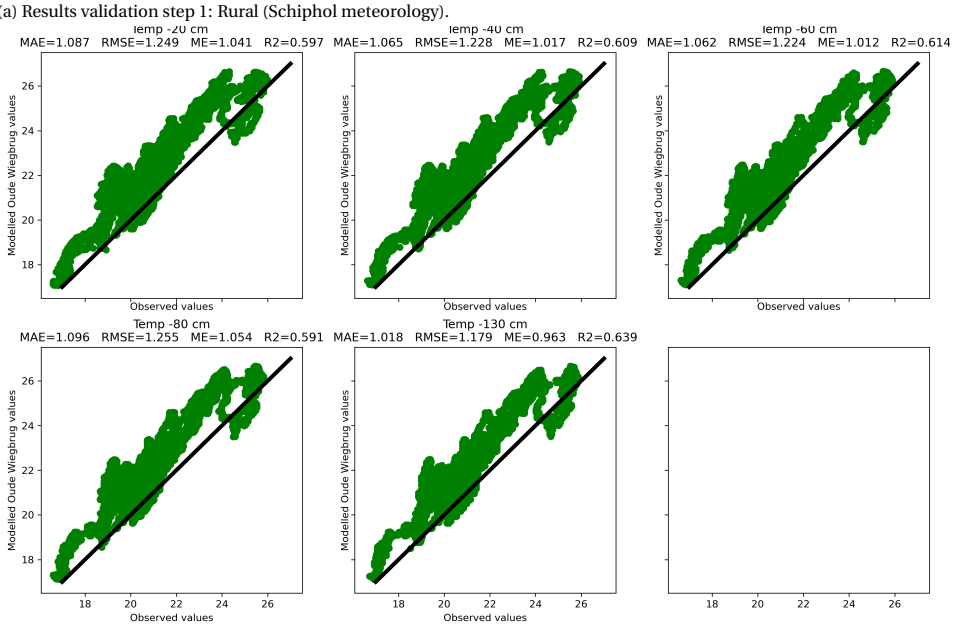

(b) Results validation step 2: Urban (Oud West Wiegbrug meteorology).

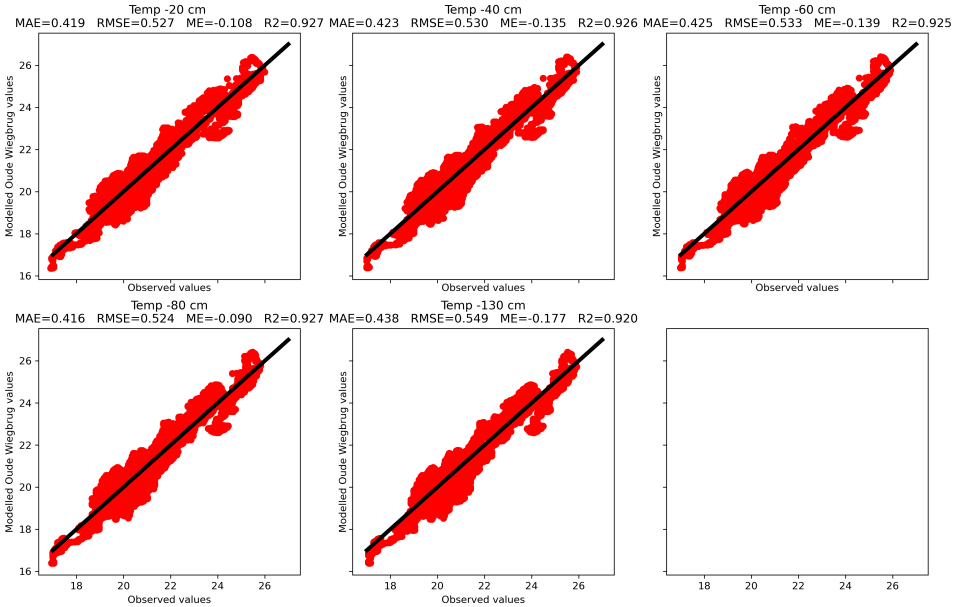

(c) Results validation step 3: Urban with shadow effects.

Figure 6.7: Scatter plots of observed (horizontal) versus modelled water temperatures (vertical) [°C] at Jacob van Lennepkanaal (measurement location JVLEN03) for different water depths and for each validation step.

It can be observed that validation step 3 with urban meteorological conditions and accounting for the shadow effects by buildings (in red), provided the best fit with the observed water temperature values on all described statistical parameters. Differences regarding the considered statistical parameters were found to be small at different depths in the water column and almost negligible. For validation step 3, the RMSE values range from 0.52 to 0.55 °C, MAE ranges from 0.42 to 0.44 °C and ME ranges from -0.09 up to −0.14 °C at measurement location JVLEN03. These descriptive statistics and the scatter plots in figure 6.7 demonstrate that the composed Delft3D model is able to represent the energy balance and related water temperatures of a city canal reasonably well. It also demonstrates the importance of carefully selecting a meteorological forcing combination appropriate for the local urban weather conditions. The incorporation of a shadow correction for the incoming shortwave solar radiation for example, since it the largest meteorological model force in terms of heat flux, resulted in a considerable quality improvement of the temperature model from validation step 2 to 3 significantly for the van Lennepkanaal (RMSE reduced on average with 57% and MAE 60%).

Found ME values are small, indicating that the long term average of the thermal energy budget or change in equilibrium water temperatures over longer periods of time are accurately modelled. From the relatively high MAE and RMSE values however, it follows that the fit of validation step 3 for short term fluctuations, e.g. on a daily timescale, is less representative, which can also be observed in figure 6.6 by comparing the modelled water temperatures of validation step 3 (red line) and the measured water temperatures (blue line). During daytime of some days, water temperatures are overestimated by the model and, during nighttime, cooling processes are generally overestimated leading to an underestimation of water temperatures during nighttime. This pattern implies that modelled daily water temperature amplitudes, as calculated by equation 6.1, deviate from the daily amplitudes measured by the loggers in the city canal.

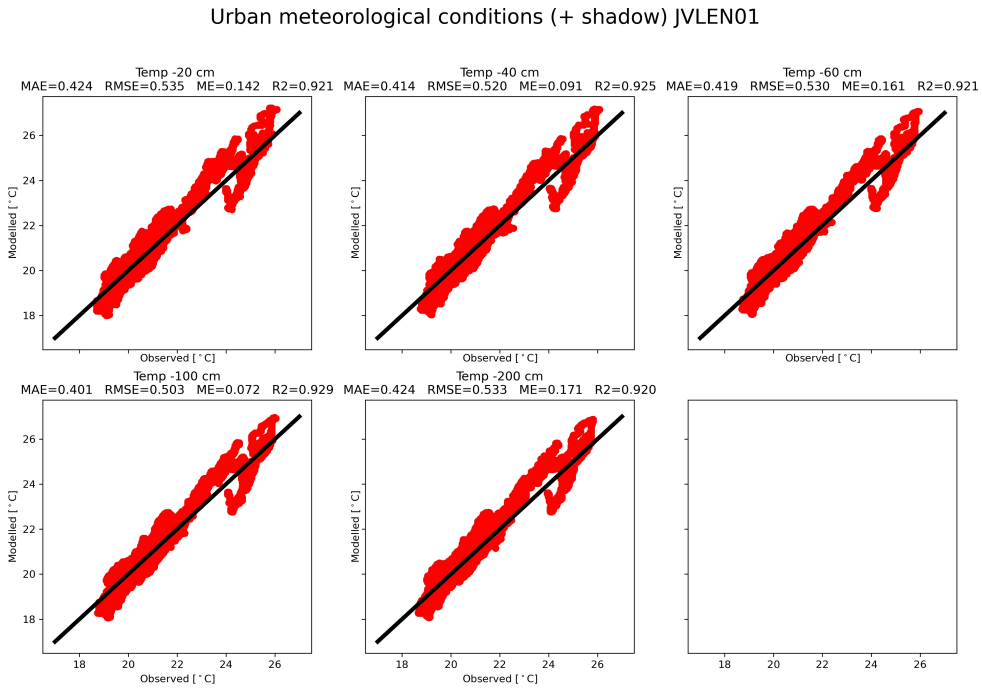

Figure 6.8: Scatter plot of observed (vertical) versus modelled water temperatures (vertical) for different water depths at JVLEN01 measurement location, validation step 3: urban meteorological conditions + shadow model.

The same analysis can be elaborated for a deeper measurement location, for example JVLEN01 in the van Lennepkanaal. The local water depth at this location is approximately 2.3 meters. In line with the findings in table 6.2, the expectation is that the daily amplitude would be slightly lower due to a reduced dampening effect of the bottom for deeper waters. From figure 6.8 it follows that descriptive statistics for this location are comparable with the JVLEN03 figures: the RMSE ranges from 0.5 to 0.53 °C, MAE ranges from 0.4 to 0.42 °C and ME from 0.1 to 0.2 °C. The positive values for ME indicate that JVLEN01 is indeed a more shadow rich location than JVLEN03 and that the model locally overestimates the water temperature over longer periods

of time. Again, this emphasizes the heterogeneity of the urban landscape where shadow and solar radiation patterns and where especially for weakly dynamic systems, such as the city canal system, differences in water temperature are visible on microscale.

6.2.1. Daily mean amplitude

To evaluate the earlier stated presumption that daily amplitudes might be overestimated by the created Delft3D model, average daily amplitudes were plotted for all validation steps and compared with the measured daily amplitudes. Figure 6.9 shows the results for both locations, JVLEN01 and JVLEN03. It can be clearly observed that daily amplitudes are overestimated by the model, especially for the shadow rich measurement location JVLEN01. JVLEN01 receives additional shadow that has not been modelled. For location JVLEN03 amplitude values modelled by validation step 3 are more accurate: 0.09 °C temperature difference in amplitude in the top layer and 0.22 °C in the bottom layer. In depth analysis showed that the difference in modelled amplitude gradient over depth between the two points can be explained by enhanced vertical mixing in the water column at JVLEN03. Comparing the averaged vertical velocity components, it was found that JVLEN03 has on average 3.4 times higher vertical transport values, resulting in a more flattened out modelled amplitude gradient over water depth and a locally less stratified temperature profile. A possible explanation is the nearby bed level gradient and the position of this location near the banks of the canal.

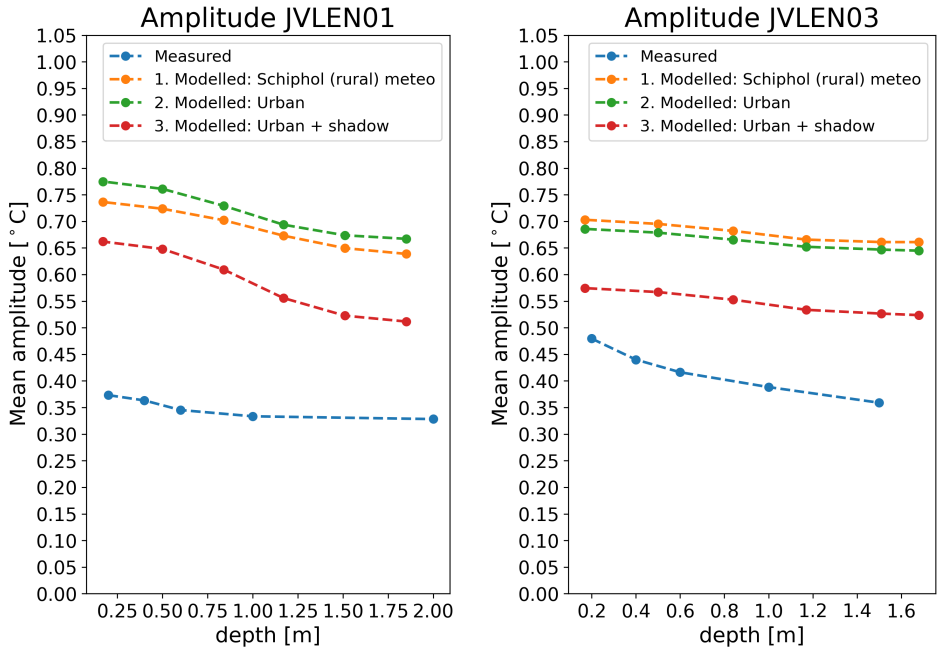

(a) Measured and modelled mean daily amplitudes at JVLEN01 location.

(b) Measured and modelled mean daily amplitudes at JVLEN03 location.

Figure 6.9: Measured and modelled mean daily amplitudes in van Lennepkanaal.

6.2.2. Error sources

When studying the sources of error, the mean daily amplitude values show that local meteorological differences have a major influence on the representativity of the local water temperature in a city canal. In the created Delft3D model, a uniform meteorological forcing was applied. This generalization leads to inaccuracies at specific locations, such as the JVLEN01 which has relatively few hours of direct sunlight. Also the blocking effect of houseboats and shadow effects of bridges were not included. This could lead to overestimation of the effect of solar radiation on the temperature profiles. Incorporating these obstacles could reduce the error in daily amplitude of the modelled water temperatures in the city canal.

Another error source is the assumption that the bottom of the city canal is non-conductive, meaning that there is no energy exchange at the bottom. Table 6.2 in section 6.1.2 clearly shows the dampening effect that

the bottom of a surface water could have. Excluding this thermal exchange at the bottom could lead to deviations in the modelled water temperatures, especially near the bottom. The bottom dampening effect is largest in shallow waters that are less than 1.2 metres deep, but could still influence the water temperature at larger depths in deeper surface waters (Boderie and Dardengo, 2003). From the measurements taken in the city canals, see figure 6.5 for example, it follows that also in city canals it is possible that the canal bottom behaves as a heat source for the deeper water layers, translating into higher temperatures near the bottom relative to the water temperature in top layers. The dampening effect of the bottom is bidirectional. However, the magnitude of thermal exchange through the bottom remains limited. Boderie and Dardengo (2003) reports an average heat flux to and from the bottom of 2.0 W/m^2 for an increase or decrease of bottom temperature of 5.0 °C within 90 days, which seems a well-reasoned estimate for the van Lennepkanaal case where the long term amplitude of the water temperature measurements over the entire summer period is around 5.0 °C (see figure 6.1, 6.2, 6.3 or 6.4).

The effect of mixing by canal navigation is currently not modelled. The blades of ship engines passing through the city canals induce extra mixing in the canal, especially during daytime. Vertical mixing induced by boats could alter the local temperature profile over the depth of the canal. Related to the mixing by navigation are the optical properties of the surface water body. Closure of the city canals for pleasure craft activities during the COVID19 crisis in 2020 showed that reduced mixing by boats translates in high water clarity (Meershoek, 2020) and higher Secchi depth values in the city canals. As described in section 4.4.1 on solar radiation, the absorption of short wave solar energy in the water column is related to the turbidity of the surface water. To account for this, the Secchi depth is used as a representative parameter in the Delft3D model. In the model, a constant average value for the Secchi depth of the canals was chosen of 1.0 metres, based on measurements elaborated on August 20, 2020, see table 6.1. However, the optical properties of canal water could significantly change spatially and temporally. During the measurement of Secchi depths at several locations, Secchi depth values ranged from 0.6 up to 1.1 metres. However, during periods of high navigational activity, Secchi depths have been reported of only 0.4 metres in the Amsterdam city canals (Meershoek, 2020). These significantly lower Secchi depths lead to increased absorption of solar radiation energy in the top layers and could enhance formation of extra thermal stratification. This effect is not accounted for in the created model.

The hydrodynamics in the canal have been modelled using historical hydrodynamic data of the year 2015. For this year, water balances of the upstream polders and discharge regimes through the sluices in IJmuiden are known. Using the hydrodynamics of another year than the meteorological forcing, namely the year 2020, induces an inevitable error in the modelled temperature profiles when comparing to the measurements. Different canal discharges could alter thermal stratification patterns and could bring thermal energy into the canal from adjacent waters or abduct thermal energy through advection, leading to either heigher or lower water temperatures. The city canals are a weakly dynamic system, where differences in discharges are limited and, for a large part, related to the local precipitation determining the discharge of surplus water from upstream polders and the discharge in the Amsterdam Rijnkanaal related to discharges in the river Rhine. From a hydrological perspective, the summer of 2015 could be characterised as dry in the month of June (27 - 30 mm) , moderately wet in July (94 - 129 mm) and wet in the month of August (137 - 146 mm), see table 6.4.

Month	Monthly rainfall KNMI 2015 [mm]	Monthly rainfall KNMI 2020 [mm]	Average Discharge ARK Weesp (2015 Rijkswaterstaat)	Average Discharge ARK Weesp (2020 Rijkswaterstaat)
June	27 - 30 mm	73 - 89 mm	44.7 m3/s	44.5 m3/s
July	94 - 129 mm	77 - 94 mm	44.9 m3/s	45 m3/s
August	137 - 146 mm	87 - 122 mm	45 m3/s	45.5 m3/s

Table 6.4: Hydrodynamic forcing data of the city canal system for years 2015 and 2020.

If all other conditions would be assumed constant, the expectation would be that discharges in the van Lennepkanaal would increase during the summer from June to August. However, modelled monthly averaged absolute discharges for the van Lennepkanaal in table 6.5 show another pattern. Although the mean discharge in 2015 of the other important hydrodynamic forcing mechanism, the Amsterdam Rijnkanaal, is regulated and indeed nearly constant in the Amsterdam Rijnkanaal (around 45 m^3/s), the direction and magnitude of the flow in the van Lennepkanaal seem less sensitive for an increase in local precipitation. At the

macroscale of the city canal system, a complex system of other factors in the water balance such as water retention and water storage in the upstream polders, the pumping regime in IJmuiden and timing of discharge peaks in the Amsterdam Rijnkanaal also influence the eventual discharge pattern in the Van Lennepkanaal. A complete study towards the hydrodynamic behaviour of the entire system could possibly clarify this system response. This is considered out of the scope of this study. Therefore, although the presented dataset in tables 6.4 and 6.5 is limited to only 3 months in the summer of 2015, it can be concluded that the order of magnitude of the discharge is comparable under different hydrological and system hydrodynamics. Also considering that there are no large differences in magnitude of rainfall and discharge in the Amsterdam Rijnkanaal for the year 2020 compared to 2015, errors within the van Lennepkanaal are assumed to be small over longer time periods and the use of hydrodynamical data of the year 2015 can be justified from this perspective.

Month	Mean modelled absolute discharge	Primary direction of flow	Minimum discharge (downstream)	Maximum discharge (upstream)
June	1.03 m3/s	Upstream towards polders (57% of time)	-5.28 m3/s	2.52 m3/s
July	1.21 m3/s	Downstream towards IJ (60 % of time)	-6.44 m3/s	2.34 m3/s
August	0.82 m3/s	Upstream towards polders (53% of time)	-4.35 m3/s	3.62 m3/s

Table 6.5: Modelled hydrodynamic data for the year 2015 in the van Lennepkanaal.

Since the validation of the model was elaborated on a larger grid for all city canals, a larger grid spacing was chosen. A grid cell for these validation computations was on average 10 x 20 metres. For each grid cell, the local bed level is averaged over the extent of the grid cell based on bed level values at the grid cell corners (grid cell nodes). Bed levels were computed for each grid cell considering all the faces of the cell and determining the bed level based on the lowest pair of grid nodes. Especially for larger grid sizes, this leads to less accurate local bed levels and related water depths. As described in sections 6.1.2 and 5.5.1, water depths have an influece on the amplitude of the water temperature. Underestimation or overestimation of water depths could lead to respectively higher and lower values for the local water temperature amplitude. For the model study towards the effects of SWH systems, a smaller grid focused on the van Lennepkanaal and smaller grid cell sizes were used, on average 2.5 x 9 metres. A sensitivity study towards the effect of grid cell size on mixing of the surface water and modelled water temperatures was not executed.

Analysis of the water temperatures and the daily temperature amplitudes in the van Lennepkanaal, showed that especially during nocturnal cooling processes the city canal water temperatures were overestimated. During nighttime, heat escapes an urban water body through long wave radiative cooling, latent heat, sensible heat and by means of conduction through the bed material. Solcerova et al. (2019) found that radiative cooling is the dominant cooling heat flux making up around 43% (± 14 %) of the total heat flux for a pond situated in an urban environment. Also in our model. (figuur met heat fluxes invoegen).. The cooling of an urban surface, such as an urban water body, is limited by the so-called Sky View Factor (SVF) denoting the ratio of visible clear sky for a specific location related to clear sky conditions in an open field (Oke, 1981), see figure 6.10 for the difference in SVF for an open field and within an urban canyon. The urban canyon situation is also applicable for a typical city canal in Amsterdam. Within such an urban canyon, the SVF value is lower than 1, meaning that the clear sky view is blocked by urban obstacles or buildings. This reduces the outgoing long-wave radiation for urban surfaces, such as a city canal, during day and during nighttime. At the same time, incoming long-wave radiation is increased due to the nearby heated urban surfaces emitting long-wave radiation. This phenomenon is at its peak at the end of the day and during nighttime when rocky urban surfaces have been heated up by the sun and attain their highest temperatures. The SVF is therefore also an important attributor to the UHI effect. The SVF was not taken into account in the considered energy balance in the Delf3D model, inducing an error, especially in the nighttime cooling process. Excluding the SVF could be an explanation for the underestimation of nighttime water temperatures and the overestimation of daily water temperature amplitudes.

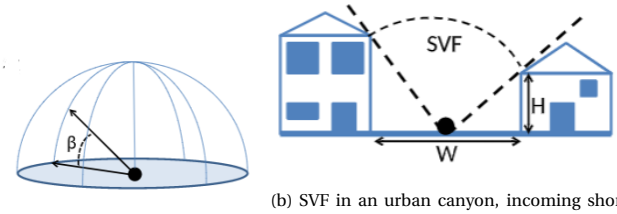

(a) 3D representation of SVF in an open field, SVF = 1.

(b) SVF in an urban canyon, incoming short wave radiation and outgoing longwave radiation is blocked by urban obstacles, SVF < 1.

Figure 6.10: Schematic representation of SVF situation in an open field and urban canyon. Figure retrieved from Dirksen et al. (2019).

6.3. Modelling results

For each of the described scenarios in section 5.6, simulations were executed with the described Delft3D model. In this chapter, the results of the model runs will be visualized and explained in the context of the scope of this research: the thermal effects of installation of SWH systems in the city canals. The first part of this chapter describes the results related to the installation of 1 system. The second part will focus on the hypothetical case with respectively 2 and 3 installed systems in the van Lennepkanaal and attempts to assess the effect of future accumulation of systems. The final part focuses on the system capacity, recirculation issues and an attempt is made to extrapolate the findings towards heating capacity of the entire city canal system of Amsterdam.

6.4. Thermal effects of a SWH system on a canal

6.4.1. ΔT profiles along the van Lennepkanaal

For the scenarios 1.50 through 1.350, with SWH system 1 extracting a maximum of $\Delta T = 5$ °C of thermal energy, temperature profiles were created within the van Lennepkanaal. Temperature differences (ΔT) are computed in relation to a reference scenario. For each intake/outfall distance, reference scenarios were modelled with an identical SWH system extracting an identical discharge Q, but without extracting heat ($\Delta T = 0$). In this way, it was assured that temperature differences in the receiving surface water originate only from thermal extraction and temperature differences due to changes in hydrodynamics were left out of the equation.

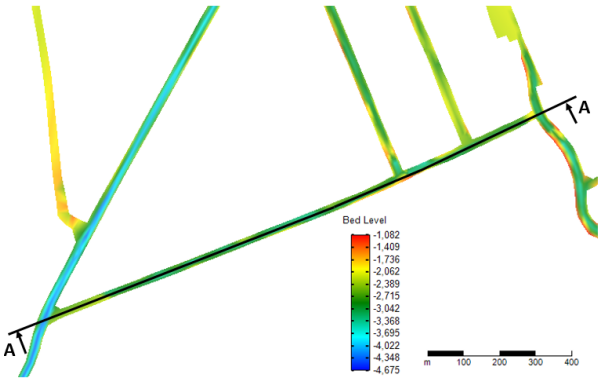

Figure 6.11: Cross section position for result analysis.

For each scenario, the model was run for the entire period between May 29^{th} and September 30^{th} of the year 2020 with hydrodynamic profiles originating from the year 2015. The results have been extracted from the model through the middle of the van Lennepkanaal, see cross section A in figure 6.11, at approximately 11 metres from both canal quay walls. For the scenario 1.200, where the designed distance between intake and outfall is 200 metres, averaged thermal profiles are displayed in figure 6.12 for two moments in time: at the end of the night 04:00 (UTC+2) and in the middle of the day 14:00 (UTC+2). These particular moments in time were chosen to provide insight in the influence of solar radiation processes.

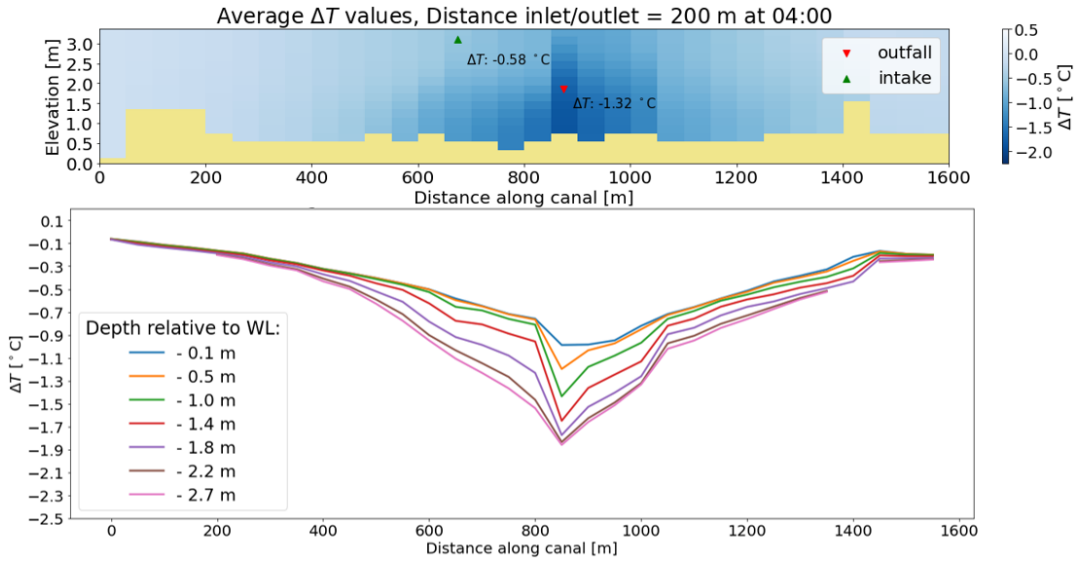

(a) Temperature profile at 04:00 (UTC+2).

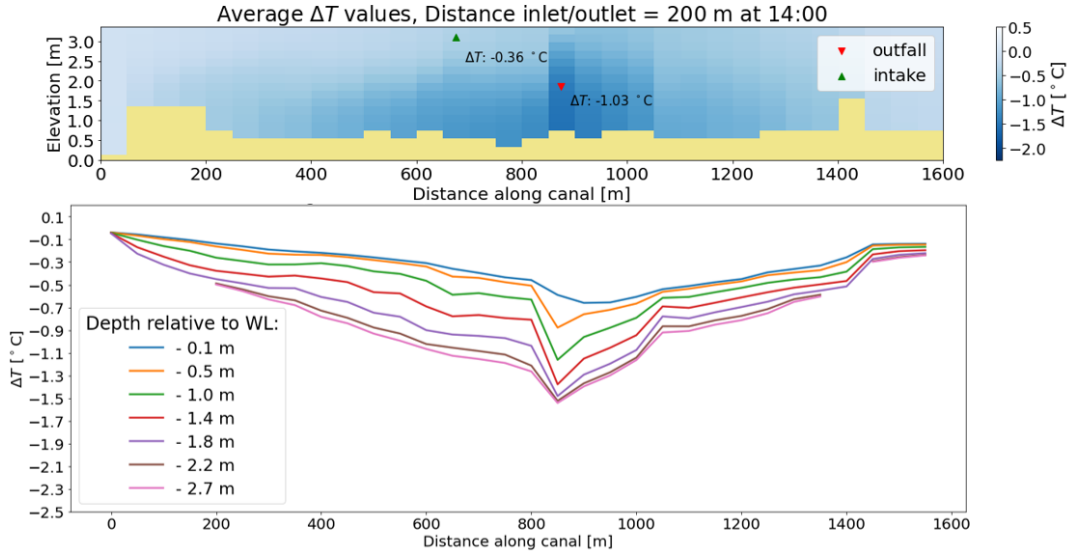

(b) Temperature profile at 14:00 (UTC+2).

Figure 6.12: Averaged temperature profiles and intake and outfall temperatures as well as their positions in the water column for two different moments in time. Profiles are presented through cross section A, see figure 6.1, approximately 10 metres away from the inlet and outfall near the canal quay walls.

From figure 6.12, the influence of radiation can be clearly observed in the 2D cross section plots. Comparing the nighttime and daytime profiles, it can be seen that the modelled radiation at 14:00 penetrates over the entire depth of the canal and reduces the average ΔT imposed by the SWH system everywhere in the canal. At the point with highest Δ_T in the profile, positioned at the bottom underneath the outfall, temperature difference ΔT decreased in magnitude from $-1.86\,°C$ to $-1.54\,°C$. A decrease was also observed at the intake in the top layer of the canal, where ΔT decreased in magnitude from $-0.58\,°C$ in the night to $-0.36\,°C$ at daytime due to the energy of the incoming sunlight. From the figure it can also be observed that the influenced area or extent of the cold water plume originating from the SWH system stretches out over the entire length of the canal.

The ΔT profiles were created by extracting information from the unstructured grid of the Delft3D model through observation stations that were implemented in the model every 50 metres along the canal. The presented 2D cross section therefore seem to have a spatial spacing of 50 metres, but in reality, the model has a grid spacing in longitudinal direction varying between approximately 6 to 9 metres nearby the SWH system and 20 metres further away along the canal. The presented ΔT values therefore seem coarser with a more

jumpy gradient, while the modelled values actually follow a more gradual coarse.

It also has to be recalled that the presented ΔT values are averaged over the entire operable period of the SWH system for a specific time of day. During system operation, the temperature profile might change considerable depending on the weather conditions at a specific moment in time. These fluctuations are not visible in the averaged ΔT values. However, the presented averaged temperature differences provide an idea of the themal influence and extent of the plume in the van Lennepkanaal. For example, another observation that can be made is that during the day, ΔT values are higher on average, but there is also more stratification visible in the ΔT profile compared to the nighttime values. Apparently, the incoming short wave radiation from the sun enhances the forming of stratification and ΔT values are less likely to mix over the vertical. An explanation for this phenomenon could be that layers higher in the water column heat up more and differences in the temperature dependent water density are increased during the day, preventing the lower layers, which are colder and therefore heavier, of mixing with the upper layers. During nighttime it can be observed that the ΔT pattern is indeed colder and more uniform over the vertical mixing.

6.4.2. Cross sectional ΔT profiles

To provide insight in the third dimension, figure 6.13 shows the cross section profiles of the averaged temperature differences at 4 locations in the van Lennepkanaal at 14:00 (UTC+2). Especially the cross section at the outfall location is interesting, figure c in 6.13. It shows the near field of the outfall and it can be derived that overall the cold water discharge sinks to the bottom, almost immediately. Only in the second row of grid cells, the discharge cold water seems to increasingly flow upward and reaches to the water surface, indicated by the lower ΔT values found at this location. This behaviour could be explained by the vertical two-equation turbulence model in Delft3D, in which turbulence parameters are transported from one grid cell to next grid cell. The large velocity gradients between the cold water discharged by the SWH outfall and the ambient water result in increased turbulence and induced mixing over the entire vertical in this particular case. The hydrostatic Delft3D model is not the ideal model to capture these type of near field processes at this scale and therefore this temperature field might not be representative, as indicated in section 4.3.1. Also, the grid spacing might not be appropriate for this problem. The forming of wakes and eddies by turbulence cannot be explicitly modelled at this grid size. However, further from the outfall, buoyancy starts to dominate the flow and the cold water sinks to the bottom and spreads out. At this scale, the mid-field and far-field, Delft3D is a suitable model, provided that the modelled near-field is not dramatically deviating from reality (Baptist et al., 2005).

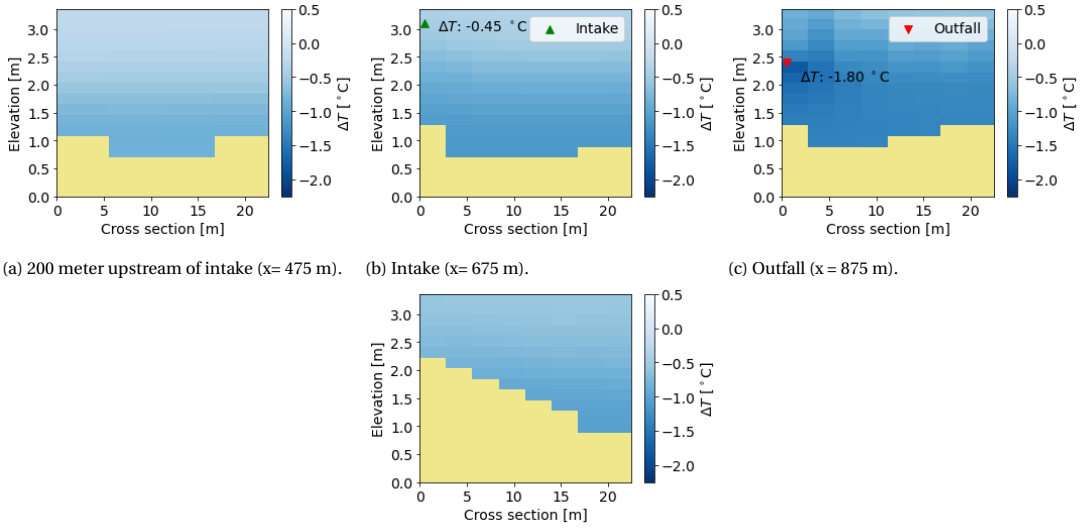

(a) 200 meter upstream of intake (x= 475 m).

(b) Intake (x= 675 m).

(c) Outfall (x = 875 m).

(d) 175 meter downstream of outfall (x = 1050 m) at Bilderdijkgracht intersection.

Figure 6.13: Cross sectional ΔT profiles at 4 locations in the Jacob van Lennepkanaal at 14:00 (UTC+2)..

6.4.3. Heat flux profiles along the van Lennepkanaal

Another way of observing the model results is by analyzing the heat fluxes passing through the water surface and exchanging thermal heat with the atmosphere along the canal. Hourly averaged heat flux differences (ΔQ) relative to the reference scenario, are displayed in figure 6.14 for scenario 1.200 with system 1 (ΔT = 5.0 °C) and scenario 1.75.200 with system 2 (ΔT = 7.5 °C). For each system, two moments during the day are selected, again at 04:00 and 14:00 (UTC+2).

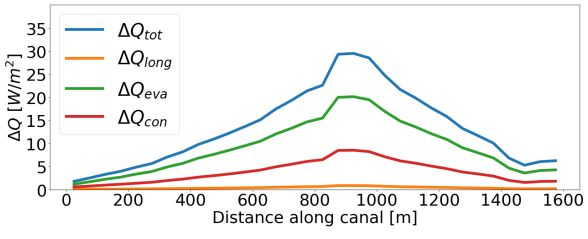

(a) Heat flux profile at 04:00 (UTC+2) scenario 1.200: system 1 (ΔT = 5.0 °C).

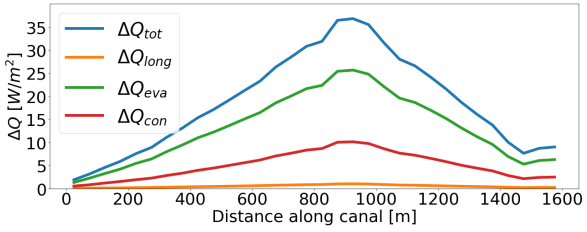

(b) Heat flux profile at 04:00 (UTC+2) scenario 1.75.200: system 2 (ΔT = 7.5 °C).

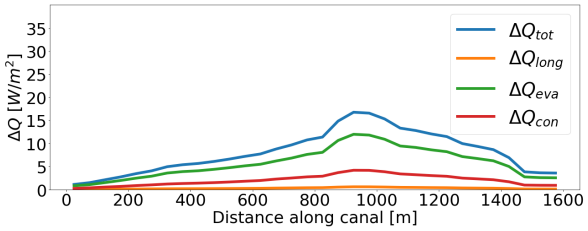

(c) Heat flux profile at 14:00 (UTC+2) scenario 1.200: system 1 (ΔT = 5.0 °C).

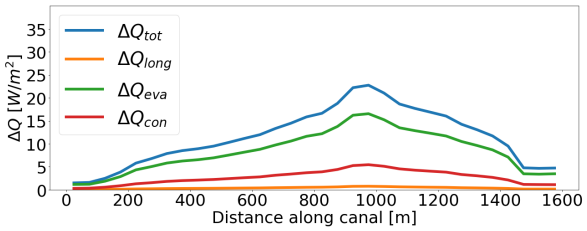

(d) Heat flux profile at 14:00 (UTC+2) for scenario 1.75.200: system 2 (ΔT = 7.5 °C).

Figure 6.14: Profiles of heat flux differences related to the reference situation at the water surface during system operation. Profiles are presented through cross section A, see figure 6.1, approximately 10 metres away from the inlet and outfall near the canal quay walls.

The ΔQ values in figure 6.14 represent the difference between the heat fluxes in the scenarios with modelled SWH systems and the reference scenario without an active modelled SWH. System 2 generates higher temperature differences (ΔT) at the water surface and, as a result, the temperature dependent heat flux components of the energy balance, i.e. the long wave radiation (Q_{long}), latent heat flux or evaporation heat flux (Q_{eva}) and sensible heat flux or conductive heat flux (Q_{con}), attain higher values in relation to the reference scenario. The modelled SWH system pushes the surface water temperature away from its equilibrium water temperature and a higher ΔT in modelled water temperatures results in a higher driving force back towards this equilibrium. In the heat balance, the magnitude of this driving force is determined by the combination of the mentioned temperature dependent heat fluxes. When the surface water is cooled, which is the case for SWH systems used for heating, the thermal deficiency is supplied by the atmosphere through sunlight, but the driving force towards equilibrium is the reduction in the outgoing heat fluxes. Another finding related to this is that, due to the effect of solar radiation, which heats the canal during daytime and reduces the ΔT especially in the top water layers, the temperature dependent heat flux differences (ΔQ) reduce in magnitude during the day and increase during nighttime. Eventually, when time evolves and the plume develops in the canal, this translates into an increase in daily water temperature amplitude within extent of the cold water plume. This higher amplitude is thus a result of the daily solar radiation and its extinction over the vertical, resulting in a stratification effect during the day and less stratification during nighttime.

Because both the values for ΔT and ΔQ at the water surface are known for the modelled results, it is also possible to find a value for the self cooling rate or heat exchange coefficient K in a simplified steady state surplus heat ΔT model, as described in section 2.2.5 of chapter 2. Since the Delft3D model of this study has been validated on meteorological forcing with actual water temperature measurements in the van Lennepkanaal, the value for K could serve as a well-founded estimate for real thermal exchange with the atmosphere averaged over an entire thermal energy extraction cycle (summer period). Boderie and Dardengo (2003) executed a study towards the use of heat exchange coefficients K for the modelling of surplus heat models. The heat exchange coefficient or self cooling rate can be derived by the following definition:

$$K = -\frac{\partial Q_{tot}}{\partial T_w} \approx -\frac{\Delta Q_{tot}}{\Delta T} \tag{6.2}$$

Boderie and Dardengo (2003) describe that derivation of K is primarily dependent on water temperature and local wind conditions and it is advised to avoid the use of constant cooling rates for water temperature differences above 3.0 °C. In this study, the water temperatures in the summer period are modelled with a meteorological validated model and change in heat flux differences are determined related to a reference scenario and subsequently averaged over the entire period. Using the average ΔQ over the entire summer period, as displayed in figure, together with the modelled water temperature differences in the top layer, average K values for the van Lennepkanaal vary within the plume between 27.6 and 28.4 $W/m^2/°C$ within the summer period. If one were to relate the self cooling rate to the average ΔT over the vertical (depth-averaged), to account for the earlier mentioned stratification effect, K values are lower and vary between 17.5 $W/m^2/°C$ near the SWH outfall and 25.6 and 26.5 $W/m^2/°C$ at the canal ends (the intersections with adjacent canals), see figure 6.15.

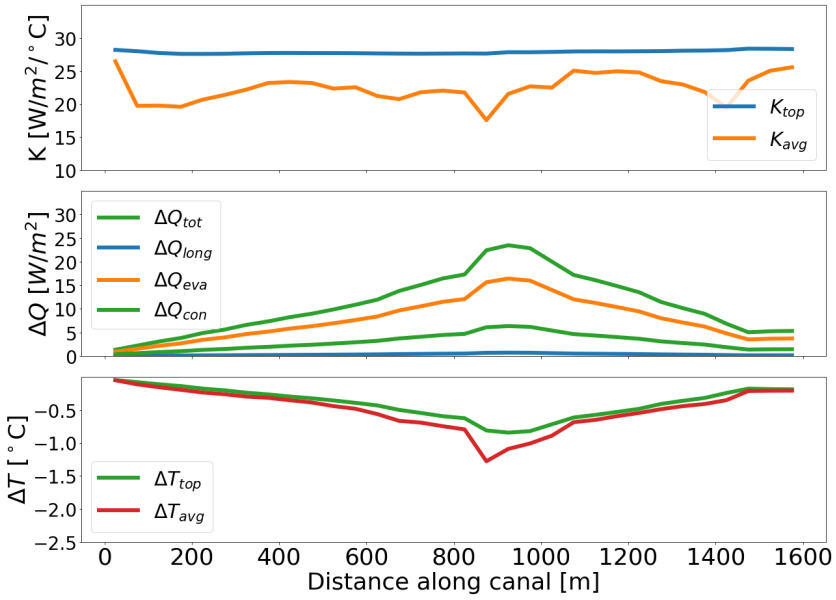

Figure 6.15: Cross sectional plots of modelled self cooling rates (K), average heat flux difference ΔQ and top and average temperature differences ΔT relative to reference scenario without SWH.

6.4.4. Steady state solutions

The result in figure 6.15 also shows the need for a three-dimensional model, where different mixing patterns over the vertical and horizontal, which result in different thermal heat exchange patterns, are to be modelled accurately. A surplus heat model, such as the simple ΔT model in chapter 2, is a simplified form of a complete heat balance and assumes one-dimensional conditions, i.e. a well-mixed water body where water temperatures are more or less uniform over the depth and horizontal cross section. Especially for cold water plumes that, according to the model results in this study have a tendency to remain at the bottom, a heat surplus model is not accurate. The origin of the these heat surplus models finds itself in hot water discharge studies where a lighter hot water plume floats on the colder water layers. In this case, a heat surplus model could be a useful estimate, since the plume is in direct contact with the atmosphere and mixes due to increased wind effects at the water surface.

However, steady state solutions could be useful in exploratory research towards application of SWH. Averaging over canal depth and longer periods of time, the ΔT from the simple ΔT model should approach the ΔT values found in the Delft3D model, especially in the far field at longer distances from the the outfall. This is also shown in figure 6.16, where both models are compared along distance measured from the outfall. The diluted solution could provide a good fit with the found results. When the outfall source is assumed to be undiluted, the simple ΔT is not accurate in the near and intermediate field. At further distances, even the undiluted solution seems to converge towards modelled values. A reason behind this is that further away

from the plume, passive diffusion processes result in a uniform water temperature over depth, which is in line with the assumptions behind the steady simple ΔT solution. For the modelling of multiple systems with a steady state solution superimposition could be applied, however, the flow velocities in the canal could also alter significantly due to the application of multiple systems. This should be checked before applying this solution. The steady state solution does not provide insight in stratification, which could alter significantly at local scale, see section 3.5.2, and temperature differences during start up and shut down of the system.

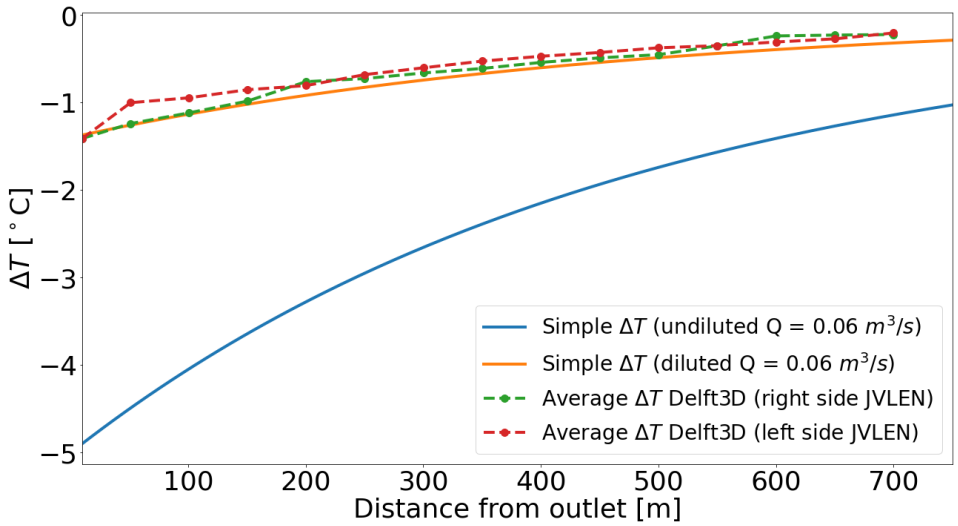

Figure 6.16: ΔT values for the Simple steady ΔT model (diluted and undiluted) and the depth and time averaged Delf3D values over the entire recovery period (for the left and right side seen from the outfall location) for a single SWH system in the van Lennepkanaal. Assumed uniform self cooling rate for the steady state solution is K = 21.5 W/m^2K.

6.4.5. Extent of the plume

Figure 6.17 shows the time series of the extent of the cold water plume in the van Lennepkanaal and considered adjacent canals, in total 6 km of city canal. The figure also shows that especially for the case of 3 systems the plume dimensions are larger than the considered grid. The presented plume extents might thus deviate from the real cold water plume.

Just as the atmospheric heat supply described in section 6.3, which is related to plume magnitude, the plume extent also fluctuates over time. An explanation for this fluctuation can be found in varying flow conditions and varying wind speeds. These two influencing factors where also found to be dominant by Aparicio Medrano (2008). The influence of wind speed is two fold. It has influence on the flow speed at the water surface and thereby the advection of the plume and through the forced convection terms for latent heat and sensible heat.

From the figure 6.17 also the order of magnitude of the start-up and shut-down times for development of the plume can be retrieved for SWH systems in the considered city canal. It follows that for 1 system the start-up time is about 25 h and for 3 identical systems the start-up time is slightly shorter about 22 h. The order of magnitude is about 1 day for both situations. The shut-down time is also interesting because it shows the resilience of urban canals to return to its natural water temperature variation after systematic temperature modification by SWH. Shut-down time for 1 system is approximately 69 h and for the case of 3 systems 90 h. In other words, it takes about 3 to 4 days for the canal system to return to its natural course, depending on the installed capacity.

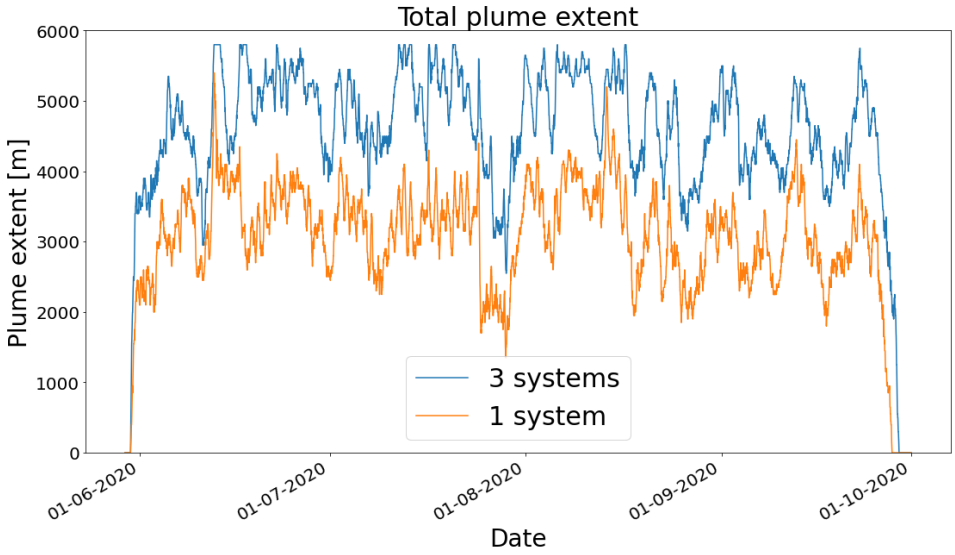

Figure 6.17: Time series of modelled cold water plume extent for installation of 1 system and 3 systems in the Jacob van Lennepkanaal. The plume is defined as the distance along the city canals where ΔT is smaller than $-0.1244\,^{\circ}\mathrm{C}$ which is rounded of to $-0.1\,^{\circ}\mathrm{C}$ in tenths of degrees, assuming that above this value thermal cooling effects are hardly noticeable.

6.4.6. The influence of a change in flow direction

The earlier presented results were averaged over longer periods of time. When looking at multiple moments in time, the influence of for example a change in flow direction in the city canal can be analyzed, see figure 6.18 for the studied event and 6.19 for the temperature difference profiles. The six profiles shown in the figure demonstrate that when the discharge changes direction, the developed stratified cold water plume to the left of the outfall is not directly displaced by the discharge from the new direction, especially in the deeper layers. The system is weakly dynamic and velocities are too low to disturb the existing thermal stratification. The top layer is however shifting towards the right in a faster pace, which can be attributed to the wind inducing higher flow speed at the top of the water column. It can also be observed that the peak in ΔT is shifted in the direction of the wind induced flow at the water surface and spreads out. The spreading of the negative peak at the water surface is also caused by the stratification effect of the solar radiation, which is increasing after it has reached its minimum during nighttime. At 07:00 AM (d in figure 6.19), the plume reaches the intersection of one of the two lateral canals at x = 1050 m. Here, the local bed elevation is shallower and water depths are in the order of only 1.0 to 1.4 metres. Colder water is elevated by the bed and mixes with the upper layers. This results in a typical vertical temperature profile where layers for a moment reach an equal ΔT.

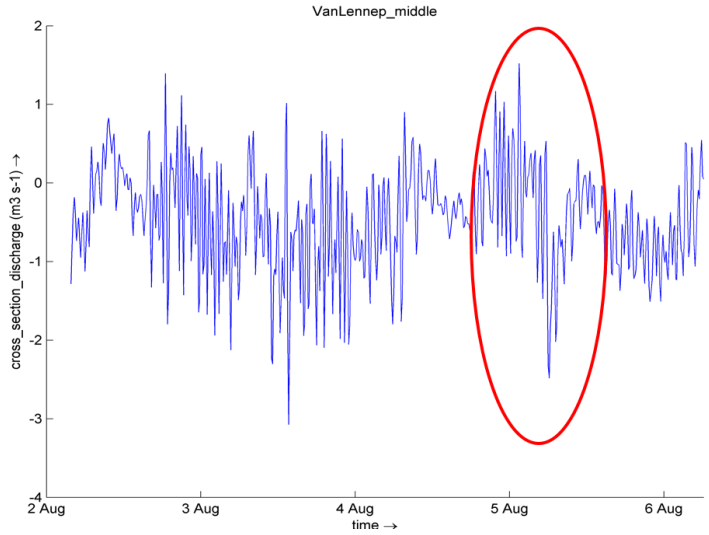

Figure 6.18: The change in flow direction in the morning of August 5^{th} used for analysis (within the red circle).

Another observation that follows from the hourly time plots in figure 6.19 is that the local dimensions and canal settings are important for the shape of the plume. At approximately x = 1050 m and x = 1275 m along the canal, two other canals are connected to the van Lennepkanaal, the Bilderdijkgracht and Da Costagracht respectively. Since at these locations severe reductions in ΔT values are observed, it can be noticed that at the intersections with these canals heat is withdrawn from the van Lennepkanaal by advection. At approximately x=675 m also a small downward jump in ΔT can be distinguished, especially in the layer layer at -1.0 metres relative to the water level. This is where the SWH takes its water in, also from the deeper and colder layers.

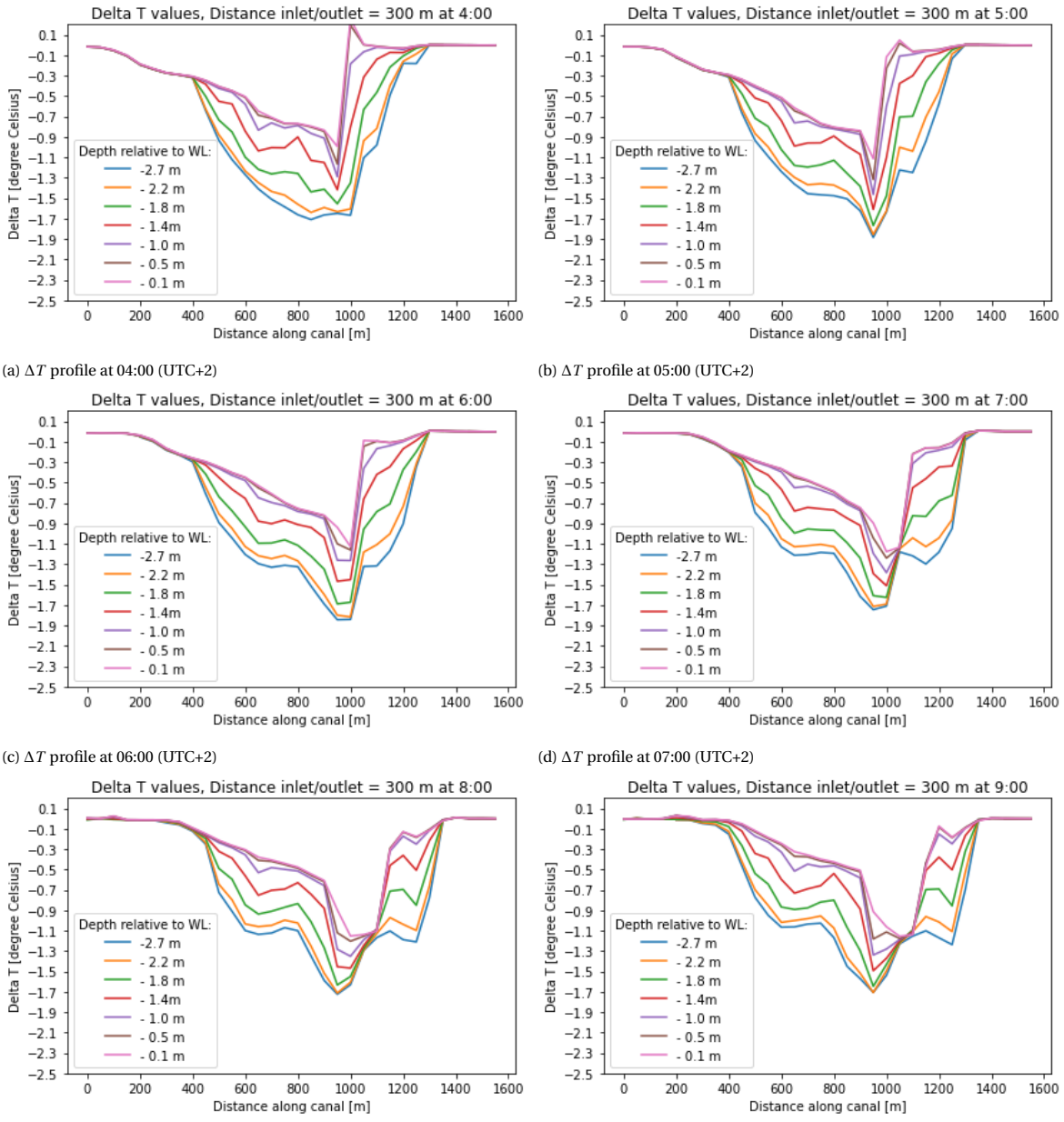

(a) ΔT profile at 04:00 (UTC+2)

(b) ΔT profile at 05:00 (UTC+2)

(c) ΔT profile at 06:00 (UTC+2)

(d) ΔT profile at 07:00 (UTC+2)

(e) ΔT profile at 08:00 (UTC+2)

(f) ΔT profile at 09:00 (UTC+2)

Figure 6.19: ΔT profiles just after a change in flow direction in the canal in the morning of August 5^{th}, 2020. The displayed hourly time fragments are retrieved from scenario 1.300 with system 1 and 300 metres between intake (at x=975 m) and outfall (at x=675 m). The flow direction is directed towards the right relative to the defined x-axis.

6.5. The thermal effect of multiple SWH systems

In the future, when sustainable thermal energy is in a further developed phase for the city of Amsterdam, a possible scenario is that multiple SWH systems are installed near the van Lennepkanaal system for the

Wilhelmina Gasthuisterrein. It is therefore interesting to look at the thermal effects when these additional systems are implemented in the city canal. The scenarios 2.300 and 3.300 with respectively 2 and 3 identical SWH systems (system 1:ΔT = 5.0 °C) were modelled to provide a first insight into future accumulation of SWH systems. Figure 6.20 shows the modelled water temperatures at the water surface for the 4 different scenarios with an intake to outfall distance of 300 metres. On first sight, it can be noticed that a large part of the cold plume escapes from the van Lennepkanaal through the Bilderdijkgracht, even for one SWH system. Temperatures in the van Lennepkanaal decrease further when installing multiple systems and a larger part of the cold plume spreads out further and also cools the adjacent canals.

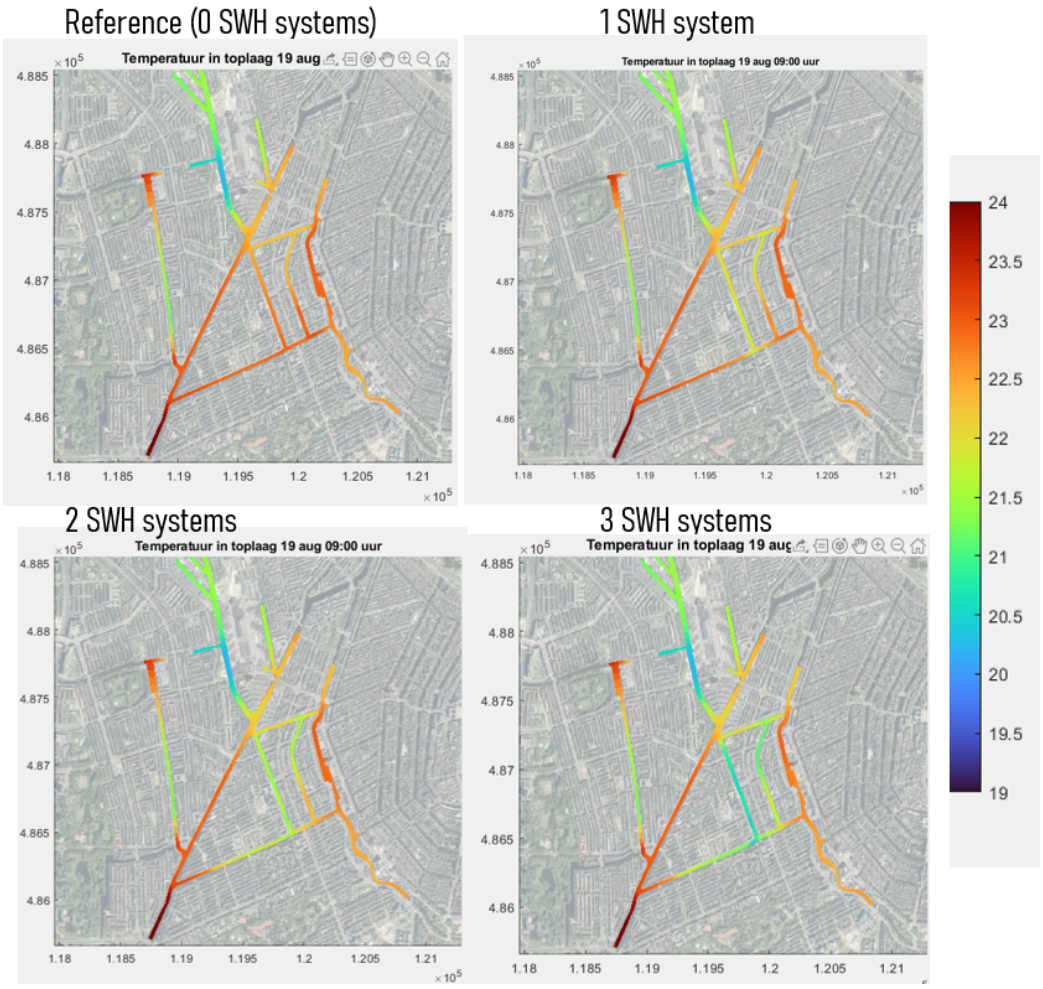

Figure 6.20: Top view on the temperature gradient in the van Lennepkanaal and adjacent canals at 09:00 AM on the 19^{th} of August. Scenarios that are displayed are the reference scenario without SWH, 1.300, 2.300 (2 systems) and 3.300 (3 systems).

Figures 6.21, 6.22, 6.23 and 6.24 show the longitudinal average ΔT values for 2 and 3 identical installed systems in the van Lennepkanaal, as described above. The figures show that by adding more systems the average temperature in the canal drops considerably. The chosen planning of the systems contains two intakes installed 50 meters apart. Together with the bed elevation at the beginning of the canal which has a shielding effect, at the Kostverlorenvaart on the left side, this results in attraction of water from the Kostverlorenvaart into the van Lennepkanaal, even though both the outfall supply the exact same flow rate. It should be noticed that even without SWH systems the dominant direction of the flow in the canal is also directed to the right. However, this local effect was not observed in the same magnitude in the situation with only one SWH system installed further away from the canal ends. It shows that the hydrodynamics and related thermodynamics are location specific and also dependent on for example the bed shape in the direct surroundings of the system. This profile also suggests that water layers at different depths in the canal also seem to be able to flow underneath each other in opposite directions. This confirms that the canal is weakly dynamic from a hydrodynamical point of view, where most of the time the wind has the largest effect on the flow at the water

surface, see previous section 6.1.4.

The case with 3 identical SWH systems, see the two figures 6.23 and 6.24 below, also indicate that water from the other end, the Singelgracht, flows into the van Lennepkanaal and discharged through the perpendicular adjacent canals, the Bilderdijkgracht and Da Costagracht. The pevailing 'pseudo tide' as described in section 3.1.1 of this report in the Amsterdam city canals seems to entrap the cold water plume from both sides within the dimensions of the van Lennepkanaal, even when the plume becomes colder and a higher amount of energy is extracted from the surface water. Meanwhile, water can be abducted through the two adjacent perpendicular canals, the Bilderdijkgracht and Da Costagracht.

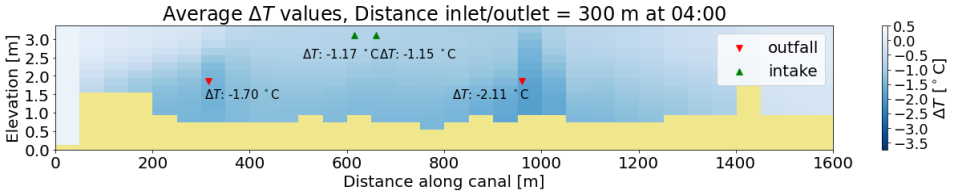

Figure 6.21: Averaged ΔT cross section of the van Lennepkanaal with 2 identical SWH systems modelled in the canal at 04:00 UTC+2.

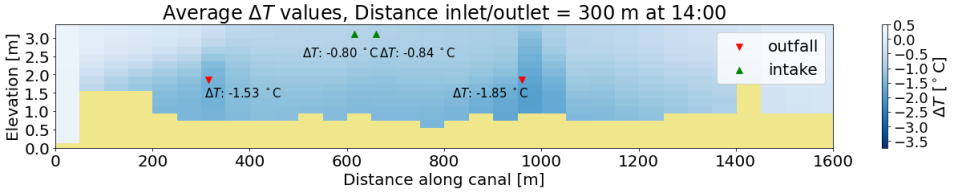

Figure 6.22: Averaged ΔT cross section of the van Lennepkanaal with 2 identical SWH systems modelled in the canal at 14:00 UTC+2.

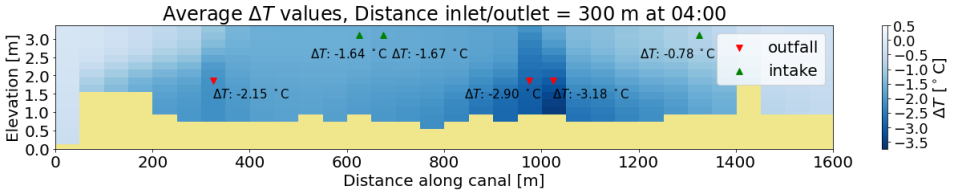

Figure 6.23: Averaged ΔT cross section of the van Lennepkanaal with 3 identical SWH systems modelled in the canal at 04:00 UTC+2.

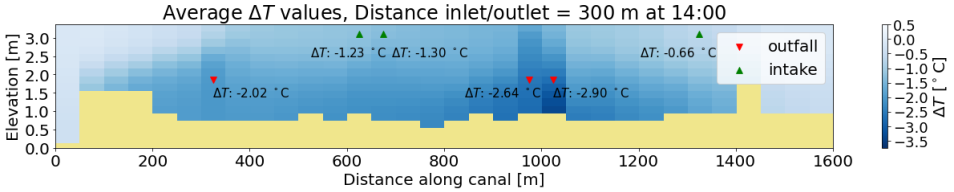

Figure 6.24: Averaged ΔT cross section of the van Lennepkanaal with 3 identical SWH systems modelled in the canal at 14:00 UTC+2.

6.6. Heat supply from atmosphere

Figure 6.25 shows the time series of the atmospheric heating power of the summed temperature dependent atmospheric heat fluxes (Q_{eva}, Q_{con} and Q_{long}) and integrated over the water surface (A [m^2]) within the considered modelled grid for 1 system in the van Lennepkanaal. Variation of heat fluxes over the width B of the canals was not included and the found total heating power is only based on longitudinal variation. Especially near the outfall, where surface water temperature also varies over the canal width, see figure c in section 6.1.2, this could lead to a slight underestimation of atmospheric heating. The other cross sectional

profiles are more uniform over the width and the calculation of total atmospheric heating power is considered more accurate for this more remote locations.

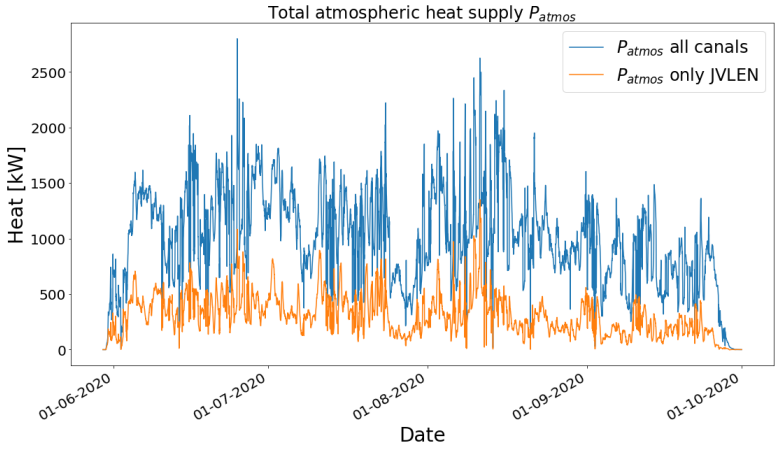

Figure 6.25: Time series of total heating power [kW] of the atmosphere within the boundaries of the van Lennepkanaal only and for the entire model domain for the installation of 1 SWH system (scenario 1.300). The entire system heat recovery period is displayed.

Figure 6.25 indicates that, apart from the day and night differences, the heating power of the atmosphere fluctuates heavily over time. In further analysis, the mean supplied heat P_{atmos} to the entire cold water plume was found to be 996 kW in this situation. The supplied heat by the atmosphere within the van Lennepkanaal dimensions was found to be only 324 kW, meaning that more than two-third of the direct atmospheric heating energy is supplied outside the dimensions of the van Lennepkanaal. Recalling that the average extracted heating power of SWH system 1 (ΔT_{max} = 5.0 °C) is 3539 kW, see table 3.2, this implies that a considerable amount of heat (roughly 72%) is not directly supplied by the atmosphere above the surface water. A reason for this discrepancy can be found in the combination of heat conduction with the ambient surface waters and advective processes displacing the outer edges of the cold water plume beyond the considered domain. At the outer edges of the plume, the process of passive ambient diffusion, as described in section 4.3.2, results in low ΔT of ΔT=0.25 °C at maximum and water temperatures are uniformly spread over the vertical. Due to the low temperature differences in this far field region, the temperature dependent driving forces in the heat balance are small, resulting in a slow gradual heat supply from the atmosphere to the cold water plume. This situation occurs especially at outer edges of the plume where the flow direction is more consistent. The cold water plume is drained away at the model boundaries where this situation occurs. The main location in the grid where this situation occurs is found at the Marnixkade boundary in the North direction of the grid. Figure 6.27 on the next page shows a longitudinal profile along a trajectory through adjacent canals, for the trajectory see figure 6.28, to the boundary at Marnixkade. At this boundary, the dominant flow direction is directed out of the grid domain, see figure 6.26, and the plume in the van Lennepkanaal is attracted to this location as a consequence.

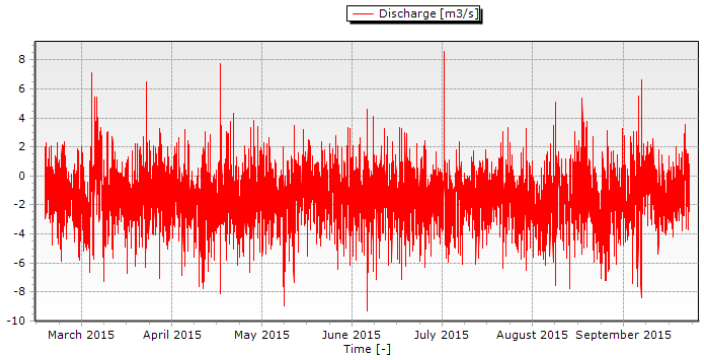

Figure 6.26: Applied 2015 time series of total discharge at Marnixkade boundary. It can be observed that dominant flow direction is directed out of the grid, indicated by the minus sign.

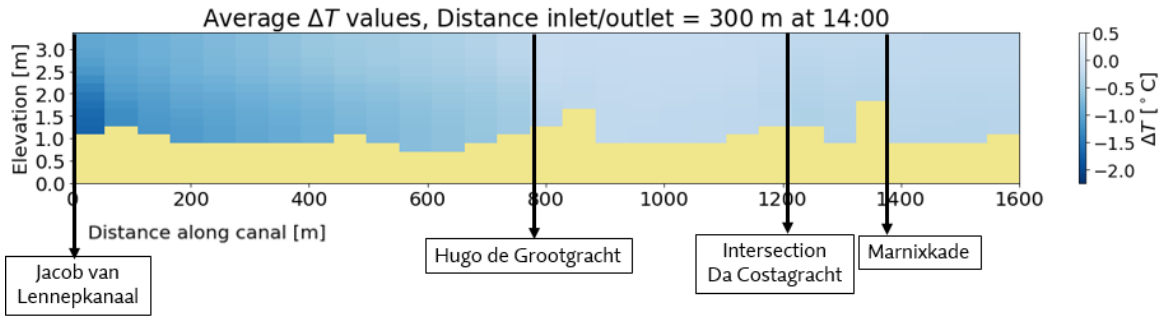

Figure 6.27: Average longitudinal ΔT profile with 1 SWH system operating in the van Lennepkanaal, starting at Jacob van Lennepkanaal and through respectively Bilderdijkkade, Hugo de Grootgracht and Marnixkade. It is visible that thermal stratification reduces and water becomes uniformly cooled due to passive diffusion processes when moving further away from the SWH system in the van Lennepkanaal. At the right, cooled water is advected out of the grid.

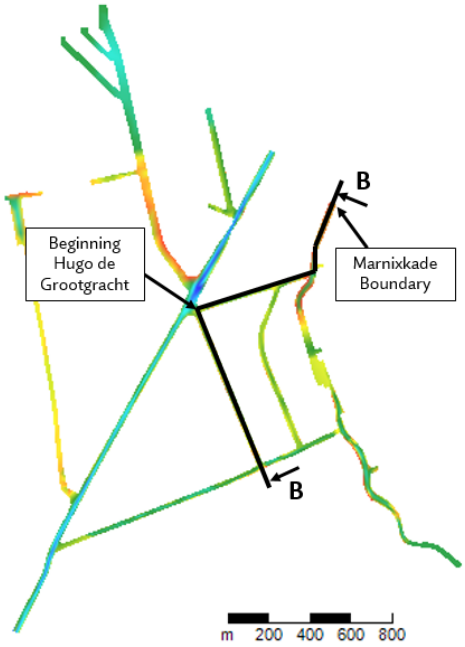

Figure 6.28: Cross section position B corresponding with longitudinal profile in figure 6.15.

Considering that in the end, the extracted heat by the SWH system is to be fully supplied by the atmosphere, it could be discussed whether the mentioned atmospheric heating power values P_{atmos} within the considered grid, as shown in figure 6.25, have any meaning. At least, it provides an insight in the atmospheric heat supply near the SWH system(s) and it shows that the van Lennepkanaal is not able to provide enough thermal energy within its own canal dimensions due to inevitable mixing of the water and spreading of the plume to other canals. For a full analysis of the trajectory of the cold water plume, a larger grid should have been applied also following the plume after full passive diffusion in the far field. Though, to gain insight in the atmospheric heating power within the considered grid, boxplots representing the atmospheric heating time series (see figure 6.25) of 4 scenarios are displayed in figure 6.29. In the case of a system 2 with a ΔT_{max} = 7.5 °C, the interquartile range has a larger spread. This is due to the higher installed power of the system and the fact that the system switches off multiple times due to the higher activation treshold water temperature (in this case 19.5 °C). The figure also shows that the atmospheric energy retrieved within the van Lennepkanaal dimensions with an increased ΔT does not result in significantly higher atmospheric power yield near the system compared to system 1 with ΔT = 5.0 °C. On the entire considered grid of 6 kilometers canal in total, the atmospheric power is slightly higher. Installing more SWH systems in the van Lennepkanaal seems to have an almost directly proportional effect on the total atmospheric power on the entire grid. It should be verified

on a larger grid whether this is indeed the case. However, within the dimensions of the van Lennepkanaal, the total supplied atmospheric power seems to flatten with the addition of the third system. A reason for this behaviour can be found in the orientation of first and third outfall near the adjacent Bilderdijkgracht. In this way, a large part of the cold water plume is abducted from the van Lennepkanaal through this perpendicular canal and thereby a larger part of the atmospheric heating energy is retrieved in the canals surrounding the van Lennepkanaal.

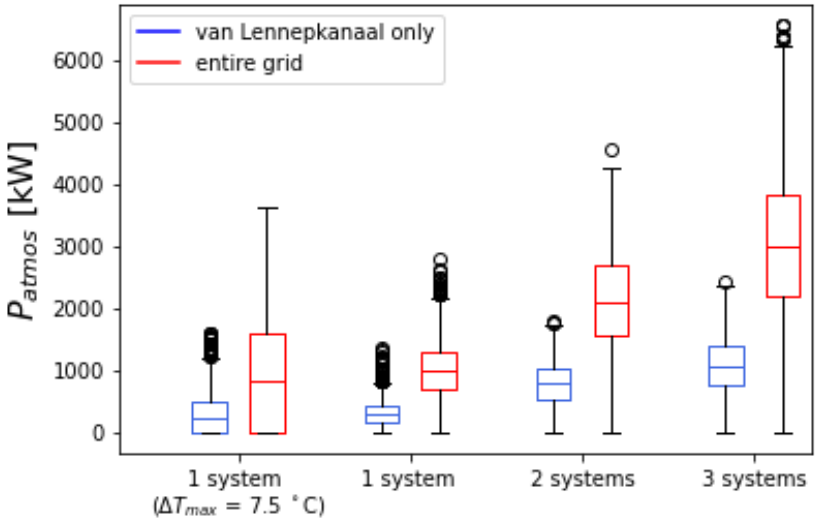

Figure 6.29: Boxplots showing the atmospheric heating power for the considered entire grid (along 6 km of canal in total) and within the extents of the van Lennepkanaal (1.4 km of canal) for 4 scenarios, each with a distance of 300 meters between intake and outfall.

6.7. Thermal system capacity and recirculation

For every scenario, time series of the water temperatures at the intake were computed. As the modelled water temperatures ΔT along the canal length have indicated, recirculation at the intake occurs in all of the scenarios and within the van Lennepkanaal recirculation is inevitable. To determine the thermal capacity or total recoverable heat of the SWH systems, hourly time series were created of the heat capacity rates ($mc_p\Delta T_{max}$) through the SWH system. Integrating over time and summation of the hourly values resulted in a total system capacity without taking recirculation issues into account. To account for recirculation, modelled recirculation temperatures at the SWH intake were substracted from the maximum recoverable ΔT_{max} of the respective system. In this way, it is presumed that the SWH system has a perfect dynamic response to water temperature changes in the adjacent water. This is hard to achieve in practice and rather a theoretical presumption. The idea behind this is to show, in the context of the envisaged restrictive legislation for system recirculation, the impact of avoiding recirculation in the thermal capacity of the system. The results of the calculations elaborated on the system heat capacity rates are summarized in figure 6.30.

The two graphs show that system capacity can be enlarged, or in other words, the occurring recirculation reduced, by increasing the distance between intake and outfall. Furthermore, the figure shows that the current thermal energy demand of the Wilhelmina Gasthuis, 27,320 GJ, can be easily achieved within the dimensions of the district. This heat demand is based on the current heat demand and therefore on the conservative side. Since district heating networks generally utilize lower system water temperatures, buildings within the district are planned to be insulated in the future. This will also reduce future heat demand. A critical note is whether it is acceptable that the thermal energy is partly recovered from adjacent canals, since the cold water plume also spreads outside the dimensions of the van Lennepkanaal. If other nearby districts would want to take part in a similar thermal energy solution, this might lead to interference issues in the future.

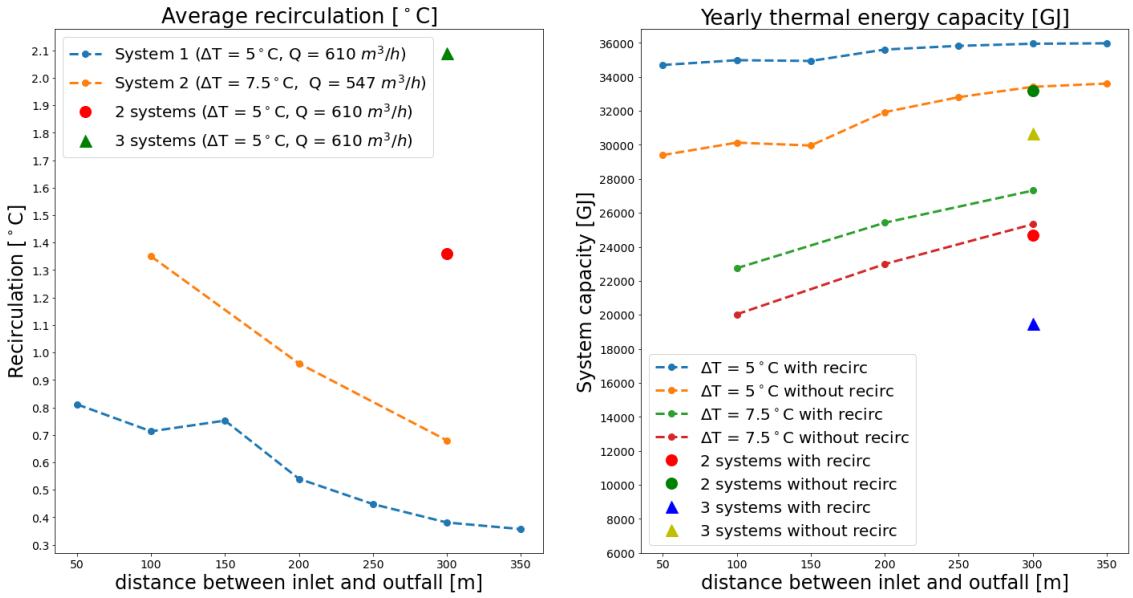

Figure 6.30: Summary of the results showing the average recirculation temperature at the intake during the heat recovery period and yearly thermal system capacity calculations for all scenarios considered.

Information that is also important to extract from figure 6.30 is that system capacity is on average 11% lower for system 1 (ΔT = 5.0 °C) and 9% for system 2 (ΔT = 7.5 °C) when recirculation is not allowed. To get a full picture of interference between systems the presented results are not sufficient. However, from the two scenarios considered, it can be observed that interference issues could become critical in the canal. Considerable losses are found. In the case of 2 systems, individual system capacity reduced with 26% and for 3 systems this loss was equal to approximately 42%. It needs to be noted that the two scenarios with multiple systems were an arbitrary choice and extraction strategies as well as well-defined policy frameworks could increase efficiency considerably.

7

Discussion

In a modelling study towards the thermal effects of energy recovery by means of open- loop SWH systems, a great amount of parameters determine the eventual outcome. Within this thesis, the created hydrodynamic and thermal Delft3D model was used for a case: the thermal modelling of a SWH system in a city canal in Amsterdam. As opposed to a modelling study focused on a sensitivity analysis, often executed under standardized conditions, a case study exists of fixed parameter choices, such as the model forcing parameters, which are set by the local conditions. The choice to perform a case study was largely motivated by the availability of water temperature measurements in the city canals. These measurements provided an opportunity to validate the reference situation in which no SWH systems were installed along the city canal. A clear disadvantage of case study modelling is the reduced applicability to other cases or locations and generalizations derived from case study results should be carefully approached. The remainder of this chapter discusses and reflects on the model accuracy, the model results and the application of SWH in a broader societal context.

7.1. Model accuracy from a CFD perspective

Approaching this study from the field of Computational Fluid Dynamics (CFD), the influence of model and computation parameters within Delft3D itself, for example the influence of grid spacing (model resolution), grid type, the choice of turbulence model and accompanying mixing parameters, e.g. the background eddy viscosities, would require more attention than this study indicated. Instead, standard and calibrated values applied in earlier CFD modelling studies of surface waters have been used. This could lead to deviations from the real local flow and thermal conditions. In this regard, the following remarks about this study should be considered:

- An example of a deviation is the influence that boats have on the mixing in the canal. This type of mixing is excluded in this study and is not included in mixing parameters such as the chosen background eddy viscosities. Moreover, including this factor would require more research.
- Another concern in the field of CFD is the relation of water temperature with the chosen turbulence model responsible for the modelling of the mixing patterns. In the van Lennep case study the two-equation k-ϵ turbulence model was chosen. As was indicated by the study of Dijkstra (2014), results on performance of two equation turbulence models for modelling of water temperatures and thermal stratification in lakes and oceans provided poor as well as good results. In accordance, the question was raised whether this type of turbulence model is actually capable to accurately model temperature profiles and thermal stratification patterns within lakes and oceans. It led to the discussion whether good results for temperature modelling with two-equation turbulence models are due to correct physical modelling or a result of calibration of other parameters in the temperature model, such as chosen bulk coefficients and background eddy viscosities. In this study, a heat model usually applied to ocean and large lakes was also applied to a city canal, which is a water body at a substantial smaller scale and where stratification is less developed. The validation performed for water temperatures at multiple depths in the city canals, demonstrated good agreement with the actual (measured) stratification in the city canal. For the van Lennepkanaal, RMSE values in the best fit validation step varied between 0.5 and 0.55 °C at all different depths. Still it remains unsure whether the processes are accurately modelled

in the case where an external force such as a SWH system alters the water temperatures and stratification in the canal.

- More generally, it should be noted that heat recovery from surface waters is still a relatively untouched subject in the scientific field. This imposes a considerable amount of uncertainties and assumptions in the modelling. Only recently, a study towards the knowledge gaps regarding aquathermal systems identified that there is still insufficient knowledge about natural variation in surface water systems, temporally as well as spatially (Harezlak, V. and Boderie, P., 2021). The presented extensive validation of the reference situation without SWH with the measured water temperatures in the city canal is an attempt to partly fill this knowlegde gap. Still uncertainties remain. An example of such an uncertainty in the modelling of SWH systems is the buoyant behaviour of the discharged cold water plume. Especially in small-scale surface waters such as city canals, where processes such as friction with the bottom and quay walls, deflection by ambient current and water body boundaries, in combination with the stratification effect of sunlight, form a complex mix, all affecting the spread of the cold water plume.

- Another important question in this light is whether a hydrostatic model such as Delft3D is accurate enough for the modelling of buoyant outfalls. Hydrostatic models exclude vertical momentum and the effect of immediate vertical bed deformations as well as immediate buoyancy effects. This leads to unrealistic behaviour and unsmooth model solutions in the near field of the outfall (Baptist et al., 2005). It was noted by Zijl (2002) that this could also lead to unrealistic representations in the modelling of buoyant jets or plumes in the far field, especially under certain conditions, such as high appearing vertical velocities, high density difference between discharge water and ambient water (ΔT_{max}) and the vertical postition of the outfall near the bottom in case of an upward positively buoyant flow (warm water discharge). The weak dynamic character of the studied city canal, together with installation of the cold water SWH outfall near the bottom for this negatively buoyant case, were assumed to keep buoyant vertical water displacements to a minimum and prevent inaccurate solutions in the far field of the cold water plume. The validity of this assumption was not verified.

7.2. Reflection on model results

The model was tested for the thermal influence of two different SWH design parameters: the extracted ΔT in the SWH heat exchanger and distance between intake and outfall. Although, the focus on only design parameters of the SWH systems limits the degrees of freedom in the analysis, still a large amount of parameter combinations could be created. Reminding that three-dimensional modelling of surface waters is a computationally expensive process, this would not be a convenient situation. In order to understand the main processes in recovering heat from surface waters and to visualize the thermal effects, a limited set of model scenarios was created for the case study location, the van Lennepkanaal. This limitation in chosen scenarios and the locality of , also limited the applicability of this study. In this light, the following points on the presented model results in this study are to be discussed:

- In this report the analysis of the results was mainly performed in longitudinal visualizations of the studied canal, the Jacob van Lennepkanaal. As described in section 7.1 and section 6.3 earlier in this report, the cold water plume reaches further into adjacent canals. This spreading towards other canals can play an important role in the longitudinal profiles at local scale. For the van Lennepkanaal case, the prevalent pseudo tide in the canal results in a continuously changing flow direction, see section 6.1.4. A situation evokes where the cold water plume is entrapped within the canal ends, which was confirmed by the modelled longitudinal profiles for ΔT. An entirely different picture emerges in canals with other local hydrodynamics, such as the adjacent Bilderdijkgracht. Here, the cold water plume originating from the Jacob van Lennepkanaal is advected towards the other end over the entire length of the canal and there is considerably less change in flow direction. The hetereogeneity in canal characteristics shows that the modelling and interpretation of surface water models in a complex city canal system needs thorough and locally tailored analysis.

- The SWH systems were modelled as time series in a spreadsheet model containing basic thermodynamical relations for heat exchangers with water temperatures as input from the Delft3D heat model. Ideally, the SWH model and Delft3D model are fully coupled, meaning that it is for example possible for the SWH system, modelled as a coupled source and sink in Delft3D, to change its heat extraction program based on the modelled water temperatures at the intake of the system. In this way, also more

intellligent controlled SWH systems could be modelled within Delft3D, which is especially needed in the future case of interfering systems. The lacking of such a feature, resulted in less realistic scenarios, especially for the two multiple system scenarios.

- For the considered case study, the SWH system discharge, or the discharge through the heat exchanger, was based on current known heating demand of the Ketelhuis WG district. In the future, the idea is to renovate the insulation of the connected building envelopes, resulting in a lower future heating demand. In the light of this future development, the mentioned heating demands in this report and corresponding SWH system designs are on the conservative side and even more buildings could potentially be supplied with the heat provided by the modelled systems, without altering the thermal effects in the city canal.

- *Accumulation* of systems was studied with two scenarios containing 2 and 3 SWH systems identical to the Wilhelmina Gasthuis district case. In practice, the heating demand between districts along the canal varies depending on the local building characteristics and magnitude of the considered district. If individual SWH systems would be applied for seperate districts in Amsterdam, this results in a variation of SWH system design dimensions, extracted heat and magnitude of the system discharges. It could be questioned whether the presented scenarios containing identical systems are realistic. However, this situation was chosen for simplicity to explore what would happen with multiple SWH systems in the canal.

- On the issue of *interference* between accumulated SWH systems, the results are rather marginal and only two scenarios were modelled. Caution is advised interpreting and extrapolating these results. It should also be remarked that in a further scale-up of SWH system in the city canal system, ambient waters are also cooled by upstream and downstream installed systems. Even if systems are installed far away from each other, far-field passive diffusion leads to an almost permanent reduction of water temperature in the canals far away from the system over the entire vertical during system operation. The temperature differences in this region are relatively small, slowing down the heating of the water by the temperature-dependent heat fluxes. In other words, energy retrieved by the SWH system is supplied by the atmosphere over a wide spread in the canals and the cold water plume can have a long 'tail'. In this study, only the total atmospheric power supplied in the direct surroundings of the van Lennepkanaal was investigated, the outer parts of the cold water plume were not included. To encapture the full atmospheric energy supply and trajectory of the cold water plume, a larger grid should have been chosen.

Based upon these findings, it was concluded that in this stage of research it is not possible to generalize the results into a total heat potential of SWH concepts in the city canals of Amsterdam. However, the results have clarified a number of important mechanisms influencing the thermal effects in the canal and retrieved heat capacity of the SWH systems, such as the existence of stratification and its dampening effect on atmospheric heat exchange, the role of certain hydrodynamic properties on cold water plume trajectory, a locally applicable relation between the inlet and outfall distance and recirculation temperatures and, finally, a preliminary research towards accumulation of multiple systems. In future design and modelling of SWH systems, these processes are important to take into consideration. In the next section, the relevant mechanisms that need attention in future modelling and research are discussed an described in more detail.

7.3. Relevance for further research

The thermal influence of open-loop SWH systems was studied for one specific location. As discussed, such a case study has the disadvantange of capturing location specific characteristics being less applicable to other cases. However, it is worthwile to reflect on the applicability of the found results for further research. On this subject, the following comments and lessons could be enumerated:

- Water temperature measurements were taken at 17 locations and 6 locations were further analyzed for stratification in water temperatures. All locations indicated that thermal stratification exists in city canals in varying orders of magnitude, depending on the local characteristics. The analyzed canals existed of varying hydrodynamic profiles, different bathymetric profiles and different orientations with respect to incoming solar radiation. Based on these results, it is very likely that thermal stratification also occurs in other (city) canal settings. The studied longitudinal profiles of the atmospheric heat

exchange coefficient K indicated that stratification effects have an important role in exchange with the atmosphere. The choice of this coefficient should be taken carefully and should consider thermal stratification effects in future research.

- An attempt was presented in this study to create a representative heat model by validation on meteorological model forcing data. It was shown that opportunistic incorporation of meteorological data from a nearby weather station without corrections for urban wind and shadow effects could lead to overestimation of the water temperatures over longer periods of time, expressed in mean error values (ME). For the modelling of thermal effects of SWH and the calculation of system capacities, this could result in inaccuracies due to incorrect system operation times which are in turn dependent on the modelled water temperature. For further research, it is advised to carefully select the meteorological data considering the local climate conditions and apply corrections if needed. Validation with measured local water temperatures is in this case a necessity.

- The modelled ΔT profiles indicate that far-field mixing processes spread out the cold water plume over long distances from the SWH system outfall. In other words, the thermal influence of a SWH systems reaches far for relatively shallow waters such as the city canals, albeit with relatively low temperature differences relative to the reference situation. The modelling grid in this study, existing of about 6 km of city canals, was not large enough to capture the entire plume and part of the plume was advected out of the modelled domain. For further research, it is important to account for these far-field effects, especially when considering the interference between multiple systems. Far-field processes originating from other systems far away could alter the background or reference situation, resulting in permanent reduction of the water temperatures during heat recovery. The appropriate model grid size might therefore be larger than intuitively thought and should be chosen carefully.

7.4. SWH in a broader context

In large societal challenges such as the energy transition, there are also a large number of other aspects that are not accounted for in this primarily technical thesis. In the first place, highly related to the thermodynamics are the water quality and environmental assessment. Ecological effects have not been part of this thesis. In a broader perspective, another challenge for the implementation of SWH systems in the quay walls of Amsterdam is the spatial implementation. SWH systems, often combined with heating networks and ATES systems, need a considerable amount of subsurface space, which is a limited resource in highly urbanized areas. Also the fact that these systems are capital-intensive and in need of pre-financing is a difficulty, economically as well as in terms of social equity. However, these economical considerations also depend on the scale of the project and the amount of buildings served by the respective system, which could improve economical viability in case of a system scale-up.

SWH is a promising technique that could reduce the carbon footprint considerably. However, electric energy is still required for the functioning of pumps and heat pumps in the system. To find a way to recover and store electricity sustainably remains one of the largest challenges. A way to partially cover this major issue, is to find efficient symbiosis between sustainable electric energy supply and ways to store this energy. For example, next to ATES systems often installed next to SWH nowadays, other storage applications for open-loop systems are also conceivable, even on another scale of application. In Diemen near Amsterdam for example, energy company Vattenfall is currently developing a large electric boiler to supply the already installed city heating network. The idea is to heat the boiler only when a surplus of sustainable solar and wind energy is available with the goal to synchronize sustainable energy supply and demand. Instead of the planned purely electric boiler, SWH systems installed in nearby surface waters in combination with heat pumps could be an even more energy efficient alternative due to relatively high COP values of the heat pumps. This is only one example of the many other configurations in which aquathermal solutions could be applied in practice.

Finally, it needs to be remarked that, comparable to ATES systems in the subsurface, surface waters could also be considered a common-pool resource. Following the precautionary principle, it is important to use and exploit such a source efficiently, sustainably and socially responsible.

8

Conclusions and recommendations

8.1. Conclusions

In this report, as the main research question indicated, insight in the thermal effects of open-loop SWH applications is obtained for a city canal. To that end, a Delft3D model was built validated on meteorological forcing parameters. Validation was performed with water temperature measurements taken in the city canal system at several depths. In order to find an answer to the main research question, in the remainder of this chapter the posed sub-questions are answered that together provide a full overview of the most important thermal effects concerning open-loop SWH systems.

S1: How are SWH systems applied in practice?

The national policy of the Netherlands prescribes that the ideal scale to tackle the energy transition from GHG emitting sources towards sustainable energy sources in the built environment is at district level. In the first part of this thesis, it was concluded that planning of SWH systems occurs within such district heating networks. To provide sufficient heating energy at district scale, open-loop SWH systems are currently the preferred option. Open-loop SWH systems have a rather simple design and exist of a radial screen functioning as a filter before the inlet, an outlet construction and a plate heat exchanger which transports the heat to the building side of the system. The outlet construction is often designed as a simple pipe discharging into the receiving surface water, although other options exist.

S2: What kind of existing regulation and calculations related to the thermodynamic modification by SWH systems are currently used in the Netherlands?

Although there is increased interest in aquathermal energy, until date no policy framework exists for the planning of SWH systems. A conceptual framework was created in 2019 which prescribes normative values for maximum extracted ΔT values and minimum water temperatures after artificial modification. The basis of the chosen norms lies in a study towards natural variation of water temperatures in surface waters within Hoogheemraadschap Delfland.

Calculations exist for assessing the thermodynamic modification SWH systems. In practice, executed calculations are often steady state one-dimensional and presume that the receiving surface water body is well-mixed. This is an assumption that doesn't hold for negative buoyant flows in stratified surface waters, especially in the near field of the outfall of the system. However, steady state solutions could provide insight in the average extent of the thermal effects, provided that the water temperature in the near-field at the outfall source is calculated as diluted or mixed and the heat exchange coeffient or self-cooling rate K is properly estimated. The steady state solution does not provide insight in stratification, which could alter significantly at local scale, and variations in the cold water plume over time.

S3: Do the water temperature measurements indicate the existence of thermal stratification in a city canal?

Both the water temperature measurements and the Delft3D modelling exercises in this study, indicate that thermal stratification develops over the depth of the city canal. This is an important conclusion since it has

a considerable effect on the thermal heat exchange with the atmosphere above the water. For the thermal stratification in city canals the following other conclusions could be drawn:

- The hydrodynamic mixing processes in a city canal are generally not strong enough to disturb the built-up of stratification. The system is therefore considered weakly dynamic. Due to related buoyancy forces, the thermal stratification enhances separation of cold water at the bottom and hot water at the water surface.
- Thermal stratification varies locally in the city canal system, depending on a combination of local water depth, clear sky view and local flow velocity.

S4: Can a 3D city canal model be developed that accurately models daily variations in water temperature and thermal stratification?

It was demonstrated within the case study area that it is possible to validate a Delft3D model on its meteorological forcing based on water temperature measurements at several depths in the Amsterdam city canals. Several validation steps were executed to increase model accuracy. A combination of local weather data of a nearby amateur station at approximately 500 meters, a shadow model also previously used by Aparicio Medrano (2008) and a simple urban canopy wind model introduced by Di Sabatino et al. (2008), provided best agreement with the measured water temperatures. The validation on meteorology resulted in a model that is moderately accurate; average MAE=0.42 °C and RMSE=0.52 °C at location JVLEN03. However, the three-dimensional thermodynamic model appeared to be even more accurate over longer timescales expressed by the mean error, which amounted to ME=-0.12 °C and ME=+0.15 °C for the JVLEN03 and JVlEN01 measurement locations. From analysis of the validation results, the following conclusions could be drawn:

- The model locally underestimates water temperatures for shallow surface waters receiving direct solar radiation and overestimates the mean water temperatures at locations with more shadow and indirect solar radiation.
- The model overestimated nocturnal cooling processes, indicating that water temperature amplitudes are also overestimated. An analysis and comparison of the daily mean water temperature amplitudes with the water temperature measurements confirmed that this was indeed the case, an overestimation varying between 0.09 °C and 0.22 °C with increasing depth.
- As potential error source, apart from uncertainty in meteorological forcing data, the omission of blocking of outgoing long wave radiation by urban structures and extra incoming longwave radiation from heat emitting buildings, together summarized in a Sky View Factor (SVF) is indicated. Another potential error source, especially near the bottom, is the omission of the dampening effect of the bed material. These error sources were not verified.

S5: Where is the cold water plume, discharged by SWH systems, located in the water column?

Concerning the position of the cold water plume, the following conclusions can be drawn:

- Downward directed buoyancy or negative buoyancy, forces the cold water discharged by SWH systems to sink. At the bottom, the plume spreads out. The warmer layers on top function as insulation and prohibit the cold water plume from exchanging heat with the atmosphere.
- Analysis of the cross sections in the longitudinal direction of the van Lennepkanaal of average ΔT values showed that stratification and temperature differences in the vertical are also dependent on local physical characteristics of the canal. Local changes in bed level and intersections with lateral canals influence the thermal profile. They emphasize the need of three-dimensional, or at least two-dimensional modelling over the vertical (2DV modelling) of small scale surface waters for detailed study of thermal effects over time.
- Before far-field processes such as passive diffusion begin to dominate and the entire vertical water column is uniformly cooled by the SWH, in the intermediate field, stratification is enhanced by the SWH system and the plume is concentrated at the bottom.

S6: Can the local heating demand for the case study situation be met, considering different distances between SWH intaken and outfall and related interferece and recirculations issues?

According to the created Delft3D model the required heat capacity for the Wilhelmina Gasthuis district can be met. However, the following conclusions provide further insight in the implications of the installed system capacity:

- The cold water plume also spreads outside of the van Lennepkanaal dimensions, where far-field processes start to dominate.
- After a shut-down of the modelled SWH systems, the time it takes for the city canal to return to its natural temperature profile is relatively short. Analysis of the results showed that the order of magnitude is 3 to 4 days, depending on installed capacity. It can be concluded that SWH systems are thermodynamically resilient.
- Recirculation within the van Lennepkanaal cannot be avoided, but decreases with distance between intake and outfall. Recirculation is the main limiting factor for installed system capacity within the dimensions of the canal. However, this also depends on chosen norms in future legislation and policy frameworks concerning this topic.
- From analysis of the total supplied power in the considered city canal domain, it follows that increasing ΔT_{max} through the SWH heat exchanger does not result in significant higher local yield of atmospheric heat in the direct surroundings of the outfall.
- Installation of multiple systems results in interference between systems, also depending on mutual distance between systems. The accumulation of multiple systems was modelled with only two scenarios and no further general applicable conclusions can be drawn yet.

8.2. Recommendations

This research forms a start in the investigation of thermal effects of open-loop SWH systems in an urban context, used for heating purposes. The findings in this study are applied to a case study in the van Lennepkanaal. To form a basis for research that is also more generally applicable, this section poses a set of recommendations that can be used in practice and in future research projects on the subject of SWH. The first three paragraphs in this section are related to subjects that could be researched in direct follow-up studies. The last part on the accumulation of multiple systems and the formation of a SWH policy is a subject that could be researched in a more advanced phase of research. The order of the paragraphs also indicate the priority of the follow-up research topics.

8.2.1. Monitoring of future SWH systems

In most real world modelling studies the biggest challenge is the availability of sufficient observations for proper validation of the created model. Therefore, especially for the first set of SWH applications installed in the inner city canals, it is important that future SWH projects are well monitored, preferably with multiple water temperature measurements spatially distributed around the outfall and intake, horizontally as well as vertically. The results of these monitoring exercises would help to get more grip on the temperature distribution horizontally as well as vertically. In such a monitoring campaign, the following surface water parameters are advised to be measured:

- *Inlet and outfall temperatures*: inlet and outfall temperatures should be logged during system operation.
- *Discharge through SWH system*: monitoring of the water discharge through the system at the surface water side of the system.
- *Water Temperatures*: a high measuring density with a Distributed Temperature Sensor (DTS). An alternative is a measuring campaign with temperature loggers, similar to the performed water temperature measurements in this research. However, it is advised in this case to increase the horizontal and vertical distribution in the vicinity of a future SWH system.
- *Local flow properties*: local flow measurements could be organised around the system which could be used to verify the hydrodynamic behaviour of available hydrodynamic surface water models.
- *Local meteorological parameters*: it is recommended to also have a local weather station installed in the direct surroundings of the monitored SWH system to provide an accurate meteorological forcing pattern to the heat model. In this study, This weather station should at least measure air temperature and local wind speed above the water body. Furthermore, the incoming and outgoing short- and longwave radiation could be measured with a radiometer, containing upward and downward facing pyranometers measuring the total radiation and pyrgeometers measuring upward and downward radiation within the long-wave spectrum. An example of meteorological measurement setup can be found in the paper of Solcerova et al. (2019).
- *Optical properties*: preferably also the optical properties of the respective water body are monitored, such as the measuring of transparancy and light extinction parameters over time. This could be achieved by periodical Secchi depth measurements or turbidity assessment of periodical water quality samples. Another option would be to apply light intensity sensors over the depth of the surface water body.

Together, the measurement of this set of parameters would create an important complete testing dataset where future SWH outfall modelling studies could be validated upon. The combination of observations provides a Also specifically for the city canal case, the external mixing effects, such as produced by the passing boats, would be represented by the measurements in this case, provided that the measurements are executed over a longer period of time.

8.2.2. Further research towards ecological effects

The effect of cold water discharges on ecology has been researched by Van Megchelen (2017) for a small ditch or waterway near a building area. In this study it was found that open-loop SWH systems, by cooling the connected surface waters, have a minor impact on ecological parameters and growth of certain plant species.

Considering that all surface waters have their own characteristics and differ also from a water quality perspective, it would be useful to monitor ecological effects of SWH systems at multiple places and in different types of water bodies. Optionally, ecological models could be coupled to created thermodynamical and hydrodynamical models. Furthermore, not only the cooling effects could be researched, but also the ecological impact of system cleaning substances used in SWH settings should be researched.

8.2.3. Heat model improvements

Delft3D is a hydrostatic approximation model based on RANS equations, meaning that immediate buoyancy effects, sudden vertical movements and vertical momentum are left out of the equation. This is a limitation of the model and might lead to inaccuracies for buoyancy related problems such as the behaviour of cold water plumes. However, in this thesis the cold water plume was injected at depth in the water column. In this way, immediate vertical movements are limited and the use of a hydrostatic model could be justified, also recalling that the prime interest went out to mid-field and far-field, for which Delft3D is more suitable. For further research, the following recommendations for further research are proposed:

- Modelling with a non-hydrostatic CFD model could be an interesting improvement. Alternatively, a combination between an analytical expert model such as CORMIX or the Langrangian model JETLAG combined with a hydrostatic model such as Delft3D. In this last case, the Distributed Entrainment Sink Approach (DESA) method by Choi and Lee (2007) has been succesfully used in the coupling of near-field and mid-field or far-field models. The basic idea of the DESA method is to represent the turbulent entrainment by the jet or plume in the near-field by a trajectory of sinks and sources in a far-field model. In this study, the near-field around the SWH outfall was modelled with only one source at the point of discharge. This method is referred to by Choi and Lee (2007) as the Actual Source (AS) method, where the near-field is solved as part of the far-field model. Applying the DESA method provides better agreement with the near-field.

- To assess and verify the right scale for stable numerical modelling with models such as Delft3D, a sensitivity analysis could be elaborated on model geometry parameters such as grid spacing and number of vertical layers. In this way, the ideal model properties could be determined, also regarding computational efficiency. Since Delt3D is originally a model applied to problems at larger scale than a city canal e.g. estuaries, lakes and shores, this might be an interesting small-scale exercise to elaborate upon.

- In the area optimization of the heat model, the Sky View Factor (SVF) and thermal exchange with the bed material could be incorporated in the chosen model to obtain more accurate results. Furthermore, the spatially varying meteorological data and shadow effects could be incorporated in a more advanced model. These optimizations could further reduce errors in an urban water temperature model. However, the effect of these model optimizations on the thermal effects by SWH systems, which is primarily related to relatively small temperature differences instead of absolute water temperatures, is expected to be marginal. This recommendation has therefore less priority in the light of this study.

8.2.4. SWH applications

Many different configurations for SWH systems exist. In this study only one type of systems was modelled: an open-loop SWH system. An example of another way of heat recovery from city canal waters is by using the entire quay walls along the canals as a large heat exchanger. In this way, problems of open-loop SWH systems such as clogging and biofouling of the heat exchanger could be avoided. The thermal effects of this type of system configuration could also be researched in more detail. Also the scale of SWH application could be further studied by varying the magnitude of extracted thermal capacity.

The thermal effects of SWH were analyzed only during the summer period of 2020. The effect of a relatively colder or warmer summer was not considered. Also the effect of a wet or relatively dry summer was not investigated. Meteorological and hydrological differences in the recovery period could alter the retrievable heat capacity of a SWH system. A model simulation for recovery periods during multiple years would create better insight in SWH system capacities and effects on the long run.

8.2.5. Accumulation of SWH systems

Research towards a policy framework for future spatial planning of SWH systems is needed, based on a chosen planning strategy for installation of the systems. For the heating potential of surface waters, it is by all means important that such a framework or another form of future legislation on SWH systems clearly indicates the maximum allowable recirculation at the intake, the maximum temperature difference through the heat exchanger (ΔT_{max}) and the minimum allowable water temperature after artificial modification.

In this context, interference between SWH systems in surface waters needs to be studied in greater detail with more scenarios on for example a standardized grid and under standardized conditions. A wide variety of system configurations and planning strategies could be studied. For example, the combination of different SWH system sizes, different ΔT_{max} and different system control methods. Another possibility is to perform a comparable study to the presented study in this report on a larger grid, for example the entire inner city canal area with connection to the IJ, with more systems installed. Such a larger grid is available for the Amsterdam city canals and also used in this study for the creation of the nested grid of the van Lennepkanaal. On a large grid, the grid would need further refinement to an appropriate scale to keep the generation of model results computationally efficient, see the recommendation in the previous section 8.2.3. An unstructured grid with varying grid spacing is also a possibility in this situation.

In an even further phase, the use of methods such as agent-based modelling, as for example presented in the study by Jaxa-Rozen et al. (2019) for the spatial plannning of multiple ATES systems in the subsurface, could also be used to research the accumulation of SWH systems in the city canals of Amsterdam. An agent-based model could also be able to test the implications of implemented certain rules or norms in a future framework on total retrieved heating potential from the entire city canal system.

A

Criterions for Recirculation and Mixing zone in Delfland

Based on the relation described in section 2.2.5, two criterion calculations were developed by Hoogheemraadschap Delfland. They are explained below.

Recirculation criterion

In Delfland, the criterion for recirculation in a SWH system is the requirement that at the intake the temperature difference is 0.5 °C at maximum. When the maximum temperature difference is 5 °C, recirculation is then allowed for 10% of the maximum temperature difference at the outfall. The main motivation for limiting the recirculation rate is that a part of the water system is completely deviant from the described natural temperature pattern. When implementing this criterion in the Delta-T model the maximum capacity of the SWH system, based on the recirculation criterion, can be determined as:

$$P < A_{\text{circ}} K \beta_T \Delta T_{\max} f(b/L) \tag{A.1}$$

where P is the permittible SWH capacity (W), A_{circ} is the recirculation water surface area between intake and outfall (m^2), β_T is the recirculation factor (-) following from the Delta-T model and the criterion (10% translating in a factor of 1/2,3) and $f(b/L)$ is a form factor for the respective water body (for linear shaped water bodies $f = 1$). This form factor becomes important in larger water bodies, such as lakes, where the cool water discharge is not able to mix over the total volume of the water body during stagnant flow conditions.

Mixing zone criterion

The surface area of the mixing zone is also derived from the Delta-T model. The mixing zone is defined as the area where ΔT is larger than 3 degrees Celsius. The surface area of the mixing zone is required to be lower than 25% of the total recirculation surface area, in line with the CIW guidelines. In the proposed national assessment framework, a higher temperature difference of 5 degrees Celsius is accepted at the edge of the mixing zone. The size of the mixing zone is required to be smaller than 10% of the ecohydrological unit. The exact definition of the ecohydrological unit is not yet known and it is unclear whether 10% is defined volumetrically or in terms of surface area. When applying the Delfland values to the Delta-T model, this leads to the following criterion for the size of the mixing zone:

$$P < K A_{\text{circ}} \Delta T_{\max} \beta_{\text{meng}} \tag{A.2}$$

where:

$$\beta_{\text{meng}} = 0,25 / \left(-\ln \left(\Delta T_{\text{edge}} / \Delta T_{\max} \right) \right) \tag{A.3}$$

where ΔT_{edge} is the temperature at the edge of the mixing zone (°C) and β_{meng} is the mixing zone factor (-) when a maximum mixing zone surface area is allowed of 25%.

The decisive criterion

Water permit requests are examined for both criterions and one criterion is decisive for the specific case. Since both criterions have been written in the same form, under the assumption that the form factor $f(b/L) = 1$, which is the case for canals and linear water bodies, a tabular overview can be generated in which for different ΔT_{max}, the only changing variable β is determining which of the criterions is decisive for the permittable SWH capacity, see figure A.1. From this table, it can be observed that recirculation is the main limiting factor for SWH installations with a ΔT_{max} lower than 5 degrees Celsius. However, if higher rates of recirculation are allowed, the mixing zone becomes decisive. Also, for higher ΔT_{max}, the size of the mixing zone becomes the limiting factor.

	ΔT_{max} [°C]	7	6	5	4	3
Recirculation	β [-]	0.295	0.361	0.489	0.869	-
2.5%	0.271	recirc	recirc	recirc	recirc	recirc
5%	0.334	mixing	recirc	recirc	recirc	recirc
10%	0.434	mixing	mixing	recirc	recirc	recirc
20%	0.621	mixing	mixing	mixing	recirc	recirc
40%	1.091	mixing	mixing	mixing	mixing	recirc

Figure A.1: Table with decisive criterions for SWH systems sorted by the maximum temperature difference and recirculation rate, according to Hoogheemraadschap Delfland (2020)

B

Modelled water temperatures for the entire grid

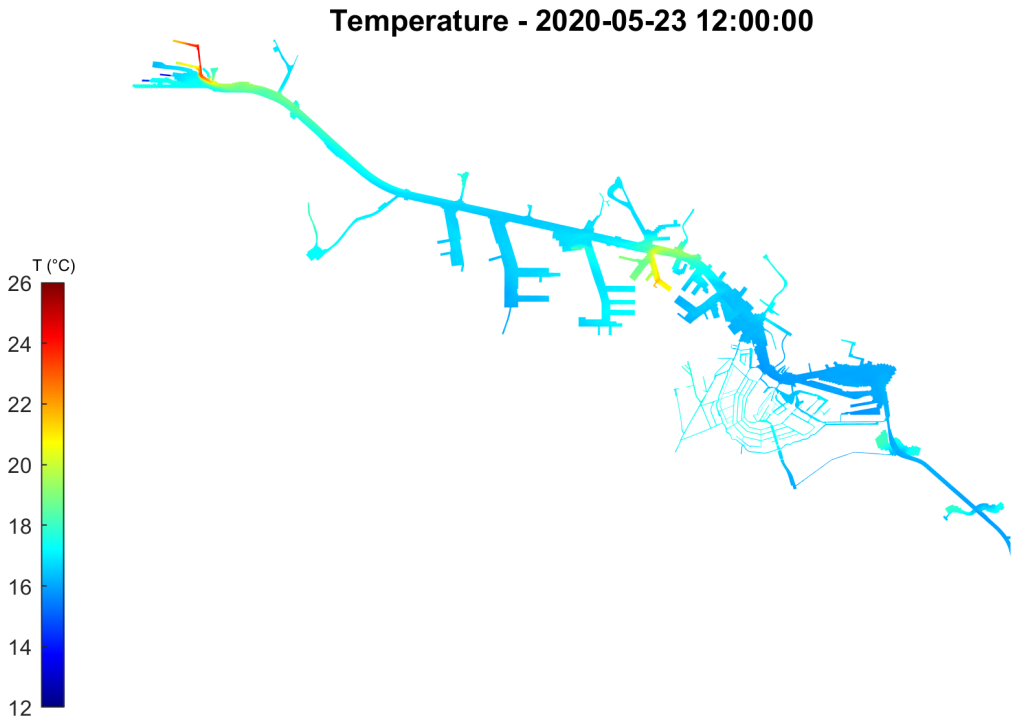

Figure B.1: Plot of water temperatures in top layer (-0.34 m under surface water level) at 12:00 PM on May 23rd 2020 for the IJ, Amsterdam Rijnkanaal (ARK) and the city canal system. Model was created by Deltares and Arcadis.

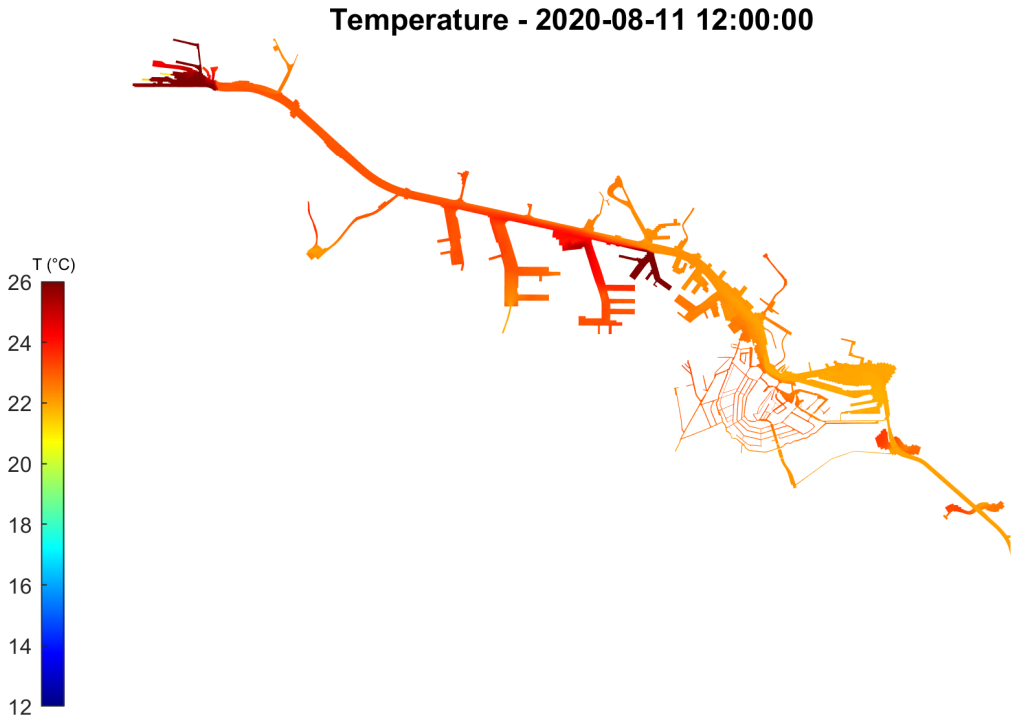

Figure B.2: Plot of water temperatures in top layer (-0.34 m under surface water level) at 12:00 PM on August 11^{th} 2020 for the IJ, Amsterdam Rijnkanaal (ARK) and the city canal system. Model was created by Deltares and Arcadis.

C

Value sheet heat capacity and recirculation at the intake

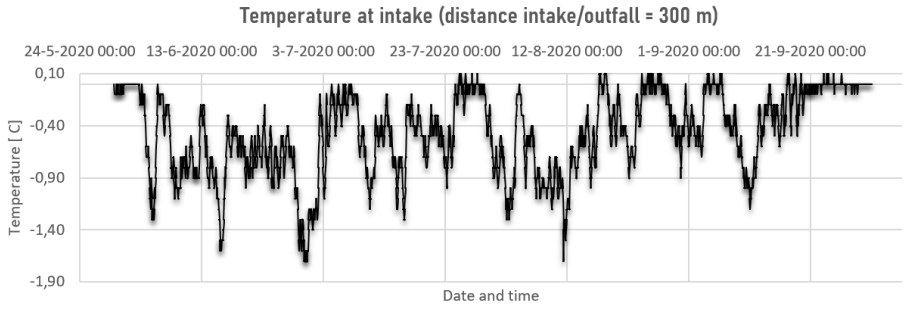

Wijkspecifieke gegevens	
Aantal woningen	1,443
Warmtevraag vermwarmd tapwater [kWh/m2 BVO]	20
Aantal m2 woningen	100,471
Warmtevraag warm tapwater [GJ]	7,234
Warmtevraag [GJ] + 10% onzekerheidsmarge/leidingverlies	40981
Rekenwaarde Coefficient of Performance (COP)	3.0
Benodigde bronenergie (WKO + direct uit TEO) [GJ]	**27320**

Potentie (zonder kortsluiting)				Potentie (met kortsluiting)	
Totaal gewonnen GJ	33421	max kortsluiting (grad C)	1.7	Totaal gewonnen GJ	30683
Direct uit bron voor warm tapwater [GJ] -10%	1321			Direct uit bron voor warm tapwater [GJ] -10%	1321
Naar WKO [GJ]	32100			Naar WKO [GJ]	29362
Totaal beschikbare warmte uit WKO	35310	gem kortsluiting (grad C)	0.5	Totaal beschikbare warmte uit WKO	26426
Totaal beschikbare bronenergie (WKO + Direct uit TEO) [GJ]	**36631**			Totaal beschikbare bronenergie (WKO + Direct uit TEO) [GJ]	**27747**

Figure C.1: Sheet displaying the recirculation at the intake for scenario 1.300 together with additional system capacity calculations

D

Calculation sheet heat exchanger and time series

Wijkspecifieke gegevens	
Aantal woningen	1,443
Warmtevraag vermwarmd tapwater [kWh/m2 BVO]	20
Aantal m2 woningen	100,471
Warmtevraag warm tapwater [GJ]	7,234
Warmtevraag [GJ] + 10% onzekerheidsmarge/leidingverlies	40,981
Warmtevraag [GJ/woning]	28.4
Warmtevraag [MWh]	11,383

Constanten	
Volumetrische warmtecapaciteit water [J/m3*K]	4.18E+06
Porositeit bodem [-]	0.3
Verbrandingswarmte aardgas [MJ/m3]	31.65
Volumetrische warmtecapaciteit aquifer [J/m3*K]	2.80E+06

TEO	
Benodige bronenergie [MWh]	7,826
Benodige bronenergie [GJ]	28,174
TEO vermogen [kW]	3,539
Aantal dagen warmtewinning [d]	97
Debiet TEO [m3/h]	610
max Delta T	5.0

Figure D.1: Spreadsheet containing the district specific data of Ketelhuis WG.

Systeemgegevens		
Average discharge waterside [m3/h]	610	
Minimum Temperature (Tsyst_off)	14.9	
Temperatuur Koude (Tsyst_in) [degrees Celsius]	9	
Temperatuur Warme bron (Tsyst_uit) [degrees Celsius]	15	
Avg Surface water temp. Operable [degrees Celsius]	20.0	16.5
min Log Mean Temp Diff [K]	5.5	1.5
Heat transfer coefficient HX (k)	2400	
Heat exchanging A [m2]	270.0	
Cu_max = m_water * C_water [kJ/sK]	708	
Number of Transfering Units (NTU) = U*A/C_min	0.92	
HX effectiveness (see graph below, in case of R=Cmin/Cmax=1.0)	0.63	

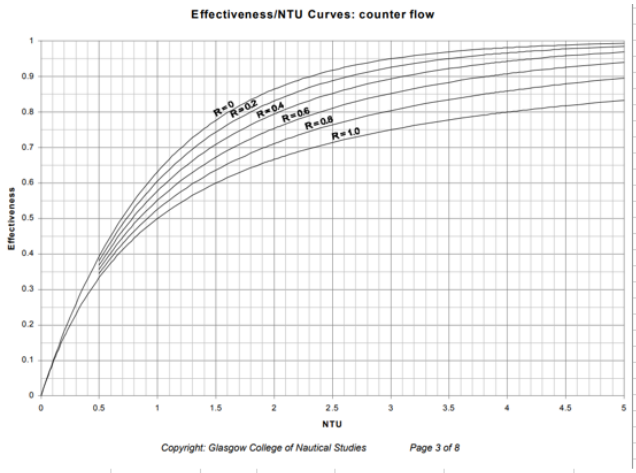

Pompregime	Min Temp	Max Temp	Discharge[m3/s]	C_min [kJ/Ks]	C_r [-]	NTU [-]	Effectiveness [-]	q_act [kJ/s or kW]	Delta T opp [degrees Celsius]	
Level 0: 16-17 graden	16	17	0.12	514	0.7	1.3	0.75	2892	4.1	(waterzijde)
Level 1: 17-18 graden	17	18	0.18	732	1.0	0.9	0.57	3544	5.0	(waterzijde)
Level 2: 18-19 graden	18	19	0.14	564	0.8	1.1	0.66	3538	5.0	(waterzijde)
Level 3(1): 19-19,5 graden	19	19.5	0.11	472	0.7	1.4	0.73	3534	5.0	(waterzijde)
Level 3(2): 19,5-20 graden	19.5	20	0.10	426	0.6	1.5	0.77	3529	5.0	(waterzijde)
Level 4: 20-21 graden	20	21	0.09	368	0.5	1.8	0.83	3511	5.0	(waterzijde)
Level 5: 21-22 graden	21	22	0.07	305	0.4	2.1	0.92	3509	5.0	(waterzijde)
Level 6: 22 and higher	22	23	0.07	276	0.4	2.3	0.94	3501	4.9	(waterzijde)

Figure D.2: Spreadsheet containing the most important parameters of the heat exchanger. In the table at the bottom a pumping regime is assumed for the SWH system dependent on sensored surface water temperature.

		Topp_in	T_TEO_uit	Topp_uit	T_TEO_in	Debiet systeem [m3/	Debiet waterzij	Temperatuur v	Gewonnen warmte [J]	Gewonnen warmte [GJ]
Date	time [s] to ref date									
29-5-2020 14:00	739560	15	0	0.0	0	0.0	0.0	0.0	0.00E+00	0.00
29-5-2020 15:00	739620	15.4	0	0.0	0	0.0	0.0	0.0	0.00E+00	0.00
29-5-2020 16:00	739680	15.6	0	0.0	0	0.0	0.0	0.0	0.00E+00	0.00
29-5-2020 17:00	739740	15.7	0	0.0	0	0.0	0.0	0.0	0.00E+00	0.00
29-5-2020 18:00	739800	15.6	0	0.0	0	0.0	0.0	0.0	0.00E+00	0.00
29-5-2020 19:00	739860	15.5	0	0.0	0	0.0	0.0	0.0	0.00E+00	0.00
29-5-2020 20:00	739920	15.4	0	0.0	0	0.0	0.0	0.0	0.00E+00	0.00
29-5-2020 21:00	739980	15.4	0	0.0	0	0.0	0.0	0.0	0.00E+00	0.00
29-5-2020 22:00	740040	15.4	0	0.0	0	0.0	0.0	0.0	0.00E+00	0.00
29-5-2020 23:00	740100	15.3	0	0.0	0	0.0	0.0	0.0	0.00E+00	0.00
30-5-2020 00:00	740160	15.3	0	0.0	0	0.0	0.0	0.0	0.00E+00	0.00
30-5-2020 01:00	740220	15.3	0	0.0	0	0.0	0.0	0.0	0.00E+00	0.00
30-5-2020 02:00	740280	15.2	0	0.0	0	0.0	0.0	0.0	0.00E+00	0.00
30-5-2020 03:00	740340	15.2	0	0.0	0	0.0	0.0	0.0	0.00E+00	0.00
30-5-2020 04:00	740400	15.1	0	0.0	0	0.0	0.0	0.0	0.00E+00	0.00
30-5-2020 05:00	740460	15.1	0	0.0	0	0.0	0.0	0.0	0.00E+00	0.00
30-5-2020 06:00	740520	15.1	0	0.0	0	0.0	0.0	0.0	0.00E+00	0.00
30-5-2020 07:00	740580	15.1	0	0.0	0	0.0	0.0	0.0	0.00E+00	0.00
30-5-2020 08:00	740640	16.1	15	12.2	9	442.8	609.5	-3.9	9.86E+09	9.86
30-5-2020 09:00	740700	16.3	15	12.3	9	442.8	609.5	-4.0	1.01E+10	10.13
30-5-2020 10:00	740760	16.5	15	12.4	9	442.8	609.5	-4.1	1.04E+10	10.41
30-5-2020 11:00	740820	16.7	15	12.5	9	442.8	609.5	-4.2	1.07E+10	10.69
30-5-2020 12:00	740880	16.9	15	12.6	9	442.8	609.5	-4.3	1.10E+10	10.97
30-5-2020 13:00	740940	17.1	15	12.3	9	630.0	609.5	-4.8	1.22E+10	12.16
30-5-2020 14:00	741000	17.2	15	12.4	9	630.0	609.5	-4.8	1.23E+10	12.31
30-5-2020 15:00	741060	17.3	15	12.4	9	630.0	609.5	-4.9	1.25E+10	12.46
30-5-2020 16:00	741120	17.5	15	12.5	9	630.0	609.5	-5.0	1.28E+10	12.76
30-5-2020 17:00	741180	17.7	15	12.6	9	630.0	609.5	-5.1	1.31E+10	13.06
30-5-2020 18:00	741240	18	15	12.7	9	486.0	609.5	-5.3	1.35E+10	13.51
30-5-2020 19:00	741300	18.2	15	13.4	9	486.0	609.5	-4.8	1.23E+10	12.34
30-5-2020 20:00	741360	18.3	15	13.4	9	486.0	609.5	-4.9	1.25E+10	12.47
30-5-2020 21:00	741420	18.4	15	13.5	9	486.0	609.5	-4.9	1.26E+10	12.60
30-5-2020 22:00	741480	18.4	15	13.5	9	486.0	609.5	-4.9	1.26E+10	12.60
30-5-2020 23:00	741540	18.4	15	13.5	9	486.0	609.5	-4.9	1.26E+10	12.60
31-5-2020 00:00	741600	18.5	15	13.5	9	486.0	609.5	-5.0	1.27E+10	12.74
31-5-2020 01:00	741660	18.5	15	13.5	9	486.0	609.5	-5.0	1.27E+10	12.74
31-5-2020 02:00	741720	18.6	15	13.5	9	486.0	609.5	-5.1	1.29E+10	12.87
31-5-2020 03:00	741780	18.7	15	13.6	9	486.0	609.5	-5.1	1.30E+10	13.01
31-5-2020 04:00	741840	18.6	15	13.5	9	486.0	609.5	-5.1	1.29E+10	12.87

Figure D.3: Impression of spreadsheet containing the created time series of the discharge and ΔT in the heat exchanger

E

Delft3D model parameters

Canal geometry	Unstructered grid	
	Varying grid size	near outfall: 2.5 x 9 m
	20 vertical layers	layer depth = 0.21 m
Computed time	Start time	29-5-2020 14:00 (UTC+2)
	End time	30-9-2020 23:00 (UTC+2)
	Time step	1 to 10 seconds
Atmospheric model	Air temperature T_a	Oud-West Wiegbrug weather station (500 meter from JVLEN)
forcing	Wind speed U_{10}	Schiphol KNMI weather station corrected with urban wind model of Di Sabatino et al. (2008) and Mertens (2003)
	Cloud fraction F_c	MODIS from NASA MERRA 2 reanalysis
	Solar radiation	Delft3D heat model corrected with shadow model of \citet{shashua2003geometry}
Model physics	Uniform horizontal eddy viscosity ($\nu_{Huniform}$)	0.1 $[m^2/s]$
	Uniform horizontal eddy diffusivity (α_H)	0.1 $[m^2/s]$
	Uniform vertical eddy viscosity ($\nu_{Vuniform}$)	5E-5 $[m^2/s]$
	Uniform vertical eddy diffusivity (α_V)	5E-5 $[m^2/s]$
	Temperature model	Composite (ocean) model, see section 4.4
	Dalton number related to evaporative/latent heat flux (E)	$c_E = c_D$
	Stanton number related to sensible heat flux (H)	$c_H = c_D$
	Bottom roughness	White-Colebrook and Strickler formulations with Nikuradse roughness k between 0.05 and 0.15 meter
	Wall roughness	k = 0.005 m (rubble masonry (Mashau, 2006))
	Secchi depth	$H_{Secchi} = 1.0 m

Bibliography

Abbasi, A. (2016). *Energy Balance and Heat Storage of Small Shallow Water Bodies in Semi-Arid Areas*. TU Delft Repository.

Addad, Y., Benhamadouche, S., and Laurence, D. (2004). The negatively buoyant wall-jet: Les results. *International journal of heat and fluid flow*, 25(5):795–808.

Aparicio Medrano, E. (2008). *Urban Surface Water as Energy Source & Collector*. TU Delft Repository, Delft, the Netherlands.

Aparicio Medrano, E., Wisse, K., and Uittenbogaard, R. (2009). *ENERGY CAPTURE USING URBAN SURFACE WATER: MODELLING AND IN-SITU MEASUREMENTS*. Eleventh International IBPSA Conference, Glasgow, Scotland.

Bach, B., Werling, J., Ommen, T., Münster, M., Morales, J. M., and Elmegaard, B. (2016). Integration of large-scale heat pumps in the district heating systems of greater copenhagen. *Energy*, 107:321–334.

Baptist, M., Uijttewaal, W., Stelling, G., and Labeur, R. (2005). Transport and mixing of cooling water. *Report WL| Delft. Internet*.

Barlow, J. F. (2014). Progress in observing and modelling the urban boundary layer. *Urban Climate*, 10:216–240.

Blocken, B., Janssen, W., and van Hooff, T. (2012). Cfd simulation for pedestrian wind comfort and wind safety in urban areas: General decision framework and case study for the eindhoven university campus. *Environmental Modelling & Software*, 30:15–34.

Bloemendal, M., Olsthoorn, T., and van de Ven, F. (2015). Combining climatic and geo-hydrological preconditions as a method to determine world potential for aquifer thermal energy storage. *Science of the Total Environment*, 538:621–633.

Boderie, P. and Dardengo, L. (2003). Warmtelozing in oppervlaktewater en uitwisseling met de atmosfeer. *Report Q3315, WL| Delft Hydraulics*.

Boderie, P. and Troost, T. (2020). *Aquathermie als maatregel voor vertering waterkwaliteit in de Sloterplas - Een voorverkenning*. Deltares.

CE Delft, Deltares (2018). *Nationaal potentieeel van aquathermie*. Delft.

Choi, K. and Lee, J. H. (2007). *Distributed Entrainment Sink Approach (DESA)-a New Method for Modelling Mixing and Transport in the Intermediate Field*. University of Hong Kong.

de Jong, K. (2010). *Warmte in de Nederlanden*. Stichting Warmtenetwerk.

de Lange, M., Jacobs, C., and Boderie, P. (2017). *Deltafact Ecologische effecten koudwaterlozingen*. STOWA, Deltares and Wageningen University.

Deilami, K., Kamruzzaman, M., and Liu, Y. (2018). Urban heat island effect: A systematic review of spatio-temporal factors, data, methods, and mitigation measures. *International journal of applied earth observation and geoinformation*, 67:30–42.

Deltares (2020). D-flow flexible mesh user manual.

Di Sabatino, S., Solazzo, E., Paradisi, P., and Britter, R. (2008). A simple model for spatially-averaged wind profiles within and above an urban canopy. *Boundary-layer meteorology*, 127(1):131–151.

Dijkstra, Y. (2014). *Turbulence modelling in environmental flows: Improving the numerical accuracy of the k-epsilon model by a mathematical transformation*. TU Delft repository.

Dirksen, M., Ronda, R., Theeuwes, N., and Pagani, G. (2019). Sky view factor calculations and its application in urban heat island studies. *Urban Climate*, 30:100498.

European Commission (2019). *The European Green Deal*. European Union, Brussels.

Falkoni, A., Soldo, V., Krajačič, G., Bupič, M., and Bertovič, I. (2020). Utilization of renewable energy sources using seawater source heat pump with and without energy storage: Comparison of thermal and battery energy storage. *Thermal Science*, 1(00):279–279.

Ferziger, J. H., Perić, M., and Street, R. L. (2002). *Computational methods for fluid dynamics*, volume 3. Springer.

Fischer, H. B., List, J. E., Koh, C. R., Imberger, J., and Brooks, N. H. (2013). *Mixing in inland and coastal waters*. Elsevier.

Fisher, H., List, J., Koh, C., Imberger, J., and Brooks, N. (1979). Mixing in inland and coastal waters, 302 pp.

Garnier, E., Adams, N., and Sagaut, P. (2009). *Large eddy simulation for compressible flows*. Springer Science & Business Media.

Gemeente Amsterdam (2019). *WKO Strandeiland: open publiek warmtenet?* Amsterdam.

Gill, A. E. (1982). Atmosphere-ocean dynamics. *Int. Geophys. Ser.*, 30:662p.

Gunawardena, K. R., Wells, M. J., and Kershaw, T. (2017). Utilising green and bluespace to mitigate urban heat island intensity. *Science of the Total Environment*, 584:1040–1055.

Hage, K. (1975). Urban-rural humidity differences. *Journal of Applied Meteorology and Climatology*, 14(7):1277–1283.

Harezlak, V. and Boderie, P. (2021). *Effecten van koudelozingen op het ecologisch functioneren van oppervlaktewatersystemen*. Netwerk Aquathermie.

Hicks, B. (1975). A procedure for the formulation of bulk transfer coefficients over water. *Boundary-Layer Meteorology*, 8(3):515–524.

HOBO (2019). *Datasheet Onset HOBO MX Pendant Data Logger*. Onset Computer Cooperation.

Holmer, B. and Eliasson, I. (1999). Urban–rural vapour pressure differences and their role in the development of urban heat islands. *International Journal of Climatology: A Journal of the Royal Meteorological Society*, 19(9):989–1009.

IF Technology bv (2017). *Business case voormalig Beursgebouw Leeuwarden*. Arnhem.

IF Technology bv (2019). Een mooie samenwerking levert energie uit de stadsgracht. `https://www.iftechnology.nl/meerwaarde-door-samenwerken`. Accessed: 16-12-2019.

Intergovernmental Panel on Climate Change (2018). *Summary for Policymakers*.

Isemer, H. and Hasse, L. (1987). *The Bunker climate atlas of the North Atlantic Ocean. Volume II: Air-sea interactions*.

Jaxa-Rozen, M., Kwakkel, J. H., and Bloemendal, M. (2019). A coupled simulation architecture for agent-based/geohydrological modelling with netlogo and modflow. *Environmental Modelling & Software*, 115:19–37.

Jirka, G. H., Doneker, R. L., and Hinton, S. W. (1996). *User's manual for CORMIX: A hydrodynamic mixing zone model and decision support system for pollutant discharges into surface waters*. US Environmental Protection Agency, Office of Science and Technology.

Joint Panel on Oceanographic Tables and Centre interuniversitaire d'études européennes and International Council of Scientific Unions. Scientific Committee on Oceanic Research and International Association for the Physical Sciences of the Ocean (1981). *Background papers and supporting data on the international equation of state of seawater 1980*, volume 38. Unesco.

Kadaster (2020). *Basisregistratie Adressen en Gebouwen (BAG)*. Kadaster.

Ketelhuis WG (2019). *Presentatie buurtbijeenkomst 11 november 2019*. Accessed: 18-12-2019.

Koole, M. (2016). *Rapportage WOW-NL evaluatie: vergelijking WOW met KNMI waarnemingen*. KNMI.

Kruitwagen, G. (2019). *Verslag workshop thermische energie uit oppervlaktewater: ontwikkelen afwegingskader koudelozingen*.

Kyrou, E. (2019). *Design of thermal energy balancing strategies for the ATES system on the TU/e campus: investigating operation strategies of the Atlas building and future design solutions for the ATES system*.

Landsberg, H. E. (1981). *The urban climate*. Academic press.

Lee, D. O. (1991). Urban—rural humidity differences in london. *International journal of climatology*, 11(5):577–582.

Liu, W., You, H., and Dou, J. (2009). Urban-rural humidity and temperature differences in the beijing area. *Theoretical and applied climatology*, 96(3):201–207.

Ludikhuize, D., de Koning, J., and Berserik, J. (2020). *Beoordelingsmethode thermische lozingen voor energiewinning (TEO)*. Hoogheemraadschap Delfland.

Macdonald, R. (2000). Modelling the mean velocity profile in the urban canopy layer. *Boundary-Layer Meteorology*, 97(1):25–45.

Macdonald, R., Carter, S., and Slawson, P. (2000). Measurements of mean velocity and turbulence statistics in simple obstacle arrays at 1: 200 scale. *Thermal fluids report*, 1.

Mashau, M. S. (2006). *Flow resistance in open channels with intermediate scale roughness*. University of Witwatersrand.

Meershoek, P. (2020). *Het water in de grachten was nog nooit zo helder*. Het Parool.

Mertens, S. (2003). The energy yield of roof mounted wind turbines. *Wind engineering*, 27(6):507–518.

Miltenburg, I. et al. (2008). Exploring the technical and economic feasibility of using the urban water system as a sustainable energy source. *Thermal Science*, 12(4):35–50.

Mostert, E. (2020). Law and politics in river basin management: The implementation of the water framework directive in the netherlands. *Water*, 12(12):3367.

Municipality of Amsterdam (2019). *Actieplan bruggen en kademuren*. Amsterdam.

Nazari-Sharabian, M., Ahmad, S., and Karakouzian, M. (2018). Climate change and eutrophication: a short review. *Engineering, Technology and Applied Science Research*, 8(6):3668.

Nelen en Schuurmans (2005). *Wateropgave Boezemwateren*. Hoogheemraadschap Amstel, Gooi en Vecht.

Netwerk Aquathermie (2020). *Aquathermie projecten in Nederland*. Netwerk Aquathermie.

Netwerk Aquathermie, Universiteit Utrecht (2019). *Juridisch Kader Aquathermie 2019; speelruimte voor de praktijk*. Amersfoort.

Noord Hollands Archief (2011). *Waterbeheersing in Amsterdam*. Oneindig Noord Holland.

Octavio, K., Jirka, G., and Harleman, D. (1977). Vertical heat transport mechanisms in lakes and reservoirs. ralph m. parsons laboratory, tech. rep.# 227, mit.

Oke, T. R. (1973). City size and the urban heat island. *Atmospheric Environment (1967)*, 7(8):769–779.

Oke, T. R. (1981). Canyon geometry and the nocturnal urban heat island: comparison of scale model and field observations. *Journal of climatology*, 1(3):237–254.

Ratti, C., Di Sabatino, S., and Britter, R. (2006). Urban texture analysis with image processing techniques: winds and dispersion. *Theoretical and applied climatology*, 84(1):77–90.

Rijksoverheid (2019). *Klimaatakkoord*. Den Haag.

Rodi, W. (1984). Turbulence models and their applications in hydraulics-a state-of-the-art review. *IAHR monograph*.

Ryan, P. J., Harleman, D. R., and Stolzenbach, K. D. (1974). Surface heat loss from cooling ponds. *Water resources research*, 10(5):930–938.

Sayegh, M. A., Jadwiszczak, P., Axcell, B., Niemierka, E., Bryś, K., and Jouhara, H. (2018). Heat pump placement, connection and operational modes in european district heating. *Energy and Buildings*, 166:122–144.

Schlichting, H. and Gersten, K. (2016). *Boundary-layer theory*. Springer.

Shashua-Bar, L. and Hoffman, M. E. (2003). Geometry and orientation aspects in passive cooling of canyon streets with trees. *Energy and Buildings*, 35(1):61–68.

Shih, T.-H., Liou, W. W., Shabbir, A., Yang, Z., and Zhu, J. (1995). A new k-e eddy viscosity model for high reynolds number turbulent flows. *Computers & fluids*, 24(3):227–238.

Snijders, A. (2005). *Aquifer Thermal Energy Storage in the Netherlands*. IFTech International BV, Arnhem.

Solcerova, A., van de Ven, F., and Van De Giesen, N. (2019). Nighttime cooling of an urban pond. *Frontiers in earth science*, 7:156.

Spitler, J. and Mitchell, M. (2016). *Advances in Ground-Source Heat Pump Systems*.

Sreenivas, K. and Prasad, A. K. (2000). Vortex-dynamics model for entrainment in jets and plumes. *Physics of Fluids*, 12(8):2101–2107.

STOWA (2017). *Handreiking voor ontwikkeling TEO projecten*. Amersfoort.

Talley, L. D. (2011). *Descriptive physical oceanography: an introduction*. Academic press.

United Nations (2020). *World Cities Report 2020: The Value of Sustainable Urbanization*. UN Habitat.

Van der Hoek, J. (2012). Climate change mitigation by recovery of energy from the water cycle: a new challenge for water management. *Water Science and Technology*, 65(1):135–141.

van der Hoek, J. P., Mol, S., Giorgi, S., Ahmad, J. I., Liu, G., and Medema, G. (2018). Energy recovery from the water cycle: Thermal energy from drinking water. *Energy*, 162:977–987.

van der Hoeven, F. and Wandl, A. (2013). *Amsterwarm: gebiedstypologie warmte-eiland Amsterdam*, volume 4. TU Delft.

van der Hoeven, F. and Wandl, A. (2015). Amsterwarm: Mapping the landuse, health and energy-efficiency implications of the amsterdam urban heat island. *Building Services Engineering Research and Technology*, 36(1):67–88.

Van Hooff, T. and Blocken, B. (2010). Coupled urban wind flow and indoor natural ventilation modelling on a high-resolution grid: A case study for the amsterdam arena stadium. *Environmental Modelling & Software*, 25(1):51–65.

Van Megchelen, C. (2017). *Cool water effects on shallow surface water*. TU Delft repository, Delft.

Verbruggen, W., van der Baan, J., and Buschman, F. (2019). Delft3d-fm pilotproject voor het nzk-ark.

Wang, J., Song, J., Huang, Y., and Fan, C. (2013). On the parameterization of drag coefficient over sea surface. *Acta Oceanologica Sinica*, 32(5):68–74.

Waternet (2015). *Waternet. Climate neutral in 2020 - Program for research and projects in the period 2015-2020*. Amsterdam.

Wauben, W. M. (2002). *J3. 2 AUTOMATION OF VISUAL OBSERVATIONS AT KNMI;(II) COMPARISON OF AUTOMATED CLOUD REPORTS WITH ROUTINE VISUAL OBSERVATIONS*. KNMI.

White, F. M. and Corfield, I. (2006). *Viscous fluid flow*, volume 3. McGraw-Hill New York.

Wieringa, J. and Rijkoort, P. J. (1983). Windklimaat van nederland. *ISBN 9012044669*.

Wood, D. (1982). Internal boundary layer growth following a step change in surface roughness. *Boundary-Layer Meteorology*, 22(2):241–244.

Wüest, A. and Lorke, A. (2003). Small-scale hydrodynamics in lakes. *Annual Review of fluid mechanics*, 35(1):373–412.

Yang, J., Shi, B., Xia, G., Xue, Q., and Cao, S.-J. (2020). Impacts of urban form on thermal environment near the surface region at pedestrian height: A case study based on high-density built-up areas of nanjing city in china. *Sustainability*, 12(5):1737.

Zanstra, Giesen en Sijmons architectenbureau (1946). *Bouwen van woning tot stad: eenige aspecten van den stedebouw, het woningbedrijf, de woningarchitectuur, de woningplattegrond en de technische voorzieningen van de woning*. van Oorschot, Amsterdam.

Zijl, F. (2002). *On the effect of non-hydrostatic simulation on buoyant jets*. Delft University Repository, Delft.